AD-A107 667 WEIDLINGER ASSOCIATES MENLO PARK CA F/G 8/11
SITE-DEPENDENT GROUND MOTIONS FROM DISTANT EARTHQUAKES. REVISED--ETC(U)
DEC 80 G L WOJCIK, J ISENBERG, W S DUNBAR F49620-80-C-0009
UNCLASSIFIED R-8065 AFOSR-TR-81-0723 NL

1 OF 2
AD A
107667

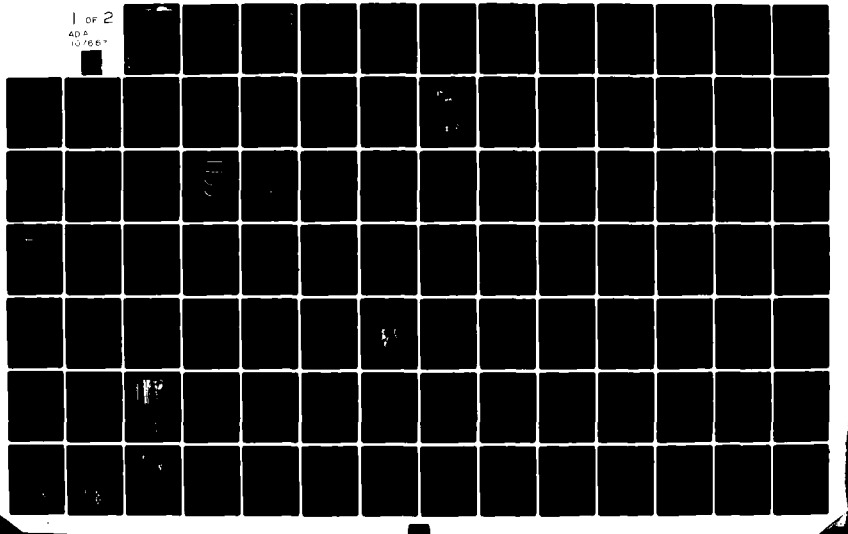

4

WEIDLINGER ASSOCIATES
3000 SAND HILL ROAD
BUILDING 4, SUITE 245
MENLO PARK, CALIFORNIA 94025

Revised Supersedes AD-A093-791

SITE-DEPENDENT GROUND MOTIONS FROM DISTANT EARTHQUAKES

By

G.L. Wojcik
J. Isenberg
W.S. Dunbar

Prepared for

Air Force Office of Scientific Research
Bolling AFB, Washington, D.C. 20332

and

Air Force Geophysics Laboratory
Terrestrial Sciences Division
Hanscom AFB, Massachusetts 01731

Final Report
AFOSR Contract F49620-80-C-0009
For the Period 1 October 1979 to 31 December 1980

UNCLASSIFIED

SECURITY CLASSIFICATION OF THIS PAGE (When Data Entered)

REPORT DOCUMENTATION PAGE	READ INSTRUCTIONS BEFORE COMPLETING FORM
1. REPORT NUMBER: AFOSR-TR- 81 -0723	2. GOVT ACCESSION NO. AD-A107 467
	3. RECIPIENT'S CATALOG NUMBER
4. TITLE (and Subtitle): Site-Dependent Ground Motions from Distant Earthquakes	5. TYPE OF REPORT & PERIOD COVERED: Final Report. 1 Oct 1979 to 31 Dec 1980
	6. PERFORMING ORG. REPORT NUMBER: R 8065
7. AUTHOR(s): G. L. Wojcik, J. Isenberg, W. S. Dunbar	8. CONTRACT OR GRANT NUMBER(s): F49620-80-C-0009
9. PERFORMING ORGANIZATION NAME AND ADDRESS: Weidlinger Associates, 3000 Sand Hill Road, Building 4, Suite 245, Menlo Park, California 94025	10. PROGRAM ELEMENT, PROJECT, TASK AREA & WORK UNIT NUMBERS: 61102F, 2309/A1
11. CONTROLLING OFFICE NAME AND ADDRESS: Air Force Office of Scientific Research, Bldg. 410, Bolling AFB, Washington, DC 20332	12. REPORT DATE: 11 Dec 1980
	13. NUMBER OF PAGES: 109
14. MONITORING AGENCY NAME & ADDRESS(if different from Controlling Office)	15. SECURITY CLASS. (of this report): UNCLASSIFIED
	15a. DECLASSIFICATION/DOWNGRADING SCHEDULE

16. DISTRIBUTION STATEMENT (of this Report)

Approved for public release; distribution unlimited.

17. DISTRIBUTION STATEMENT (of the abstract entered in Block 20, if different from Report)

18. SUPPLEMENTARY NOTES

19. KEY WORDS (Continue on reverse side if necessary and identify by block number)

Geology
Seismology
Denver Basin
Basin Resonance
Body Waves
Seismic Alarms
Minuteman Wing V

20. ABSTRACT (Continue on reverse side if necessary and identify by block number)

This study examines geological and seismological reasons for patterns of guidance alarms in Minuteman Wing V due to the 1975 Pocatello Valley, Idaho and 1979 St. Elias, Alaska earthquakes. Two features are identified which together could cause these patterns of alarms. First is the existence of lightly-damped missile suspension system modes in the period window from 2 to 6 seconds. Second is a 2 to 3 km sedimentary layer underlying the wing, with natural frequencies in this critical period window. Near-vertically-

DD FORM 1 JAN 73 1473 EDITION OF 1 NOV 65 IS OBSOLETE

UNCLASSIFIED

SECURITY CLASSIFICATION OF THIS PAGE (When Data Entered)

20. ABSTRACT (CONTINUED)

incident P and S seismic body waves which propagate directly from the source through the crust and upper mantle can interact with this structure. A Haskell-Thomson program for body wave propagation in a layered model indicates that peak ground shaking can vary by a factor of 2 at adjacent Wing V flights. Differences are due to variations in sediment thicknesses and wavespeeds, deduced from oil well log and laboratory data. Therefore, Wing V alarm patterns appear to be caused by the coincidence of three factors: 1) high gain of the 2 to 6 second suspension system modes; 2) incident body waves in this period range; and 3) sedimentary column resonance periods close to the suspension system natural periods. If the first two are sufficient to trigger alarms, then the third would cause anomalous patterns due to relative amplification between flights. Escarpments, basin edges and similar features are not likely to cause the observed distribution of alarms because they produce resonances at periods too short to affect the Missile Guidance Set. This is confirmed by a finite element analysis of the escarpment for vertically-incident body waves.

WEIDLINGER ASSOCIATES
3000 SAND HILL ROAD
BUILDING 4, SUITE 245
MENLO PARK, CALIFORNIA 94025

SITE-DEPENDENT GROUND MOTIONS FROM DISTANT EARTHQUAKES

By

G.L. Wojcik
J. Isenberg
W.S. Dunbar

Prepared for

Air Force Office of Scientific Research
Bolling AFB, Washington, D.C. 20332

and

Air Force Geophysics Laboratory
Terrestrial Sciences Division
Hanscom AFB, Massachusetts 01731

Final Report
AFOSR Contract F49620-80-C-0009
For the Period 1 October 1979 to 31 December 1980

ABSTRACT

This study examines geologic and seismological reasons for patterns of guidance alarms in Minuteman Wing V due to the 1975 Pocatello Valley, Idaho and 1979 St. Elias, Alaska earthquakes. Two features are identified which together could cause these patterns of alarms. First is the existence of lightly-damped missile suspension system modes in the period window from 2 to 6 seconds. Second is a 2 to 3 km sedimentary layer underlying the wing, with natural frequencies in this critical period window. Near-vertically-incident P and S seismic body waves which propagate directly from the source through the crust and upper mantle can interact with this structure. A Haskell-Thomson program for body wave propagation in a layered model indicates that peak ground shaking can vary by a factor of 2 at adjacent Wing V flights. Differences are due to variations in sediment thicknesses and wavespeeds, deduced from oil well log and laboratory data. Therefore, Wing V alarm patterns appear to be caused by the coincidence of three factors: 1) high gain of the 2 to 6 second suspension system modes; 2) incident body waves in this period range; and 3) sedimentary column resonance periods close to the suspension system natural periods. If the first two are sufficient to trigger alarms, then the third would cause anomalous patterns due to relative amplification between flights. Escarpments, basin edges and similar features are not likely to cause the observed distribution of alarms because they produce resonances at periods too short to affect the Missile Guidance Set. This is confirmed by a finite element analysis of the escarpment for vertically-incident body waves.

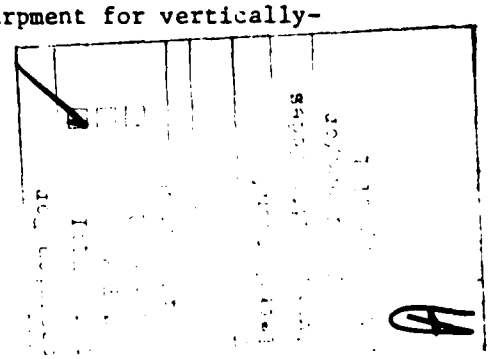

ACKNOWLEDGMENTS

The research effort reported here benefited from information and comments by a number of individuals. Dr. Ker Thomson of the Air Force Geophysics Laboratory instigated this research effort and provided preliminary data. Prof. Robert B. Smith, Prof. Walter Arabasz and Mr. Kevin Kilty at the University of Utah were consultants early in the effort and supplied preliminary geophysical data on the Denver Basin area, particularly Tertiary geology, oil well log data and Landsat imagery. Mr. Thomas S. Summers of Eyring Research Institute, Inc. was a valuable and timely source of data on Wing V seismic alarms from both the Pocatello Valley and St. Elias earthquakes. Mr. Robert Hume of TRW provided a useful discussion of unclassified data pertaining to Wing V seismic discriminants. Messrs. Norman Lipner and Gary Teraoka of TRW made available the Porter and O'Brien Wing V subsurface site investigations and related data. Prof. Amos Nur and Ms. Carol Tosaya of Stanford University supplied valuable data and discussion on rock properties. Dr. David Boore of USGS, Menlo Park, California kindly read a draft of Section 3. In addition, the technical assitance of Penny Sevison for the illustrations, Edith Durfey for much of the geologic data reduction, and Myrtle Carey and Pam Hagan for typing the report, is gratefully acknowledged.

TABLE OF CONTENTS

LIST OF FIGURES

LIST OF FIGURES (CONTINUED)

LIST OF FIGURES (CONCLUDED)

LIST OF TABLES

SECTION 1

INTRODUCTION

In 1975 a magnitude 6.0 (M_L) earthquake occurred in Pocatello Valley, Idaho, near the southeast Idaho-Utah border (Arabasz, et al. (1980)). It was located within the southern part of the Intermountain Seismic Belt (Smith and Sbar (1974)) where the last local event of comparable magnitude took place in 1962 (Cache Valley, Utah; M_L = 5.7). In addition to causing moderate damage in the epicentral region, the earthquake had a significant effect 640 kilometers east of the epicenter at the 90th Strategic Missile Wing, Wing V, near F. E. Warren Air Force Base, Cheyenne, Wyoming. Unexpected and unprecedented operational mode changes (seismic alarms) were triggered in 42% of the missile force, distributed in a southeast swath across the wing. The apparent cause was long period (2 to 6 second), low amplitude ground shaking. The subject of this report is a quantitative investigation of the phenomenon in terms of ICBM response and seismic response of the Wing V area.

The investigation was begun as a computational effort to explain the distribution of seismic alarms. Initial emphasis was on topography, particularly the apparent correlation of alarms with highland sites, which were separated from lowland sites by the Goshen Hole escarpment ($\leq$ 200 meter elevation change). Preliminary studies were conducted using finite element regional models together with seismic input derived from synthetic seismograms, Rodi et al. (1979). It soon became apparent that no significant interaction between topography and seismic waves could occur in the period window of interest, 2 to 6 seconds, so as to cause the observed alarm distribution. The synthetic seismograms exhibited considerable surface wave motion which suggested

that the interaction of surface waves with local geology may have been a cause. However, work by Hume (1980) showed that body wave arrivals were correlated with more subtle Wing V seismic discriminants from distant earthquakes, leaving the question of causative wave type unresolved.

In 1979, four years after the Pocatello Valley event, the St. Elias earthquake in southeast Alaska triggered seismic alarms in 46% of the Wing V missile force. A surface wave magnitude (M_S) of 7.1 was reported, Lahr (1980), Boatwright (1980). The alarm distribution differed from the previous case, as did the duration, phasing and amplitude of seismic waves. St. Elias seismograms recorded at Golden, Colorado, in conjunction with alarm timing data collected by Summers (1980) suggested that body waves were responsible for the St. Elias seismic alarms. This is consistent with Hume's observations.

After reevaluating the Wing V problem, an effort was made to collect data on Wing V system response, seismic inputs, local geology and tectonics, in order to narrow the choice of possible causative mechanisms. It was necessary to characterize three types of behavior: 1) response of the Minuteman ICBM, its suspension system and the surrounding silo (structure response); 2) nature of the seismic input (source and path effects); and 3) ground response due to the interaction of seismic waves with local geology (site response). These are basic features of any problem in engineering seismology. In the following sections, these data are described and finally applied to a calculational model in Section 5.

The present report consists of five sections. Section 1 introduces the problem and provides background data on the Wing V system and previous Air Force sponsored work addressing local response within Wing V. Section 2 describes the geological evolution of the area in order to identify geologic and structural features relevant to the problem. Section 3 presents available

seismograms from the two earthquakes considered, and identifies significant phases. Section 4 describes velocity data in the Wing V area and velocity and density functions necessary to model the seismic response of underlying sediments. Section 5 presents models of the sedimentary column at each flight within Wing V, and calculations of surface response due to normally-incident body waves. The conclusion presented in Section 5 is that body waves in the period range of 2 to 6 seconds tend to interact with the sedimentary column underlying Wing V. The interaction is such that highland flights may experience 50-100% higher ground response than a reference lowland flight. The mechanism is differences in sedimentary column resonant periods rather than surface topography. This conclusion applies to body wave inputs. Surface wave calculations are not included here. Section 6 provides a brief summary of the effort and conclusions.

In compliance with Air Force reporting requirements, the efforts of the contributing authors are as follows. W. S. Dunbar performed part of the calculation reported in the Appendix on finite element modeling. J. Isenberg was co-principal investigator and instrumental in early stages focusing on finite element regional modeling and preliminary data, and wrote part of the Appendix. G. L. Wojcik was co-principal investigator and performed the overall research effort and report, and is responsible for its contents and conclusions.

1.1 Description of Wing V

Wing V includes 200 operational Minuteman III ICBMs, each suspended in a vertical silo, and twenty Launch Control Facilities (LCFs). It is situated approximately 700 kilometers due east of the Pocatello Valley epicenter in the Northern Denver Basin and covers over 13,000 square kilometers. Distribution of the twenty flights composing Wing V (ten ICBMs and one LCF per flight) is shown in Figure 1-1.

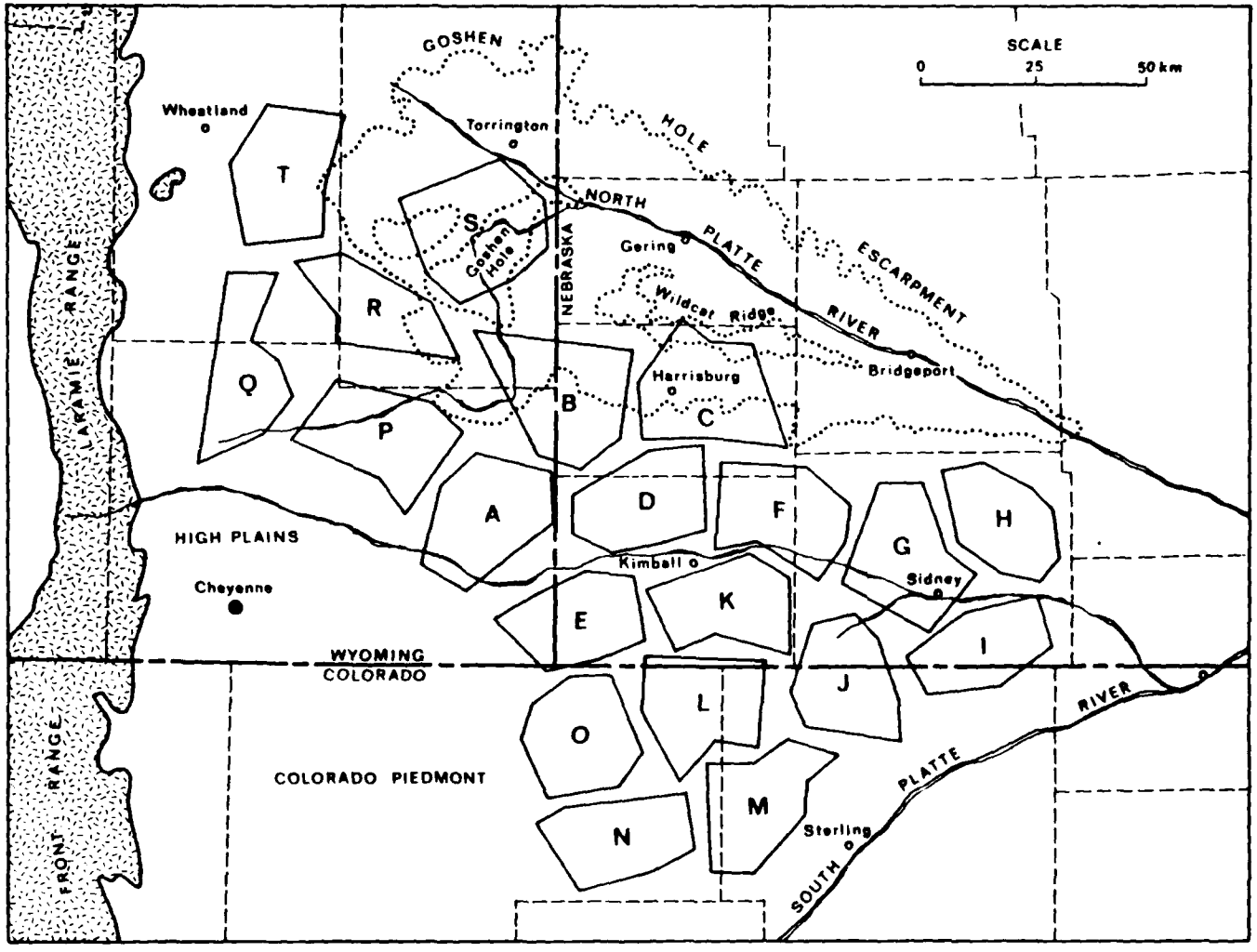

Figure 1-1. Distribution of Wing V flights (A through T) in the tri-state area of Wyoming, Nebraska, and Colorado (northern Denver Basin).

The 200 ICBMs can be viewed as an array of seismic instruments (inverted pendulums) capable of registering ground motion. This is accomplished as a secondary function by the Missile Guidance Set (MGS) which includes an inertial platform, digital computer, gravity level, gyrocompass and gyro accelerometer. Resolution of the MGS is rather crude, however, in comparison to a conventional seismic instrument. For example, the data sample interval is on the order of minutes and disruption counts are recorded rather than motion levels. The output of principal concern here is the so-called seismic alarm, an instruction (based on leveling counts) for the system to switch from a very stable gravity leveling mode to a more robust gyroscopic leveling mode (PIGA leveling). Therefore, the alarm is essentially a seismic switch indicating that motion of the MGS has repeatedly exceeded some value. Details of the alarm transfer function are presently being investigated by the Air Force under a full-scale testing program. The available data on MGS response are described below.

The Minuteman III silo mounted ICBMs in Wing V are each supported from a base ring in a missile cage which is in turn suspended by an upgraded Boeing Missile Suspension System within the silo. Boeing has represented the overall response of the system to external seismic input by a linear model with twelve coupled degrees of freedom. The coefficient matrices of the resulting linear system of ordinary differential equations are determined experimentally by "plucking" the missile in its suspension system. This is in contrast to real seismic inputs corresponding to motion of the silo (ground motion) rather than missile motion. The linearity assumption guarantees that the two approaches are equivalent. Actually, there is some suspicion that at the low amplitudes and long periods of interest here, nonlinear system response is significant. This question will be clarified by the full-scale testing program which mimics silo inputs rather than missile inputs.

The classical linear approach yields theoretical uncoupled modes of the system. The first five modes are long period (2-6 seconds) and lightly damped (damping ratio less than or equal to .01). Resonance curves for these modes are shown in Figure 1-2. The remaining seven modes have periods on the order of one second or less and are more highly damped. It has been strongly suggested that the longer period modes, specifically the 3.4 second mode, are responsible for the seismic alarms. One basis is data from more subtle MGS discriminants registering distant earthquakes, Hume (1980). These data are not generally available; nonetheless, it will be assumed in what follows that 2-6 second seismic input is the period window of concern for seismic alarms.

It is clear from the resonance curves that the long period input motion is strongly amplified. However, it takes many cycles before these amplifications are achieved. Figure 1-3 shows curves of amplification versus number of cycles; for example, it requires over 50 cycles to achieve 90% of the theoretical maximum for the 3.4 second mode. Therefore, seismic inputs must have duration on the order of minutes ($\cong$ 3 minutes for the 3.4 second mode) in order to approach the maximum achievable amplification.

1.2 Alarm Distributions and Early Hypotheses

The distribution of seismic alarms over Wing V are shown in Figure 1-4 for both the Pocatello Valley and St. Elias earthquakes. The Pocatello Valley event triggered alarms in over 42% of the wing on a clear swath trending southeast. Because neighboring silos to the north and south were relatively unaffected, this alarm pattern suggested a localized belt of ground motion enhancement. In comparison, the St. Elias event caused alarms in 46% of the wing; however, they were grouped in the southeast rather than across the wing.

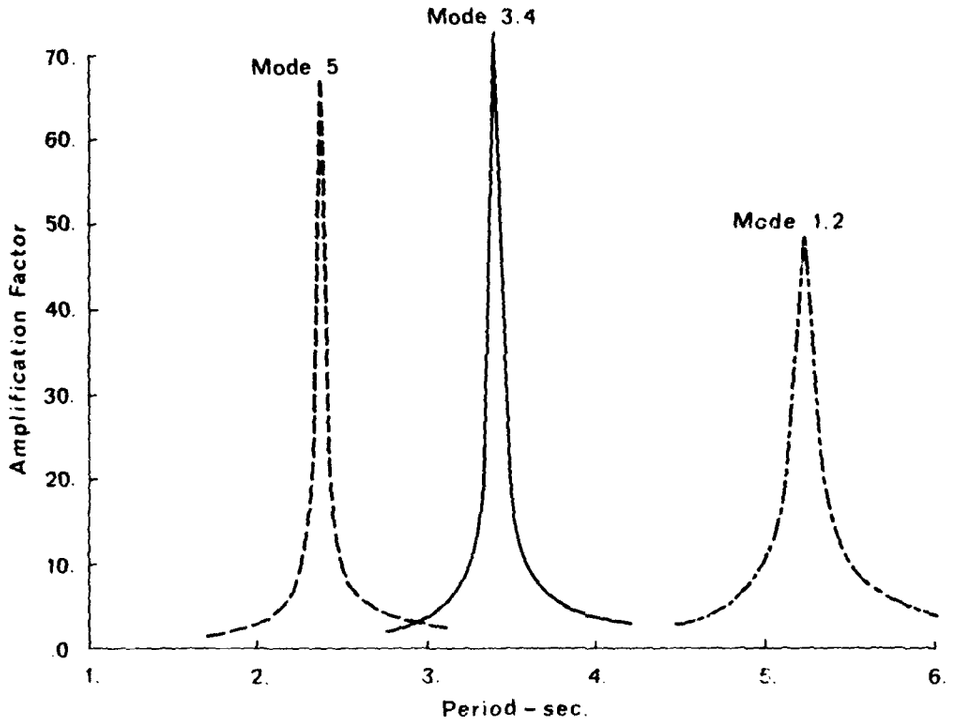

Figure I-2. Resonance curves for longer period, lightly damped modes of the suspension system.

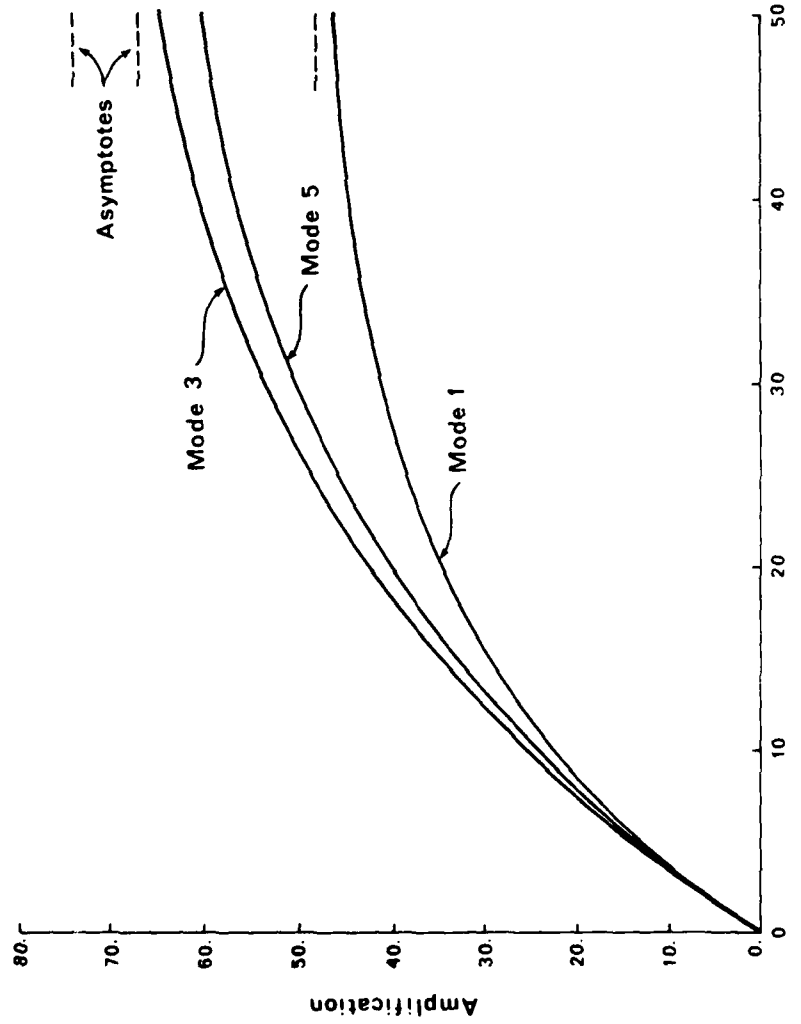

Figure 1-3. Amplitude versus number of cycles for longer period suspension system modes.

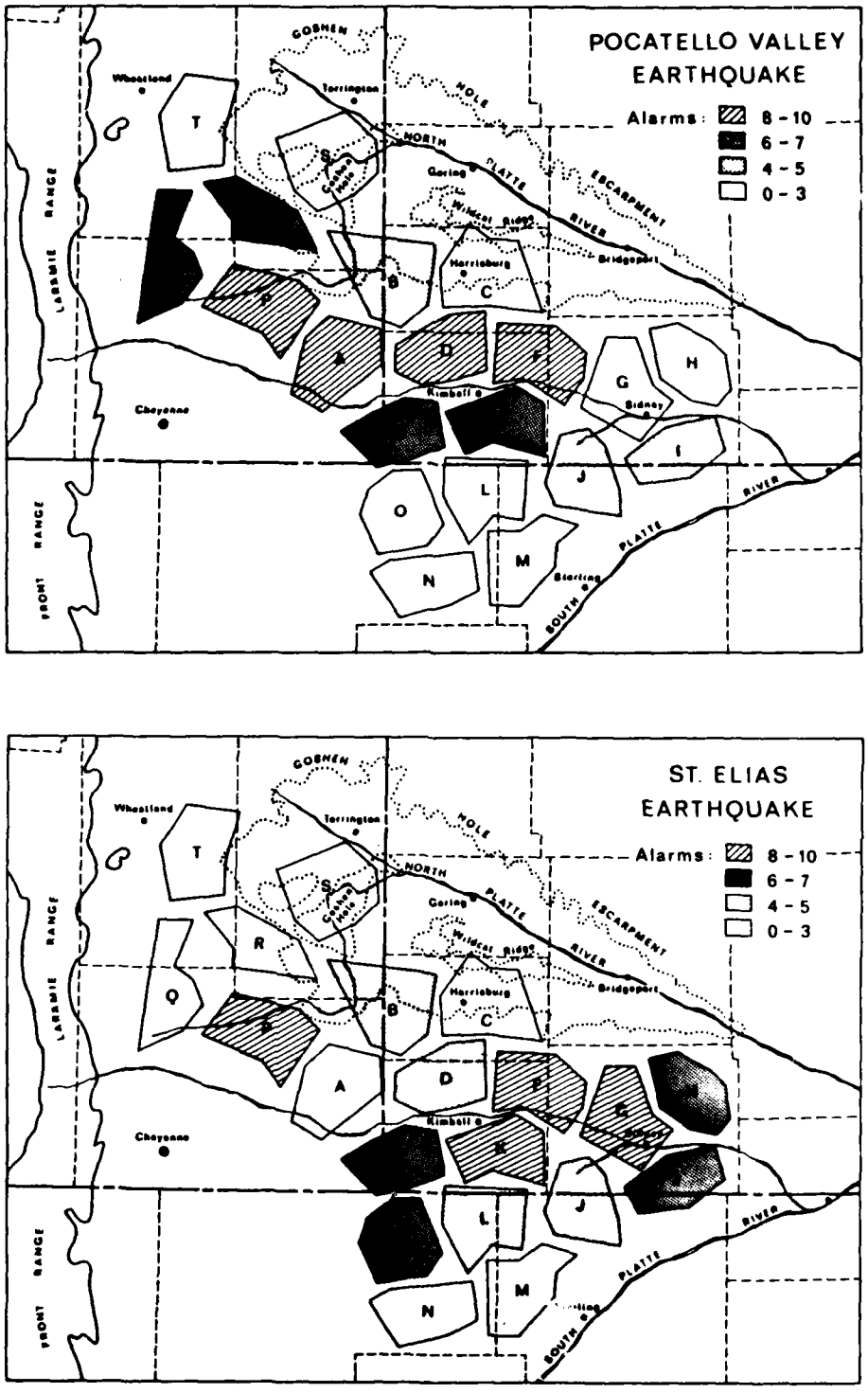

Figure 1-4. Distribution of seismic alarms caused by the 1975 Pocatello Valley and 1979 St. Elias earthquakes (from data provided by Summers (1980)).

The Pocatello Valley event graphically illustrated the sensitivity of Wing V to ground motion from distant earthquakes. Prompted by this, a number of studies have been conducted to explain the anomalies. Two of these, concerned principally with local site investigations, are described below.

A geologic literature search conducted by Riecker (1975) examined the geology of the tri-state area of northeastern Colorado, southeastern Wyoming and southwest Nebraska, encompassing Wing V. It concluded that no subsurface geologic, structural or geophysical trends conformed to the pattern of affected silos. Riecker postulated that perhaps the latest fluvial deposits (Tertiary) were significant because the southeast flow trends approximately matched the alarm pattern orientation. A second postulate concerned the structural shape of the Denver Basin and its ability to focus seismic energy along the swath of affected silos. Neither postulate was supported at this stage by quantitative data. The search revealed a great amount of geologic data from oil and water well drilling logs in the northern Denver Basin. This follows from the fact that it is the second oldest oil producing area in the United States and that late Tertiary aquifers supply large amounts of groundwater for extensive agricultural developments in the region. These and related data will be described in detail in Section 2.

In 1978 a Wing V ground motion study was reported by Ossing and Crowley (1978). The authors observed that the majority of silos affected by the Pocatello Valley event were located in the High Plains, south of the southerly Goshen hole escarpment, Figure 1-1 (≅ 200 meters of elevation change), while the lowland silos north of the escarpment were relatively unaffected. Citing evidence that motion is amplified near the top of a ridge and attenuated near the bottom, Bouchon (1973), the authors instrumented two sites on either side of the escarpment, one in Flight S and the other in Flight R. The seismograph

stations were operated for one year, November 1976 to October 1977, and recorded one earthquake with source location and magnitude approaching the Pocatello Valley event (500 km away in eastern Utah, M_L = 5.0). There were no significant differences in ground motion levels or missile effects between the two stations. In addition, the authors examined seismic risk criteria for the Wing V area and compared source characteristics from the Pocatello Valley event and a 1975 Yellowstone earthquake (M_L = 6.). The Yellowstone event did not affect Wing V due in part to a favorable fault plane orientation and attenuation through the Yellowstone caldera, both minimizing seismic radiation towards the wing. Ossing and Crowley concluded that a source-site transfer function was necessary in order to explain the anomalous Wing V effects. Such a study is described in Section 1.3.

A seismic risk evaluation program was initiated by the Air Force in response to the Wing V anomalies as well as the Palmdale uplift near Edwards Air Force Base. Battis and Hill (1977) analyzed seismicity and tectonics of the central and western US, including the Rocky Mountain region of interest here. Recurrence relations and strain release maps were developed. The Pocatello Valley event and a June 30, 1975 Yellowstone earthquake were analyzed using far-field surface wave data. It was noted that the effects at Wing V might be explained by Rayleigh wave radiation patterns, although the connection between seismic alarms and Rayleigh waves was not investigated. Additional studies included the state of knowledge concerning the Palmdale uplift in Southern California, and the state of earthquake prediction technology. In a second report, Battis (1978) conducted seismic risk studies of three military facilities in the western US, including Wing V near Cheyenne, Wyoming. These studies resulted in ground motion risk curves relating ground motion levels to annual occurrence probabilities. However, the paucity of

near-regional data limited the accuracy of risk evaluation for Wing V. A recurrence period of two years for Wing V disturbances was predicted.

1.3 Source Modeling and Synthetic Seismograms

The Pocatello Valley earthquake was one of the best documented earthquake sequences in the Basin and Range province. The University of Utah's telemetered seismic network and portable instruments deployed by the University and U.S. Geological Survey provided abundant details of the foreshock, mainshock and aftershock activity. The seismological data are discussed in detail by Arabasz, et al. (1980). The authors describe the earthquake sequence as a complex episode of Basin and Range graben subsidence that may typify similar source regions elsewhere in the Intermountain Seismic Belt.

In 1978 Day, et al. (1978) reported analytical and numerical source models for the Pocatello Valley event. These were derived by constraining the focal mechanism using the above-mentioned aftershock data and fitting synthetic seismograms to observed long and short period teleseismic P wave data. To fit the data, they had to include variable rupture velocity, variable stress drop and unilateral rupture toward the free surface. In a follow-on report Rodi, et al. (1979) used the above Pocatello Valley source model and a simplified plane, layered path model to calculate synthetic seismograms at Wing V. The overall effort described in these reports was state-of-the-art and involved a successful unification of several rather complicated analytical techniques. One purpose was to determine features of the source or path which might make the event unique among western U.S. earthquakes. Other research objectives not described here were synthetic seismograms for western U.S. earthquakes in the range of 150-250 km, modeling of the 1975 Yellowstone earthquake and initial comparisons of surface motion generated by earthquakes and large surface explosions.

In the remainder of this section, the above synthetic seismogram calculations for Wing V will be described. These were prompted by the lack of measured ground motion data in the area of interest. The calculations utilized generalized ray theory for the early arriving P waves, and modal superposition for S waves and surface waves. Both techniques were coupled to the analytical source model derived by Day, et al. (1980). Anelastic shear attenuation was incorporated using an approximate Q operator. Approximations in the wave propagation analysis included the neglect of certain weak body wave phases and truncation of modal sums at the fifth or sixth higher overtone. The authors concluded that the analysis was probably adequate for the source and epicentral distances involved. The path model used was a Northern Colorado Plateau model from Keller, et al. (1976) based on short period Rayleigh wave dispersion. The two kilometer sedimentary layer in this model was a rather crude approximation to the true propagation path so another model without the layer was employed to bound its effect. Two postulated Q models were also included to indicate the effect of anelastic attenuation.

The best estimates of ground motions were for the model with a sedimentary layer. Synthetics for the two cases are shown in Figure 1-5. Peak motion at the closest of the Wing V sites are: displacement, 0.05 cm (tangential); velocity, 0.12 cm/sec (radial); and acceleration, 0.35 cm/sec^2 (radial). Corresponding values at a site 88 kilometers further southeast are about half these. The principal difference between the synthetics with and without a sedimentary layer is the surface waves. These are highly dispersed by the surface layer and the Rayleigh wave is dominated by longer period motion. Without the layer, the surface waves are much less dispersed yielding more impulsive arrivals; in addition, the amplitudes are roughly doubled.

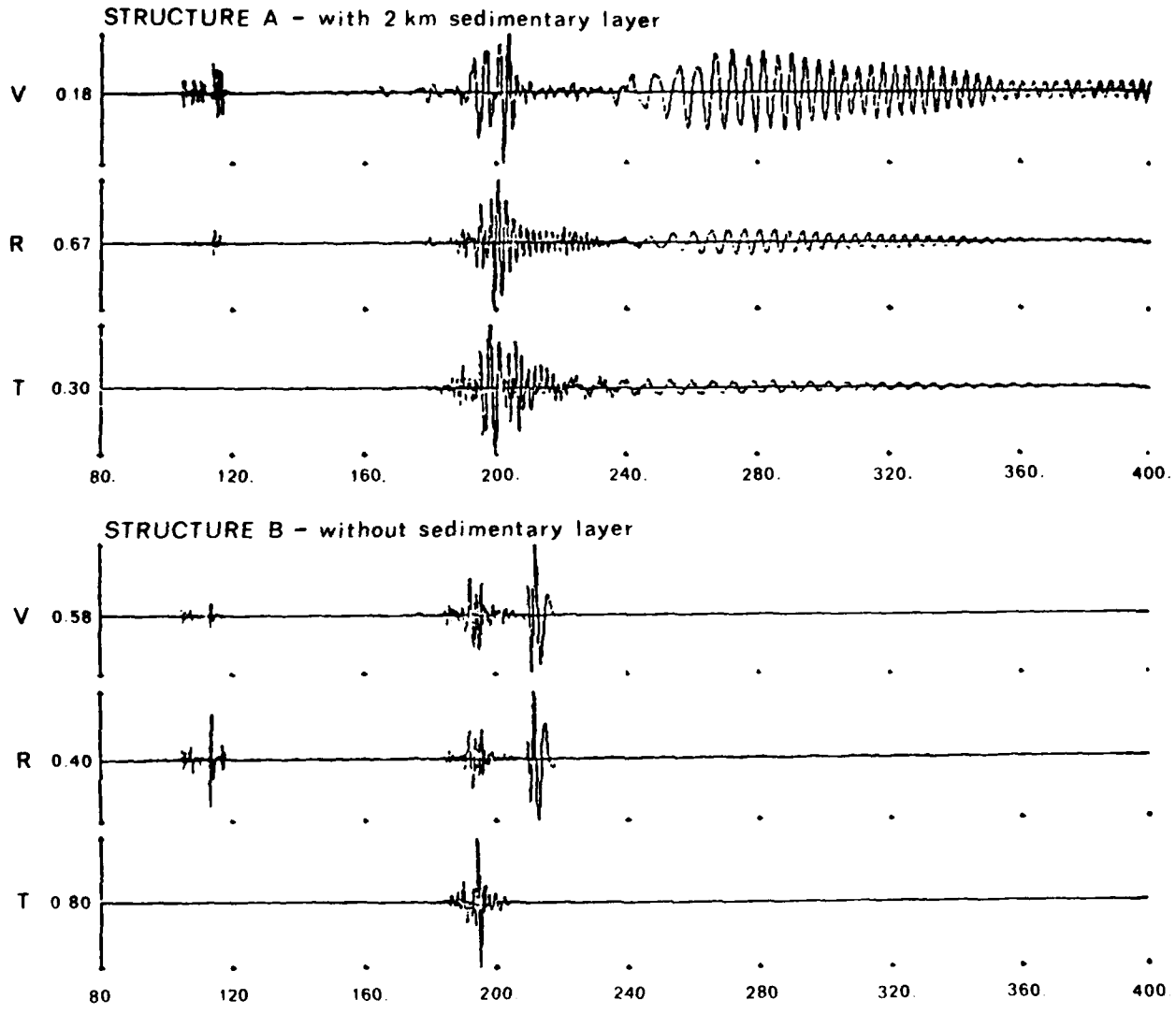

Figure 1-5. Comparison of synthetic seismograms with and without uniform sediment over travel path (Rodi, et al. (1979)).

SECTION 2

GEOLOGICAL EVOLUTION OF THE WING V AREA

Wing V is distributed over the tri-state area of Wyoming, Nebraska and Colorado in the northern Denver Basin. It is bounded to the west by the Laramie Range of the Central and Southern Rocky Mountains and to the east by the Great Plains of central North America. The principal tectonic features are illustrated in Figure 2-1 from King, et al. (1969). The structure to the west is dominated by the Cordilleran system of mountains, basins and plateaus, which extends 800-1600 kilometers inland from the Pacific Coast along the length of North America. The eastern part of the system was deformed most recently during the Laramide orogeny towards the end of the Mesozoic era. For reference, the geologic time scale is shown in Table 2-1. The principal source of information on the evolution of the region is King (1977).

2.1 Tectonic and Geologic Background

The Laramide orogeny, beginning in late Cretaceous time, affected the easternmost extreme of the Cordilleran, creating great vertical uplifts. Some raised so high that cores of basement rock were brought to the surface. The structures developed from rocks of the ancient continental platform previously deformed in late Paleozoic time. The structures have since been modified by processes during Tertiary time. These include the formation of basins soon after the main orogeny, in which Tertiary sediments were deposited; and regional uplift of broad areas which is responsible for the present height of the Central and Southern Rocky Mountains and Colorado Plateau. Streams invigorated by the uplift have etched out the ranges of the Rockies and the myriad canyons of the Plateau. A schematic illustrating structural evolution of the Front

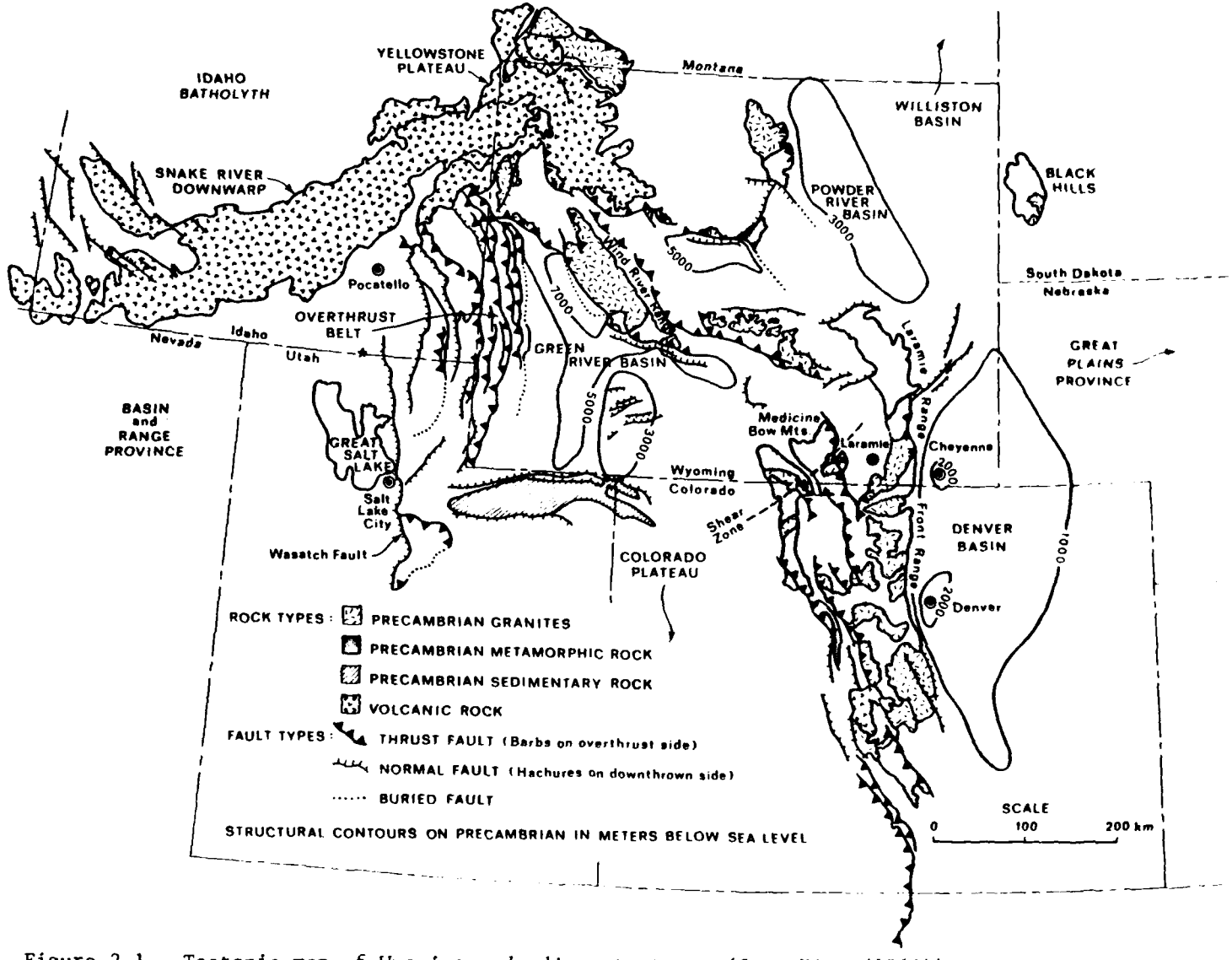

Figure 2-1. Tectonic map of Wyoming and adjacent states (from King (1969)), showing principal uplifts and basins. The Pocatello Valley epicenter is marked by a star near the border above the Great Salt Lake.

Table 2-1. Geologic Time Scale

Era	*Period*	*Epoch*	*Duration in Millions in Years*	*Began Millions of Years Ago*
Cenozoic	Quaternary	Recent	(Late archeologic and historic time)	
		Pleistocene	1	1
	Tertiary	Pliocene	12	13
		Miocene	12	25
		Oligocene	11	36
		Eocene	22	58
		Paleocene	5	63
Mesozoic	Cretaceous	(Early,	72	135
	Jurassic	Middle, or	46	181
	Triassic	Late)	49	230
Paleozoic	Permian	(Early,	50	280
	Carboniferous:	Middle, or		
	Pennsylvanian and	Late)	30	310
	Mississippian		35	345
	Devonian		60	405
	Silurian		20	425
	Ordovician		75	500
	Cambrian		100	600
Precambrian: Proterozoic and Archeozoic			900 (undetermined)	1,500

Range of Colorado is shown in Figure 2-2. Similar processes operated on the Front Range's northerly extension, the Laramie Range in southeast Wyoming. Figure 2-2a shows structure during late Paleozoic time, after formation of the Front Range geanticline, an upwarping of platform sediments. Figure 2-2b shows the situation in late Mesozoic time when the range was quiescent and buried, followed by (c) in early Tertiary time immediately after the Laramide orogeny. Figure 2-2d shows the present relations following later Tertiary regional uplift and dissection. A more general illustration of the different structural features found along edges of the uplifts is shown in Figure 2-3. These include a dipping border along the core of exposed Precambrian rocks, with the upturned sediments carved by erosion into lines of hogbacks (a); nearly vertical faults with Cretaceous and early tertiary rocks of the basin abuting Precambrian rock faces (b); faults dipping under the mountains so that Precambrian core rock is thrust over basin rocks (c); and lastly, all of these borders covered by younger sedimentary deposits which overlay the older rocks, masking structure (d).

The regional tectonic map, Figure 2-1 shows the overall configuration of mountains and basins as compiled by King. Heavily metamorphosed, steeply tilted Precambrian rocks form most of the cores of ranges in Colorado and Wyoming. The Precambrian of the ranges in Wyoming are predominately a complex of paragneiss and orthogneiss. These rocks are truncated to the south by a northeast trending shear zone (Mullen Creek - Nash Fork Shear Zone) south of which is a metamorphic complex (paragneiss) forming the basement of the Southern Rocky Mountains. Embedded in this complex and covering over half of the exposed Precambrian is an array of granitic plutonic rocks (igneous intrusions).

During Cretaceous time a broad seaway extended north across the continent from the Gulf of Mexico to the Arctic Ocean, along the eastern side of the

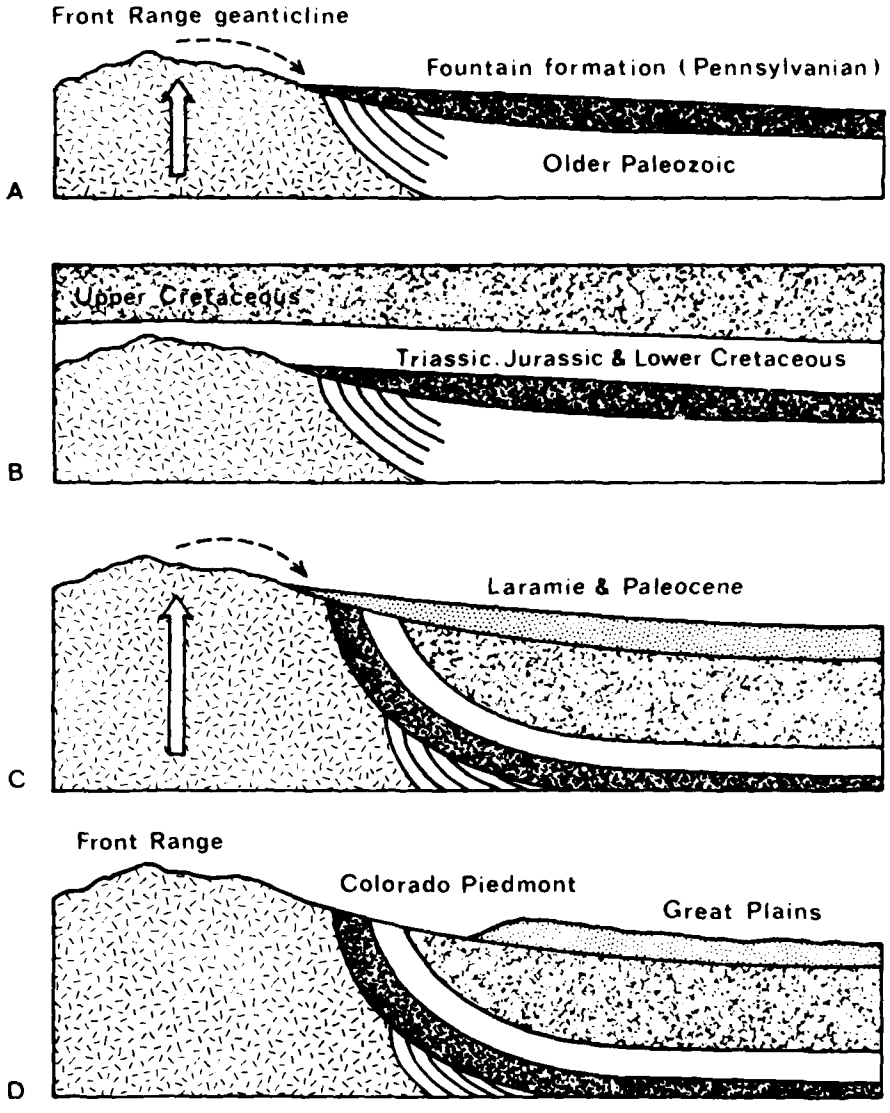

Figure 2-2. Sections illustrating structural evolution of the Front Range of Colorado (from King (1977)).

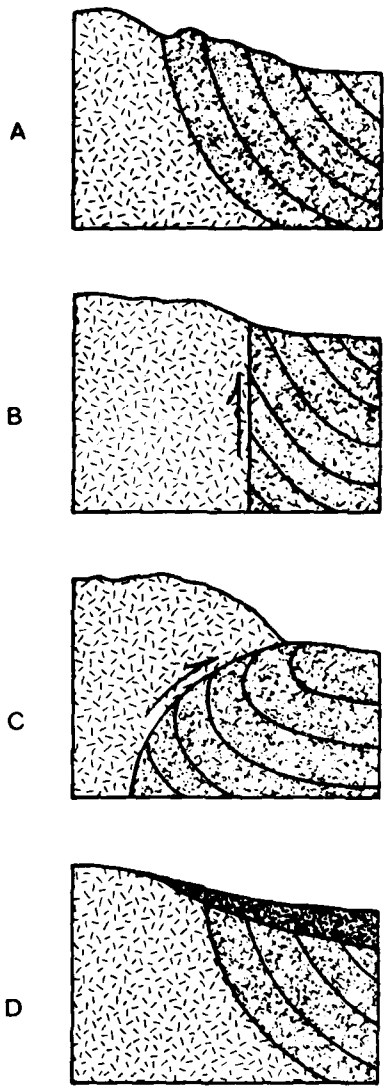

Figure 2-3. Sketches illustrating structural features found along uplifts in the Central and Southern Rocky Mountains (from King (1977)).

Cordilleran region from central Utah to Kansas, Iowa and Minnesota. In Kansas the Cretaceous deposits laid down in the seaway are no more than a kilometer thick, beginning with a sandstone, the Dakota, overlain by interbedded limestone and Niobrara Chalk below and the Pierre Shale above. Further west, near the front of the Rocky Mountains, the deposits have thickened to 3 kilometers, most of the incrase due to shales.

Overlying the main body of the earlier Cretaceous deposits are continental (as opposed to marine) and coal bearing deposits of latest Cretaceous age. These have a different pattern from the widespread earlier deposits and occur in local basins such as the Denver, Powder River and Williston Basins, indicated in Figure 2-1. The latest Cretaceous deposits were laid while the ranges about them were uplifted, during the Laramide orogeny. The ranges did not project in their present form but instead eroded as they were uplifted, shedding detritus into the basins (see Figure 2-2c).

2.2 The Denver Basin

The Denver Basin is a shallow, sediment filled depression between the front ranges of the Southern Rocky Mountains and the Great Plains. A structural contour map is illustrated in Figure 2-4. The axis of the basin lies on a line between Cheyenne, Wyoming and Denver, Colorado. West of the axis the basement has a moderate to steep dip (5^{o} to 10^{o}+) while to the east the dip is very shallow ($\leq .5^{o}$). The upper Denver Basin (Julesburg Basin) is bounded to the west by the Front and Laramie Ranges, to the northwest by the Hartville Uplift, and to the northeast by the Chadron Arch. The area geology and tectonics have been studied intensively because it is one of the oldest petroleum producing provinces on the continent and still holds promise of additional reserves. The Cretaceous reservoirs are the most important, followed by

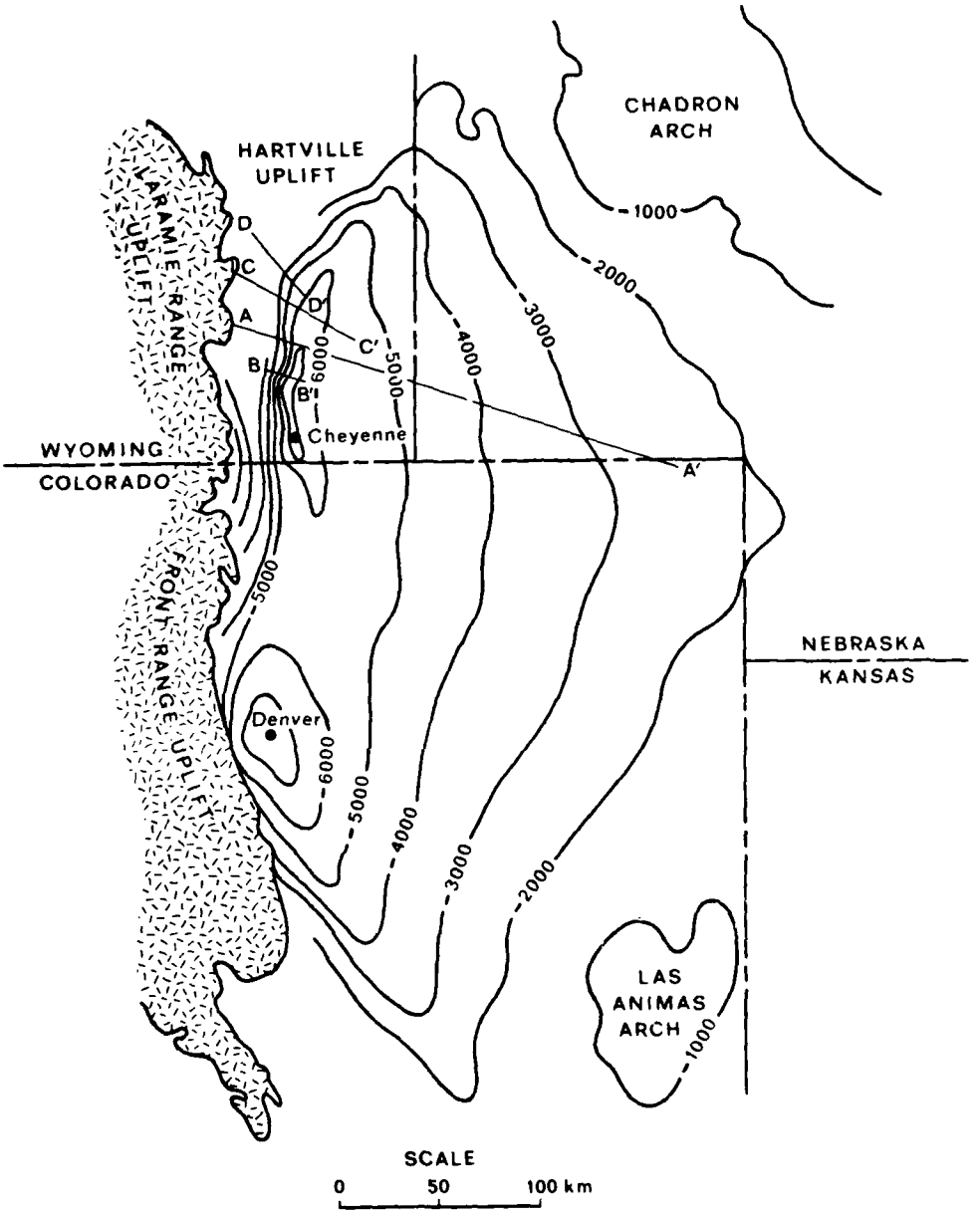

Figure 2-4. Approximate structural contour map of pre-Mississippian rocks in the Denver Basin. Contours are in feet below sea level (in part from Matuszczak (1976)).

accumulations in older rock (see Cram (1971)). Additionally the Tertiary deposits are an important source of ground water and numerous water resource studies have been done (see Rapp, et al. (1957)).

Structure surrounding the upper Denver Basin will be described briefly (see Anderman and Ackman (1963)). The mountain flank structure north from the Wyoming-Colorado border along the Laramie Range is a series of high angle thrust (reverse) faults continuing to the northeast trending fault zone on the southeast flank of the Hartville uplift (see Figure 2-1). The Hartville uplift is a doubly plunging structural high extending northeast from the Laramie Mountains to the southwest flank of the Black Hills and separates the Powder River and Denver Basins. To the northeast is the Chadron Arch (Chadron-Cambridge), a major structural feature trending northeast-southwest from the Black Hills to the central Kansas uplift.

A more detailed discussion of the faulting along the flank of the Hartville uplift is provided by Droullard (1963). During Miocene and Pliocene time additional uplifting of the Laramie Range, including the Goshen Hole area, Figure 1-1, occurred. When compression ceased, the northwest flank of the Goshen uplift collapsed forming the fault system indicated on the tectonic map, principally the Whalen and Wheatland faults of the Richeau-Jay Em fault zone. The Whalen fault has a net vertical displacement of 1.5 kilometers in Paleozoic rocks. It is a thrust fault in the Cretaceous and older rocks and a normal fault with 250 meters of displacement in Tertiary deposits.

Stratigraphy in the Denver Basin has been described in great detail in the geologic literature. An extensive catalog and description of formations is included in Bolyard and Katich (1963). Anderman and Ackman (1963) present a structural contour map of the Denver Basin based on all wells which bottomed in Mississippian or older rocks. Combining this data with isopach (thickness)

maps of the major formations provides a model of the Denver Basin deposits. Using formation thickness data in Volk (1971), a topographic map and the above structural contour map yield the cross section in Figure 2-5. This is section AA' in Figure 2-4 which is alligned with and bisects Wing V.

The Mississippian rocks, predominantly limestone, are absent in the northern Denver Basin and the Pennsylvanian rocks, chiefly sandstone, lie uncomformably on the Precambrian basement. The Permian, composed of sandstone and limestone is next, followed by the Triassic and Jurassic sandstones. The Cretaceous rocks are predominantly shales (Pierre Shale) with sandstone. In the above rocks sandstone is the principal reservoir rock for petroleum with some fracture reservoirs in the Pierre Shale and other Cretaceous rocks. Note that this description of rock type is merely indicative, and variability is the rule.

Additional cross sections near the flank of the Laramie Range are shown in Figure 2-6. Locations correspond to sections through the westernmost flights of Wing V and approximate locations are marked in Figure 2-4. Maximum dip is in the range of 5^{o} to 10^{o} for the cases shown, however depending on location dip can be much higher. Details of the flank structure are given in the structural contour map of Anderman and Ackman (1963).

The Tertiary deposits overlying the Cretaceous have been discussed in numerous papers. Their areal extent is most readily seen on the geologic map of the United States compiled by King and Beikman (1974). Figure 2-7 is redrawn from this map and shows the relative position of Wing V Flights. The bulk of Tertiary sediments were derived from erosion of the Front and Laramie Ranges and older flank sediments. Paleocene and Eocene sediments are absent so the oldest is the Oligocene (White River Group) followed by the Miocene (Arikaree) and Pliocene (Ogallala). A discussion with photographs can be

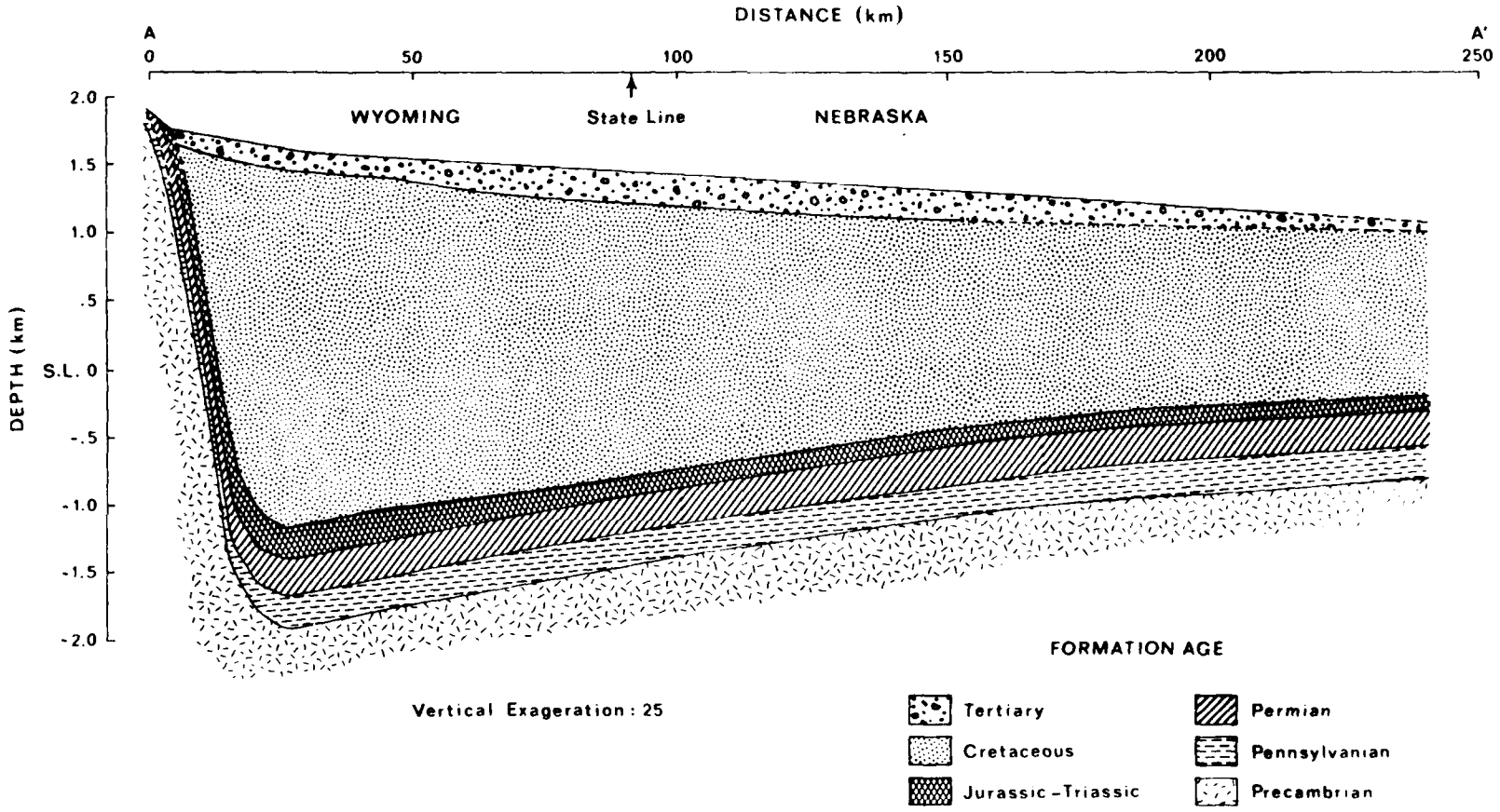

Figure 2-5. Section AA' of Figure 2-4 illustrating formation thickness in the Denver Basin on a line bisecting Wing V.

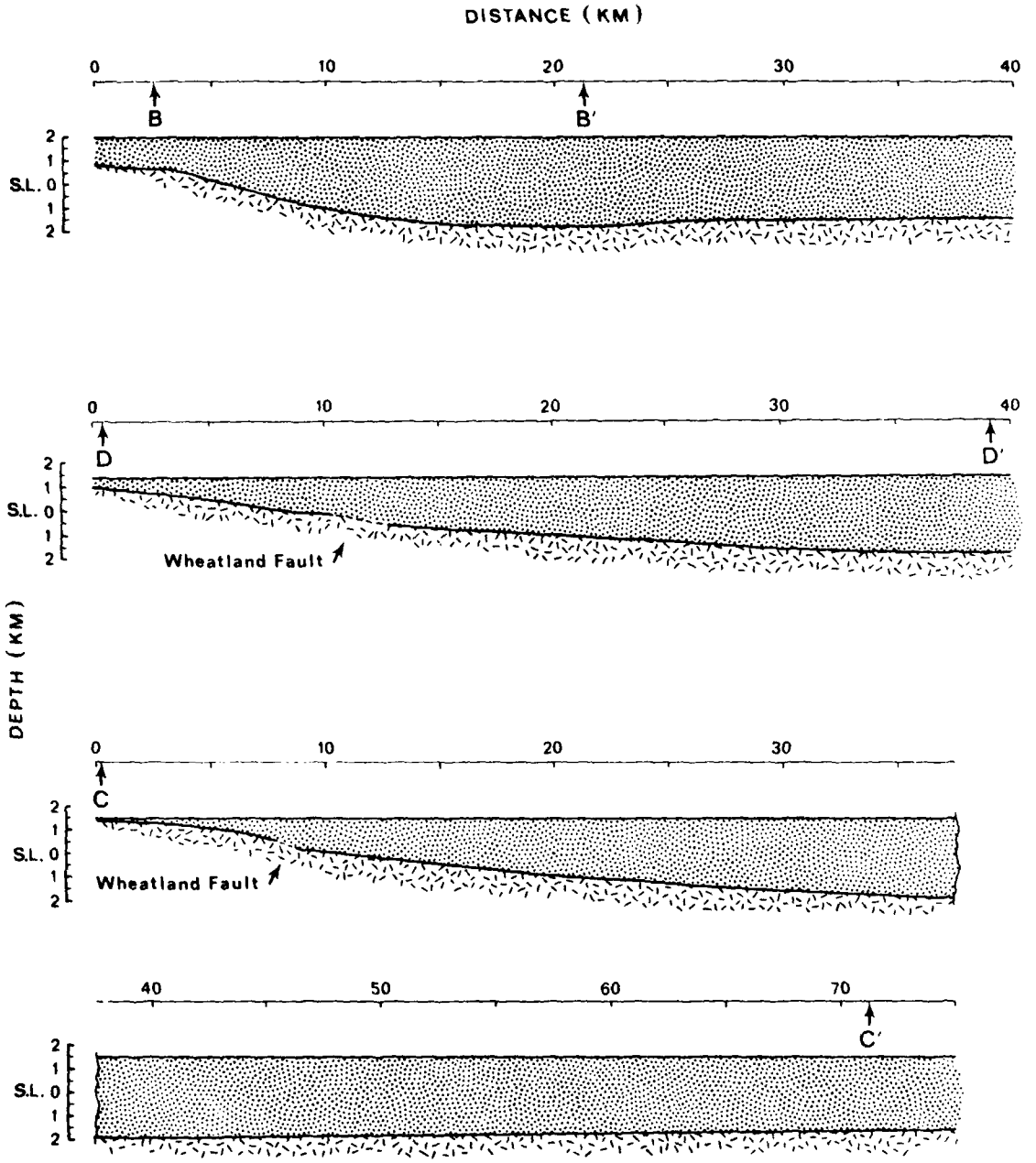

Figure 2-6. Sections in Figure 2-4 illustrating Denver Basin structure on the Laramie Range east flank.

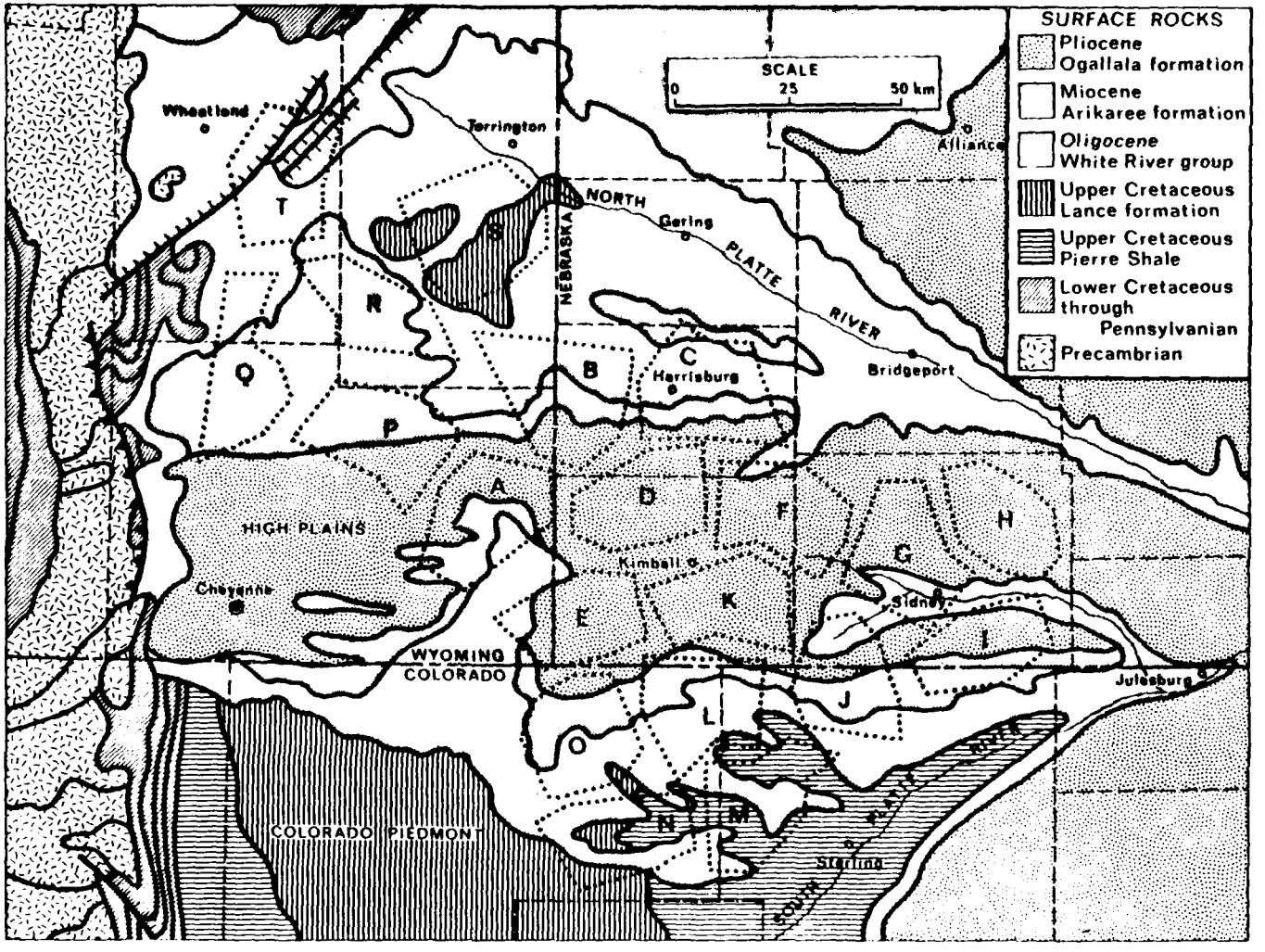

Figure 2-7. Distribution of Tertiary and older surface rocks in the tri-state area (from King and Beikman (1974)).

found in Moore (1963). The topography of Cretaceous sediments underlying the Tertiary is probably much like the Colorado Piedmont of today, i.e. a dissected irregular plane, predominantly shale, as described by Harris (1963).

The Oligocene White River Group is composed of the older Chadron member underlying the Brule member. These rocks were deposited on an erosional surface and were eroded in turn, thus total thickness may vary from 0 to 200 meters over short distances. The Chadron formation is highly variable consisting of siltstones, sandstones and conglomerates with thickness up to 50 meters. Above the Chadron are massive clays and siltstones making up the Brule formation, with thickness from 0 to 150 meters. The Brule is hard and cut by fractured zones, fissures and faults. It weathers into a badland topography but when protected by resistent younger beds forms steep cliffs like the Goshen Hole escarpment.

Miocene sediments are referred to here as the Arikaree. There is some confusion in the literature as to a consistent designation, but these rocks are for the most part siltstones and volcanic ash with a maximum thickness of 25 meters. A thin layer of Arikaree appears to form an effective cap rock for the Brule along escarpments.

Capping the High Plains is a series of sandstones, conglomerates, siltstones and limestones of Pliocene age which are included in the Ogallala formation. Thickness varies from 0 to 90 meters. Grain size decreases eastward from the mountains. Near the Laramie Range the Ogallala is a poorly sorted conglomerate with boulders a meter or more in diameter. In eastern Wyoming it is a well sorted sandstone and siltstone. The conglomerate contains fragments of nearly every rock type in the Laramie Range.

By the end of the Pliocene epoch a vast sheet of alluvium extended from the front ranges east onto the Great Plains. Only a remnant of the blanket has

survived the severe dissection that characterized Quaternary time. This is clearly seen in Figure 2-7. The major remnant is the Gangplank of the High Plains where the mountains-plains surface is continuous. Historically the Gangplank provided a natural route over the Laramie Range. Isopach maps of Pliocene, Miocene and Oligocene rocks in the tri-state area have been compiled by Denson and Bergendahl (1961). A section schematic through Wing V is shown in Figure 2-8a along with a sketch of a local section in Banner County, Nebraska illustrating the variability of formation thicknesses, Figure 2-8b.

The Tertiary deposits exhibit variable degrees of cementation from carbonates and to a lesser extent silica. These cemented areas are more resistent to erosion than the softer areas and form well defined ledges and escarpments. These features can be seen quite clearly in Landsat imagery of the region provided by Smith, et al. (1980). The escarpments are most prominent along Wildcat Ridge and the southwestern Goshen Hole area indicated in Figure 1-1, and provide up to 200 meters of vertical relief in the Arikaree and White River formations. Farther south the escarpments are found on either side of the Ogallala forming the Gangplank to the Laramie Range. On the north side the vertical relief is probably no more than 90 meters while to the south it may be on the order of 60 meters. Lesser relief features are common due to stream dissection, and Landsat pictures indicate a correlation with the distribution of Tertiary sediments shown in Figure 2-7.

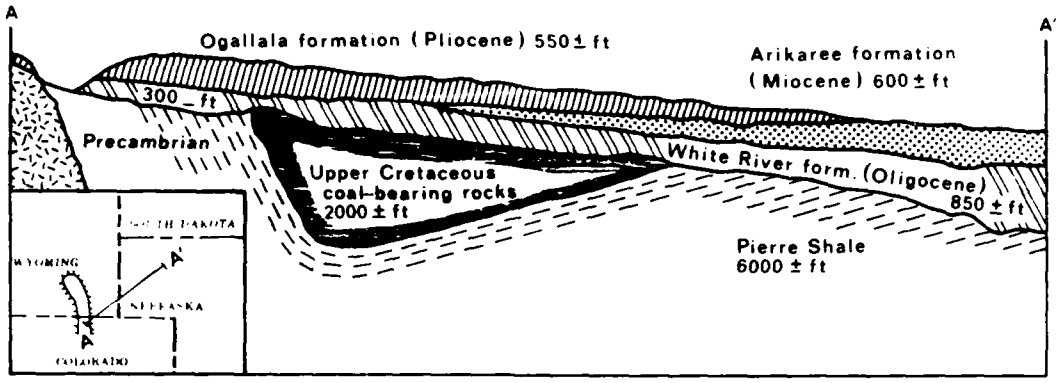

Figure 2-8a. Schematic showing stratigraphic relations of Tertiary rock on a section through Wing V (from Denson and Bergendahl (1961)).

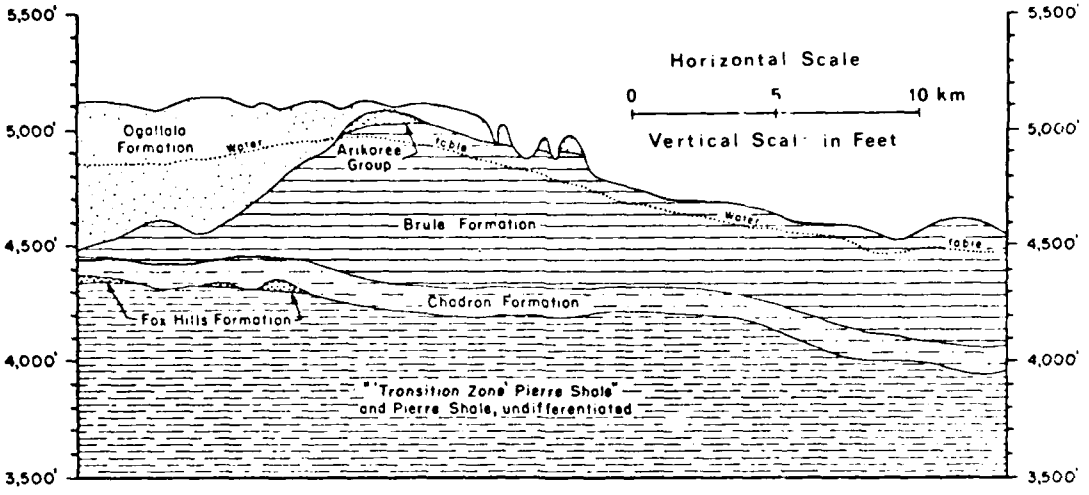

Figure 2-8b. A north-south section through Flight B illustrating topography and nonuniform thickness of Tertiary deposits (from Smith and Souders (1975)).

SECTION 3

GROUND MOTIONS FROM THE POCATELLO VALLEY AND ST. ELIAS EVENTS

Ground motions at Wing V from the Pocatello Valley and St. Elias earthquakes are not known with any certainty. The synthetic seismograms calculated by Rodi, et al. (1979) for the Pocatello Valley event provide the only available estimate of ground motion within the wing. However, seismograms are available from the seismograph station at Golden, Colorado, about 200 km southwest of the wing, within the Denver Basin. These records will be discussed here to compare and contrast motions from the two events. Observations have been overshadowed by the calculational approach in most considerations of Wing V anomalies. Recognizing that seismic alarms will probably be triggered by future earthquakes, the collection and interpretation of relevant seismograms is an important complement to ground motion calculations.

3.1 The St. Elias Earthquake

The St. Elias earthquake occurred on February 28, 1979 in southeast Alaska near 60.6°N, 141.6°W with a surface wave magnitude, $M_S = 7.1$ reported. The source was shallow, averaging about 11 km and the earthquke ruptured approximately 60 km to the southeast in three subevents with individual ruptures estimated at 12, 27 and 17 km , Boatwright (1980). The propagation path from southeast Alaska to the Wing V area was entirely continental, along the Cordilleran System, the mountain belt of western North America. Most of the path followed the demarcation between mountains and interior continental plains. Distance from the epicenter to Wing V was about 3350 km ($\Delta \cong 30°$) and the azimuth was approximately 38° northwest from Wing V.

To infer the nature of ground shaking at Wing V, seismograms recorded nearby, preferably on bedrock are most useful. The closest seismological observatory with accessable records is the Golden, Colorado WWSSN station (GOL) operated by the Colorado School of Mines. It is located on bedrock near the east flank of the Laramie Range, about 165 km south of Cheyenne, Wyoming. Seismograph recordings of the St. Elias event include horizontal Wood-Anderson records, and all components of short period and long period WWSSN (World Wide Standardized Seismograph Network) records. The Wood-Anderson seismograms are reproduced in Figure 3-1. These have been reconstructed (dashed lines) to allow easier interpretation by the reader.

The first observable P arrival is marked on the N-S component while the S arrival is more readily identified on the E-W component. Origin time of the earthquake is given as $21^h\ 27^m\ 7^s$ UTC (Universal Coordinated Time), Lahr (1980), giving a P transit of $6^m\ 17^s$ and an S transit of $11^m\ 22^s$. Distance from the epicenter to GOL is about 3415 km ($\Delta \simeq 31^o$), and as a verification travel time tables in Richter (1958) yield $6^m\ 20^s$ and $11^m\ 20^s$ for P and S respectively. This assumes a shallow focus at 25 km depth. The most prominent phases on the records are surface wave arrivals at $43^m\ 12^s$ (where the reconstruction begins) in both components, and at 46^m in the N-S component. The $43^m\ 12^s$ arrival has a predominant period of about 4.5 seconds and an observed group velocity of 3.54 km/sec (i.e. distance/travel time). The 46^m arrival has a period of 12 seconds and a group velocity of 3.01 km/sec. A longer period surface wave is seen in the E-W component at $42^m\ 12^s$. This has a period of 35 seconds and a group velocity of 3.77 km/sec.

Surface wave phases can generally be identified on the basis of period, group velocity, polarization and orbital motion. For example, the relatively

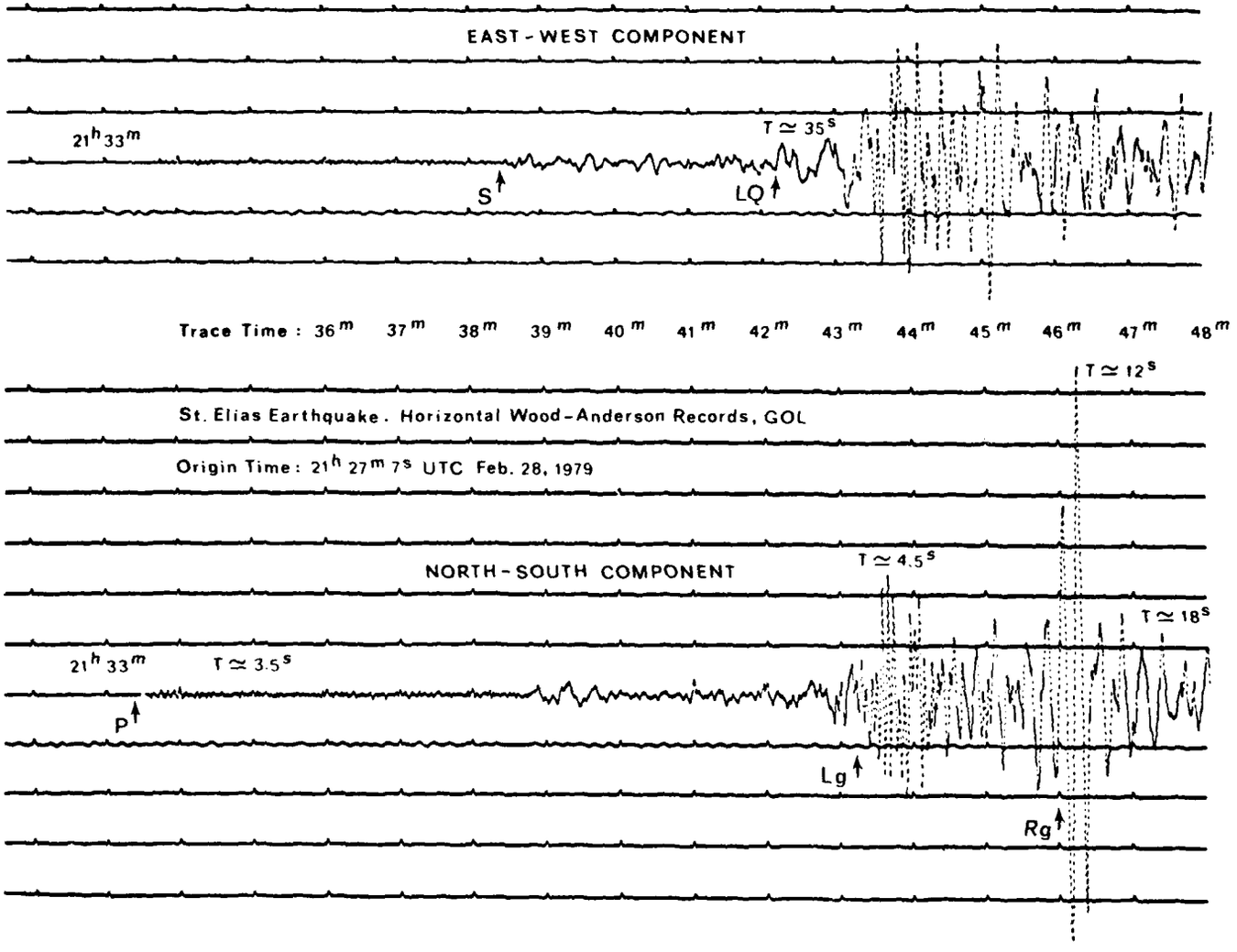

Figure 3-1. Horizontal Wood-Anderson seismograms of the 1979 St. Elias earthquake recorded at Golden, Colorado.

short period and group velocity of the $43^m\ 12^s$ arrival identify it as Lg, a phase which is routinely observed on strictly continental paths over North America. Lg is generally regarded as a complex of higher mode surface waves propagating within a crustal waveguide at nearly the granitic shear velocity of 3.51 km/sec or so (Ewing, et al. (1958)). Unlike fundamental mode surface waves, where the highest amplitudes occur at or near the surface, the Lg phase carries most of its energy deeper within the crust. Consequently it is less disturbed by surface structure and is often the dominant phase on a seismogram.

The highest amplitude surface wave arrival, at 46^m in the N-S record, is a Rayleigh wave. This follows from observed dispersion curves for continental Rayleigh waves shown in Figure 3-2a, from Ewing, et al. (1958). One of the data points, a seismogram from a March 1, 1955 Yukon aftershock recorded at Palisades, New York, is shown in Figure 3-2b from the same reference. Comparing the 1979 St. Elias N-S record to the 1955 Yukon aftershock N-S record shows a striking similarity. The Lg phase from the 1955 event has a period of about 4 seconds (compare to 4.5 seconds for the 1979 event) and the Rayleigh wave, designated Rg, has an initial 8 second period (compare to 12 seconds). Rg was identified at Palisades by orbital motion and group velocity. The Rg phase in Figure 3-2b is also notable because it exhibits reverse dispersion, where shorter periods lead longer periods in contrast to normal dispersion. The travel path from the Yukon epicenter to Palisades is about 4250 km based on travel time. Similar phasing between Lg and Rg for the two events is due to the greater distance in combination with a slightly higher group velocity of Rg recorded at Palisades. Referring back to Figure 3-1 note that the E-W component of ground motion from the 1979 event does not show the Rg phase.

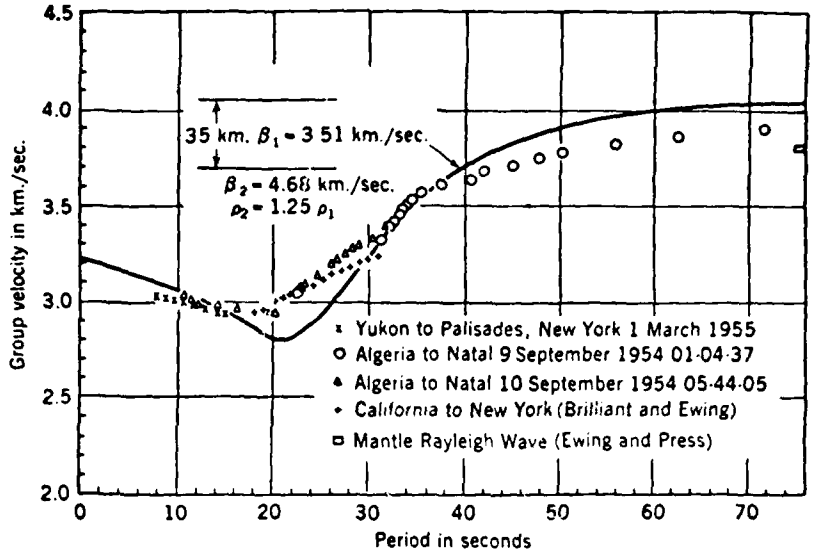

Figure 3-2a. Observed and theoretical dispersion of continental Rayleigh waves (from Ewing, et al. (1958)).

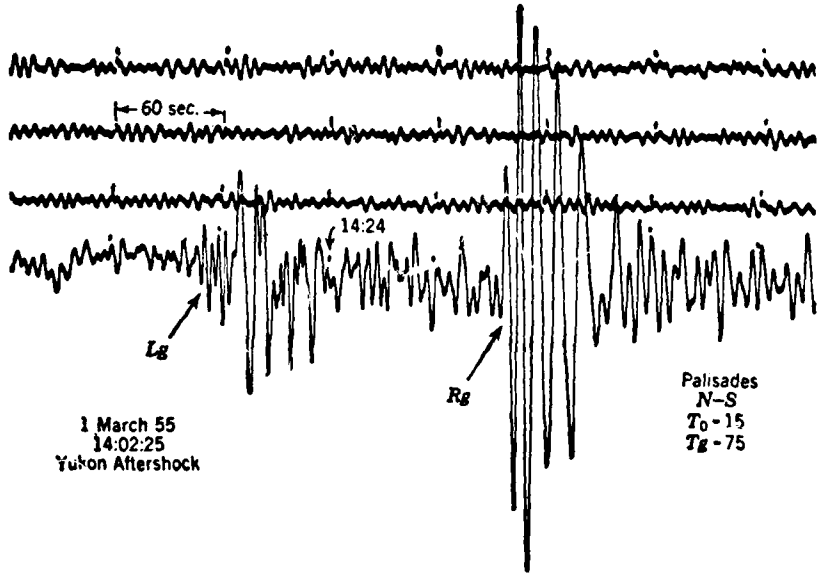

Figure 3-2b. Palisades NS seismogram of Lg and Rg waves from Yukon aftershock of March 1, 1955 (from Ewing, et al. (1958)).

This is consistent with the polarization of Rayleigh wave ground motion although some E-W component would be expected considering that the azimuth at GOL is 38^{o} northwest.

Longer period surface waves can also be identified. Figure 3-3 shows a composite of dispersion curves for Love and Rayleigh waves. The 35 second E-W arrival at $42^{m}\ 12^{s}$ fits the curve for continental Love waves and is designated LQ. The 18 second motion in the N-S component probably corresponds to a continental Rayleigh wave arriving close to the Rg Rayleigh wave.

Body waves are much weaker phases than surface waves at distances considered here, 30^{o} or so. This is primarily due to the three dimensional spread of body wavefronts as compared to the two dimensional spread of surface waves. The Wood-Anderson and short period WWSSN seismograms from GOL are used here to examine body wave arrivals. Between the P and S arrivals marked on the Wood-Anderson seismograms the travel time curves (e.g. the Jeffreys-Bullen tables, Bolt (1976)) show multiple mantle reflection (PP,PPP) and a core reflection (P_cP) of longitudinal (P) motion. Between S and the surface waves are additional transverse (S) body wave arrivals (P_cS, SS, etc.). Rather than attempt an identification of these phases a brief discussion of the period and amplitude history will be given.

Counting peaks on the Wood-Anderson seismogram between P and S yields an average period of body wave motion of 3.5 seconds. A corresponding section of the short period WWSSN seismogram (not pictured here) indicates significant motion down to 1 second but because of excessive gain and the superposition of later arrivals it is difficult to determine a predominate period or range of periods. The situation is somewhat clearer after the S arrival where the spacing of peaks indicate periods in the range 3 to 6 seconds. At the Lg

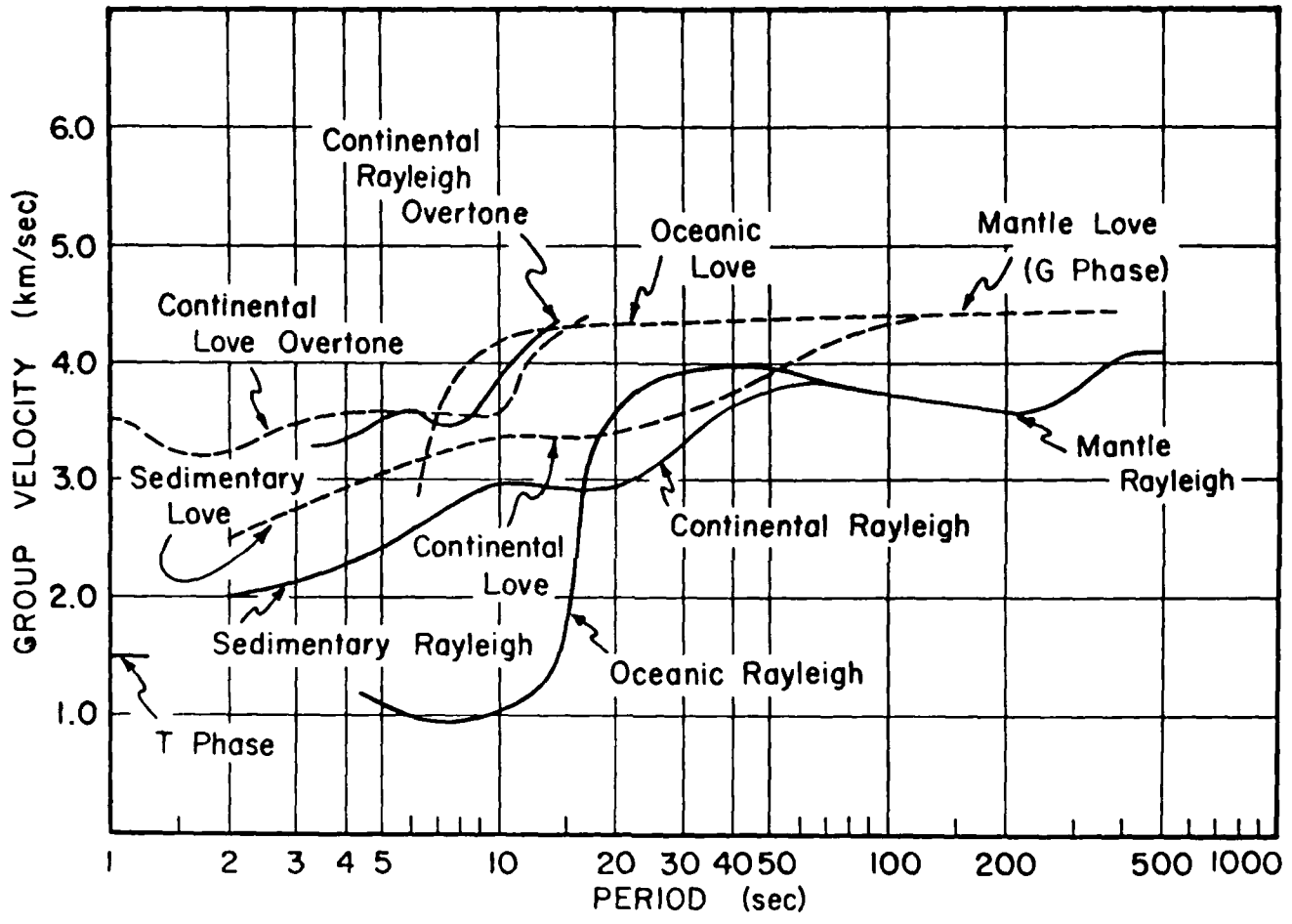

Figure 3-3. A composite of surface wave dispersion curves (from Manual of Seismological Observatory Practice (1979)).

arrival, periods in the range 2 to 3 seconds appear to be superposed on the 4.5 second Lg motion.

Few strong conclusions can be drawn from the above short period body wave observations. Suffice it to say that overall, body wave arrivals with periods in the range of interest, 2 to 6 seconds are present in the seismograms. Due to excessive gain no amplitudes can be measured with confidence from the short period seismograms, however the N-S component of Wood-Anderson record, Figure 3-1 indicates a peak P wave motion of .1 millimeter at a period of 4.8 seconds.

3.2 The Pocatello Valley Earthquake

The Pocatello Valley earthquake sequence of late March and April of 1975 was centered near the Idaho-Utah border at 42.1°N, 112.5°W. The sequence included a magnitude 4.2 (M_L) foreshock, a 6.0 mainshock, one 4.7 and two 3.8 aftershocks and over 50 lesser events greater than 3.0. The sequence is described in detail by Arabasz, et al. (1980) who attributed the events to irregular Basin and Range graben subsidence within the Pocatello Valley. The propagation path from Pocatello Valley to the Wing V area was nearly due east across the lower third of Wyoming, a distance of about 700 kilometers. The path included 180 km of the Idaho-Wyoming Overthrust Belt, 350 km of the Green River Basin of Wyoming and about 170 km of the Laramie Range and the Denver Basin. The tectonic map, Figure 2-1 shows these features and surrounding structure. The epicenter is marked by a star on the border above the Great Salt Lake.

The Pocatello Valley earthquake was a local event in contrast to the distant St. Elias event. Consequently the character of ground motion at Wing V should differ. This is clearly seen in a comparison of time scales for the

synthetic Pocatello Valley seismograms in Figure 1-5 and the Wood-Anderson record of the St. Elias event in Figure 3-1.

Long and short period WWSSN seismograms recorded at the Golden, Colorado station will be used here to infer general features of ground motion at Wing V. The epicentral distance to GOL is 650 km and the azimuth is 66^{o} east of south. The main Pocatello Valley event, $M_L = 6.0$, at $2^h\ 31^m\ 6^s$, March 28, drove the long and short period records off scale at GOL for 4 to 5 minutes. Predominant periods could not be determined. However the lesser events provided good records. The short period E-W seismogram of the first 3.8 magnitude aftershock is shown in Figure 3-4. The sequence of arrivals seen here is common to the 4.2 foreshock and the 4.7 aftershock. The first arrival, at $1^m\ 32^s$ after the origin time of $16^h\ 15^m\ 6^s$, March 28 is the P_n phase, a low amplitude refracted wave from the Moho discontinuity. This is followed by the higher amplitude P_g phase, a direct wave propagated through the granitic crust. Another arrival associated with intermediate layers in the crust may be present between P_n and P_g. The next obvious arrival is S_g, the direct shear wave through the crust. Faster refracted phases preceed this arrival but are not obvious on the record. Also Love waves including Lg may be superposed on S_g but no distinctions are obvious. The time between P_g and S_g is $1^m\ 16^s$. The spacing of peaks on the record indicate periods on the order of 1 second. The corresponding long period record shows no evidence of this event.

The only significant long period record at GOL, besides the mainshock, is the magnitude 4.7 aftershock, shown in Figure 3-5. The origin time is $13^h\ 1^m\ 20^s$, March 29. The long period arrival at $13^h\ 5^m$ has a travel time of $3^m\ 40^s$. The Z and E-W components have the higher amplitudes. Periods start

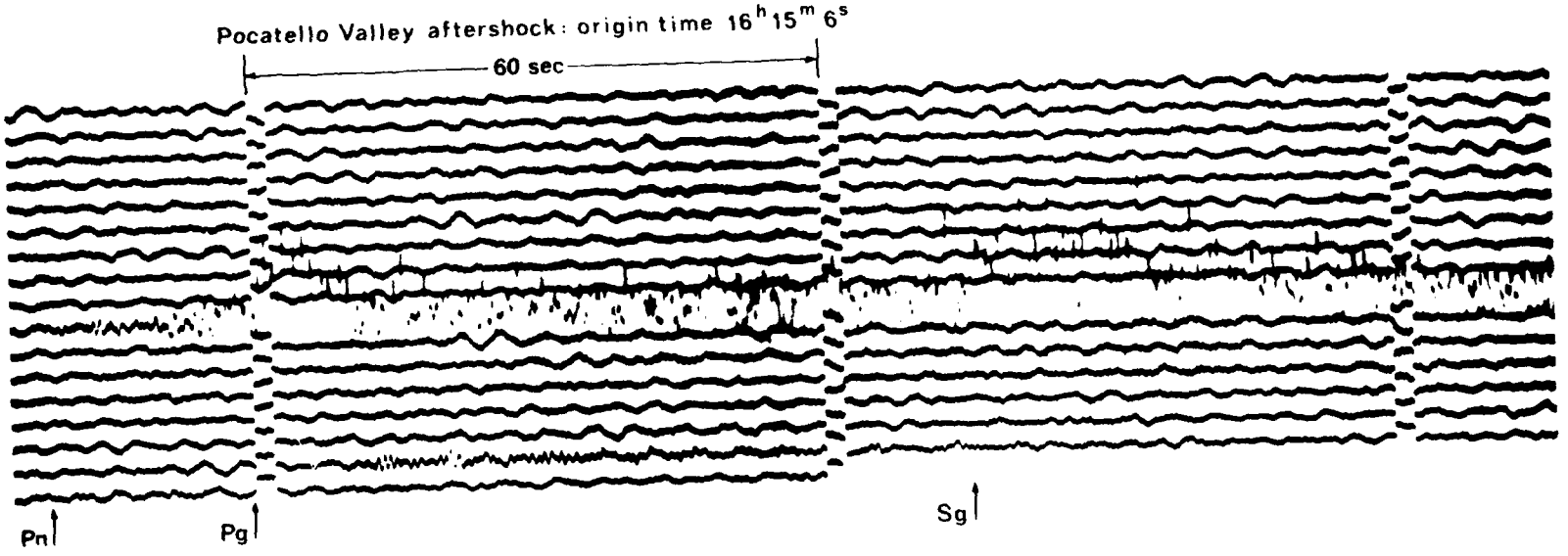

Figure 3-4. Short period E-W WWSSN seismogram of a M_L = 3.8 March 28, 1975 Pocatello Valley aftershock recorded at Golden, Colorado. First minute mark on event trace is $16^h\ 17^m$.

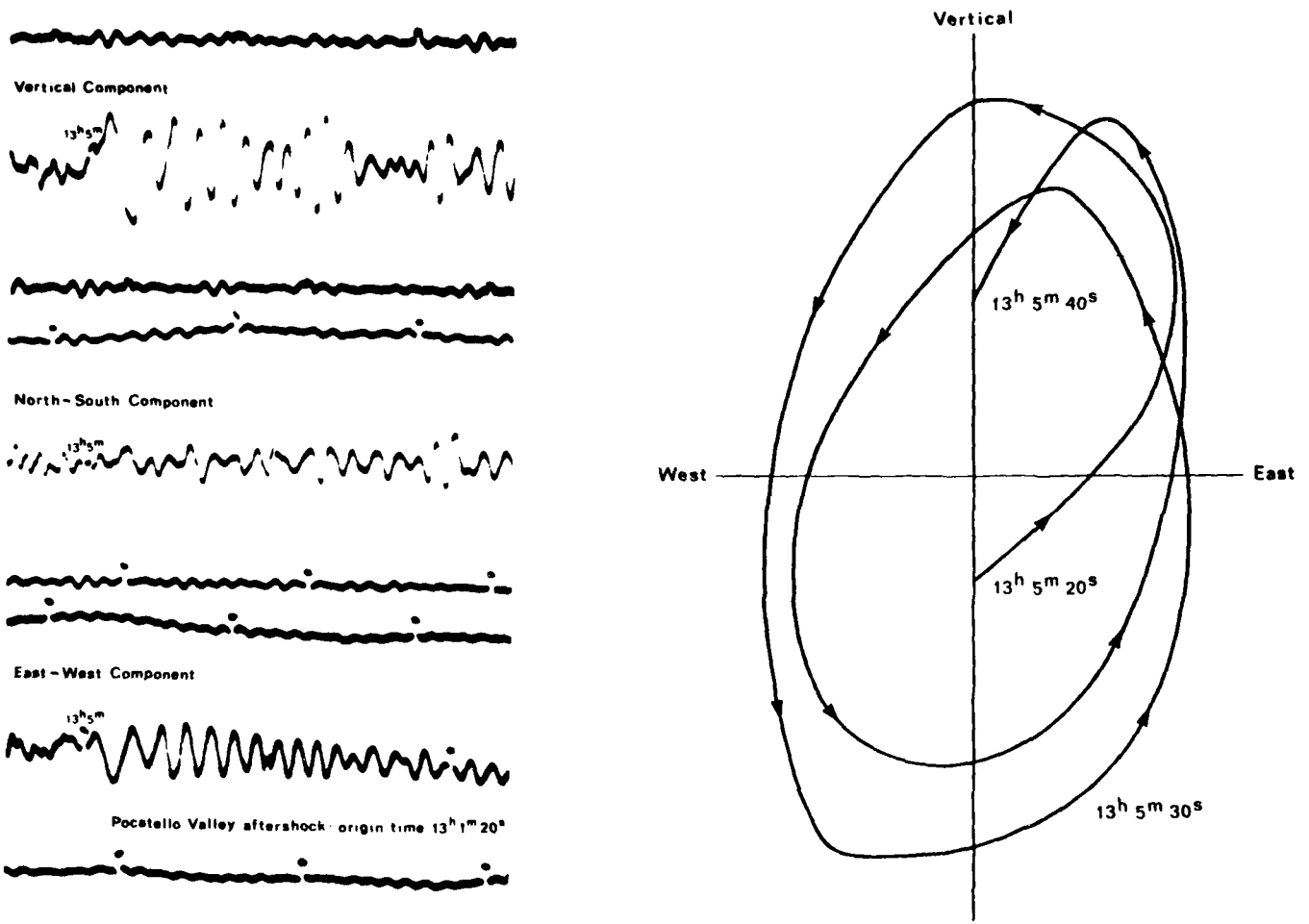

Figure 3-5. Long period WWSSN seismograms (left) of a M_L = 4.7, March 29, 1975 Pocatello Valley aftershock recorded at Golden, Colorado. The retrograde elliptical partical motion on the right identifies this phase as a Rayleigh wave.

at 12 seconds and after $1^m\ 30^s$ are down to 5 seconds. This behavior, the normal dispersion and the particle motion in the Z and E-W directions, suggests that this phase is a Rayleigh wave. Group velocity of the 12 second period is found to be 2.95 km/sec, very close to the measured values in Figure 3-2a for continental Rayleigh waves. Apparently the smaller shocks do not excite surface waves very efficiently; however, the 4.7 aftershock is seen to be an effective source and the main shock is no doubt a very rich source.

Examining the synthetic seismograms in Figure 1-5 shows that these observations at GOL are consistent with calculated body and surface wave arrivals at Wing V. The synthetics are for an epicentral distance of 680 km compared to 650 km at GOL. The first arrival in the synthetics is 95 seconds after the event, followed by higher amplitude P phases which precede the higher amplitude S phases by about 85 seconds. Depending on the near surface crustal model chosen, Rayleigh wave arrivals are between 210 and 240 seconds in the synthetics, compared to 220 seconds from the long period record of the 4.7 aftershock. Allowing for the 30 km difference in epicentral distance would give an observed Rayleigh wave arrival at 230 seconds. This arrival time and the dispersed nature of the observed Rayleigh wave suggests that the crustal model with a surface sedimentary layer is more representative of the travel path from Pocatello Valley to Wing V.

A cross section through the travel path in Wyoming is shown in Figure 3-6 . This was compiled from a tectonic map of North America, King (1969) and a state topographic map. It shows a substantial sedimentary cover over Precambrian basement which thins to the east, terminating on the west flank of the Laramie Range. The section is located near a line connecting the Pocatello Valley epicenter and a point 50 km north of Cheyenne, Wyoming on the tectonic

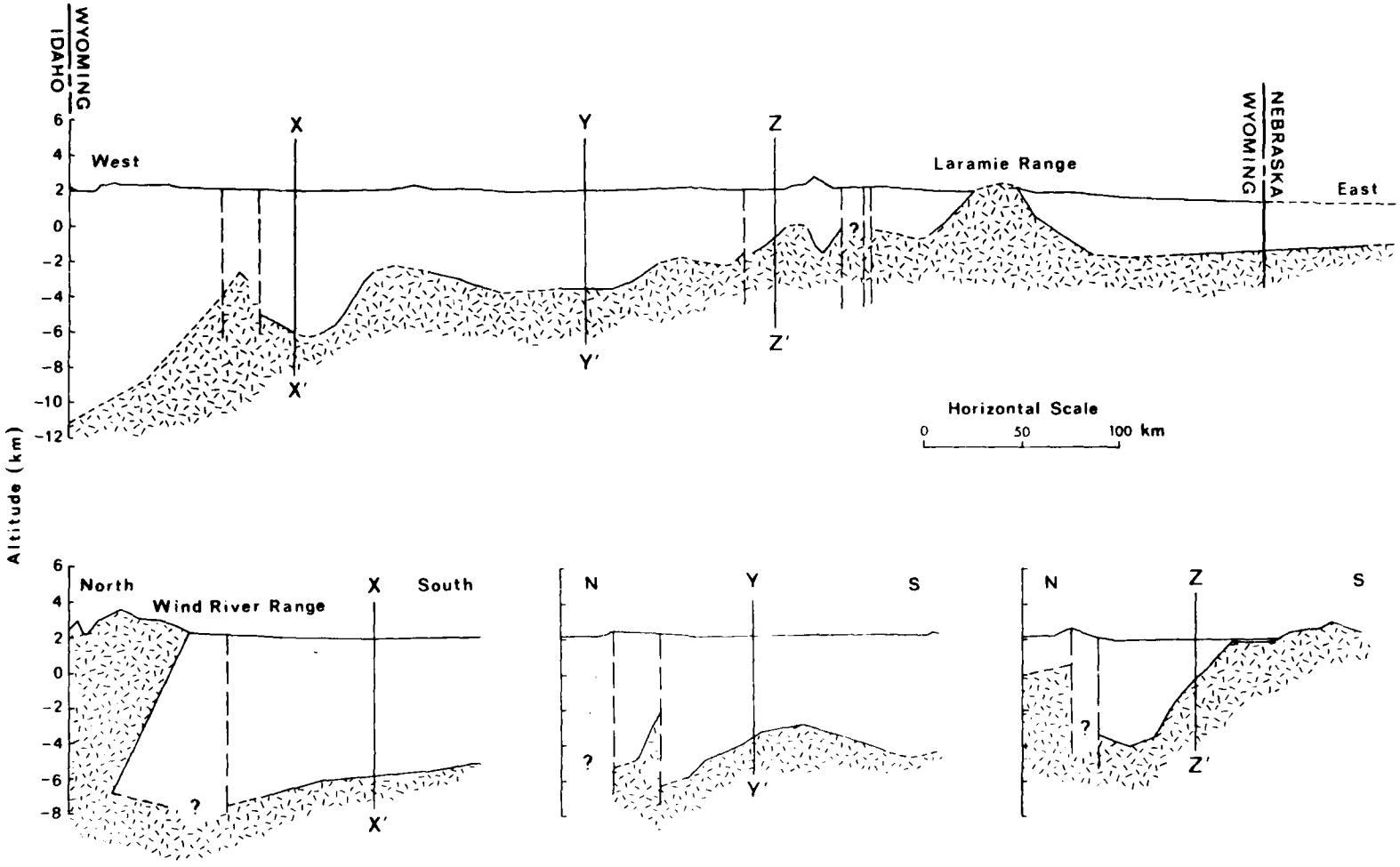

Figure 3-6. A cross-section through Wyoming aligned with the propagation path from the Pocatello Valley epicenter to Wing V.

map, Figure 2-1. The behavior of surface waves propagating across such structures is unknown, both because the path includes sections with significant updip and the presence of basement uplifts north and south of the path may channel surface wave energy. Shorter period surface waves have wavelengths comparable to the sediment thickness and therefore interact more readily with the irregular path structure than would longer period surface waves. Also, the updipping sediment cover on the west flank of the Laramie Range would be expected to have a significant effect on shorter period sedimentary surface waves. A quantitative evaluation of these phenomena is the subject of a continuing effort on surface waves in sedimentary basins and will be reported later.

SECTION 4

VELOCITY STRUCTURE IN THE DENVER BASIN

An understanding of surface ground motion over the Denver Basin begins with a realistic seismic velocity model of the basin sediments. Sources of data can include direct, local measurements such as velocity logs of wells, seismic reflection and refraction surveys, laboratory testing of rock samples, etc. Additionally, velocities can be inferred from data collected in similar lithologies (rock types) in other areas, particularly the ubiquitous shales and sandstones. In this section the available data will be described and applied to a generalized velocity model of basin deposits consisting chiefly of shales and sandstones.

4.1 P Wave Models

The most readily available velocity data in the Denver Basin are P wave well logs. These are obtained using a sending and receiving unit (sonde) lowered down the well to measure interval transit time as a function of depth, Telford, et al. (1980). The major limitation in using such logs to estimate seismic velocities is their restricted sampling region around the borehole and the unknown structural disturbance caused by drilling. Nonetheless these velocity logs are a useful source of P wave data in the absence of alternate seismic velocity meausrements. Figure 4-1a shows a collection of velocity functions from five wells within Flights S, R and P in Wyoming (see Figure 1-1), as interpreted by Smith, et al.(1980). Independent spot checks of relevant well logs from Nebraska and Colorado fall within the bounds indicated in the figure.

A determination of velocity functions from well logs on a site by site basis is beyond the scope of this investigation. The question is then, how to

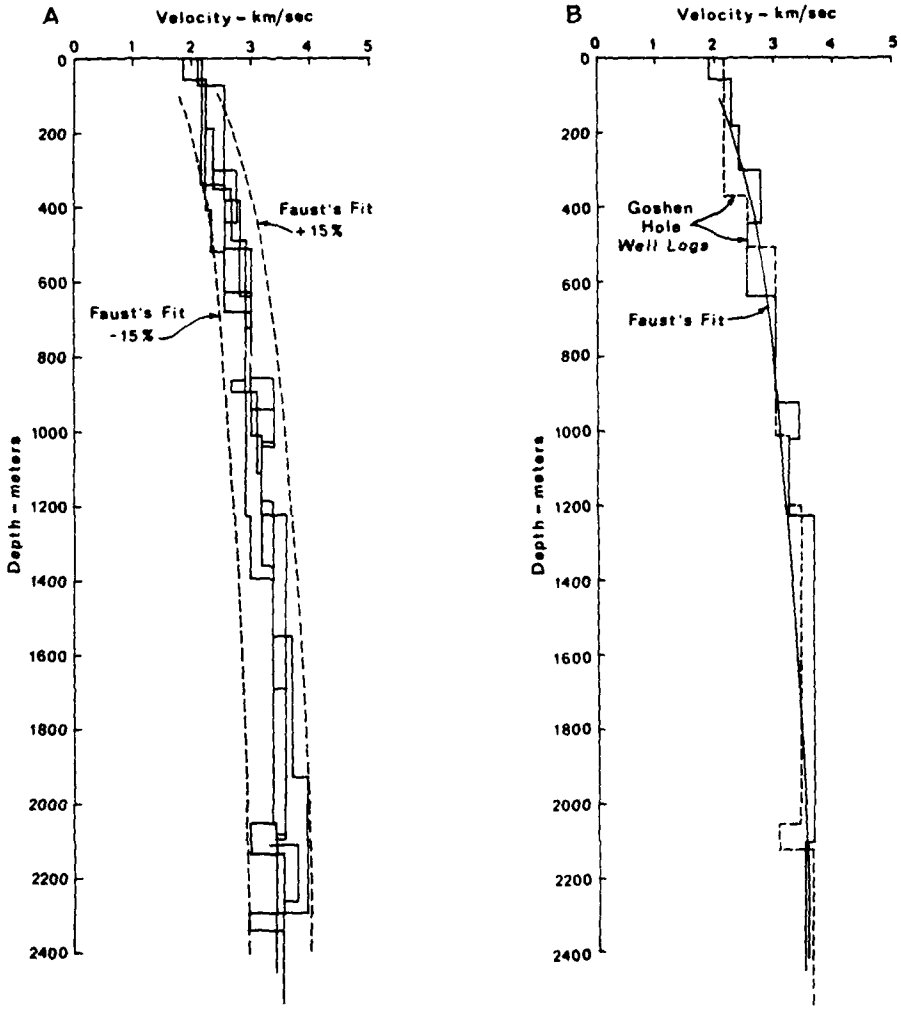

Figure 4-1. A - Velocity function from well logs within Flights S, R and P.
B - Faust's fit of velocity functions in the Goshen Hole (Flight S).

generalize the limited data in Figure 4-1a to the entire Wing V area considering the common lithologies and known formation depths? Similar questions concerning the fullest utilization of well logs have been addressed by a number of researchers over the years. For example, Haskell (1941) explored the relation between depth, lithology and velocity logs in Tertiary sandstones and shales. He found a mean vertical velocity gradient of .464 meters/sec/meter, and that on the average 78% of the gradient is due to overburden, the remainder due to age of the formation. The effect of overburden on shales is smaller than the average, while for sandstones it is larger. A crude comparison can be made with the data in Figure 4-1a where the mean velocity gradient is .43 km/sec/km for the interval between 1 and 2 kilometers depth.

A more extensive and applicable study of the question is found in Faust (1951), where velocity functions were developed for shales and sandstones of Pennsylvanian age and younger. The data used in the study came from over 500 velocity logs in the United States and Canada. Velocity was correlated with depth and age, and interval velocities were plotted as a function of depth for each age group. Log-log plots showed a common slope of 1/6 for all curves indicating that the velocity function could be fit by $AZ^{1/6}$, where Z is depth and A is a constant depending on geologic age. The constants determined by Faust were A(Cretaceous) = 967, A(Jurassic-Triassic) = 1047, A(Permian) = 1063 and A(Pennsylvanian) = 1318 (modified from Faust's to yield velocities in meters/second for Z measured in meters). The range of depths sampled was 300 to 3500 meters and Faust found reasonable agreement outside this range as well. Sandstone velocities were about 100 m/sec greater than shale velocities on the average.

An interesting note regarding Faust's fit of shale and sandstone is that such a relation is theoretically consistent with the theory of elastic waves

through a packing of small spheres, Gassmann (1951). Gassmann examined a porous solid consisting of a hexagonal close packing of equal spheres, with and without a fluid filler, using Hertz's theory of contact. Expressions were developed for the P wave velocity as a function of depth when the packing was stressed by self weight only. The velocity relation was found to be $V = AZ^{1/6}$ where A is a function of Young's modulus, Poisson ratio, sphere and fluid density and the acceleration of gravity. An example was given for granitic spheres with the pore space dry or filled with water. The numerical value determined for A(saturated) was 865, about 10% lower than Faust's value for Cretaceous shale and sandstone. Another significant finding concerned anisotropy. At a depth of 200 meters horizontal velocity was about 16% lower than the vertical velocity for the wet case and the difference increased with depth. No cross-hole tests are available to confirm this in the Denver Basin however some anisotropy should be expected.

To compare Faust's velocity function with available data in the Denver Basin consider the two curves shown in Figure 4-1b inferred from well logs 20 kilometers apart in the Cretaceous section of Flight S in the Goshen Hole area. Taking mean velocity at a depth of two kilometers as the datum gives 3500 m/sec from which A = 987. This is 2% higher than Faust's estimate based on a wide variety of Cretaceous shales and sandstones. The fit is also plotted in Figure 4-1b and is seen to agree fairly well with log inferred velocities to a minimum depth of 50 meters. Above this depth the velocities are too low.

There remains the question of velocity models in the Tertiary section overlying the Cretaceous and older sediments modeled above. A search of non-classified data showed that near surface velocities were determined prior to construction at each of the 200 Wing V silo sites by Porter and

O'Brien (1960) using uphole and refraction surveys. Telford, et al. (1980) describe the techniques. The velocity data is distributed through 20 volumes (one per flight) of Wing V geologic and geophysical reports. A review of the data shows that despite the unconformities and nonuniform thicknesses of the Tertiary strata described in Section 2 there are no notable near surface velocity anomalies below the surface weathered zone (5 - 10 meters deep). Below a depth of 40-50 meters the P wave velocity is on the order of $2 \pm .5$ km/sec. Above this level velocity structure can be classed as slow, moderate or fast, describing a surface layer 20-30 meters thick with velocity around 1000, 1500 or 2000 m/sec respectively. Assigning a numerical value of -1 to slow sites, 0 to moderate sites and + 1 to fast sites and summing over each flight results in the distribution indicated in Figure 4-2. N is the numerical sum at each flight. Referring back to the geologic map, Figure 2-7, a comparision shows that slow, moderate and fast sites correlate with Pliocene, Miocene and Oligocene surface deposits respectively. The correlation is not perfect but it serves to demonstrate that near surface velocities correspond fairly well with near surface geology. Of course many other factors can perturb surface properties including depth to groundwater, soil overburden, cementation, etc. Depth to groundwater is probably the next factor to consider. Groundwater surveys published by the U.S. Geological Survey are a rich source of data. However for the purpose of this investigation suffice it to say that the depth depends on the surface elevation and is generally greater for highland and lesser for lowland. Average water depth is around 40 meters which is on the same order as expected surface relief.

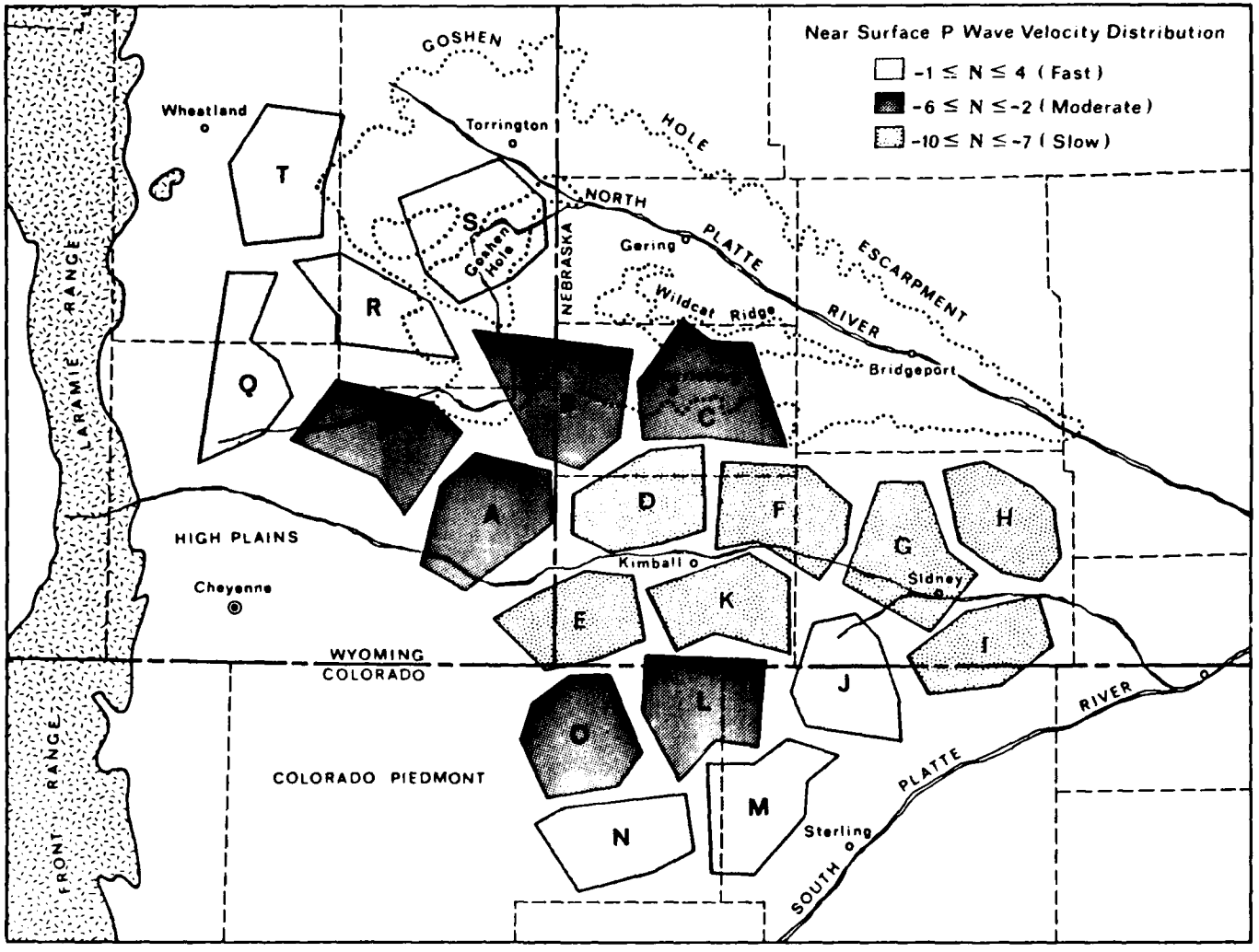

Figure 4-2. Distribution of fast, moderate and slow velocities in near surface rock. See text for description.

4.2 S Wave and Density Models

The above data provide a reasonable model of the P wave velocity function in the Denver Basin deposits. This model is consistent with velocity logs of wells in the area and also with logs in similar lithologies at comparable depth elsewhere in the United States and Canada. However, a complete seismic velocity model must also include S wave velocity and density functions. For this purpose the available data come from laboratory tests of rock samples and empirical relations developed in geophysical exploration.

Geophysical testing of rock samples under laboratory controlled conditions of pressure, saturation, etc. is a valuable source of data, particularly in conjunction with field observation. A timely example is preliminary data provided by Tosaya (1980) on recent laboratory tests of Pierre Shale samples from a South Dakota oil well in Williston Basin sediments. Sediments in the Denver and Williston Basins have the same depositional history and test results should indicate common properties. Core samples provided by Tosaya included a shale specimen from 1 km depth which was clayey in appearance with a gritty fracture surface and many small fossil fragments; another shale specimen from 1.5 km depth was dark and hard, appearing more rock like with no fossil fragments in evidence; and a third specimen from 2 km depth, with an appearance somewhere between the previous two, turned out to be virtually all limestone. Laboratory velocity measurements were made on the 1.5 km shale specimen and some of Tosaya's results are shown in Figure 4-3. Samples were either dry or saturated with deionized water, confining pressure ranged from atmospheric to 1.2 kilobars (1216 atmospheres) and a maximum pore pressure of 410 bars was applied.

Figure 4-3a shows P and S velocities, V_P and V_S, for dry and saturated Pierre Shale. Velocities increase rapidly with confining pressure at low pressures due to closure of microcracks and the resulting decrease in porosity.

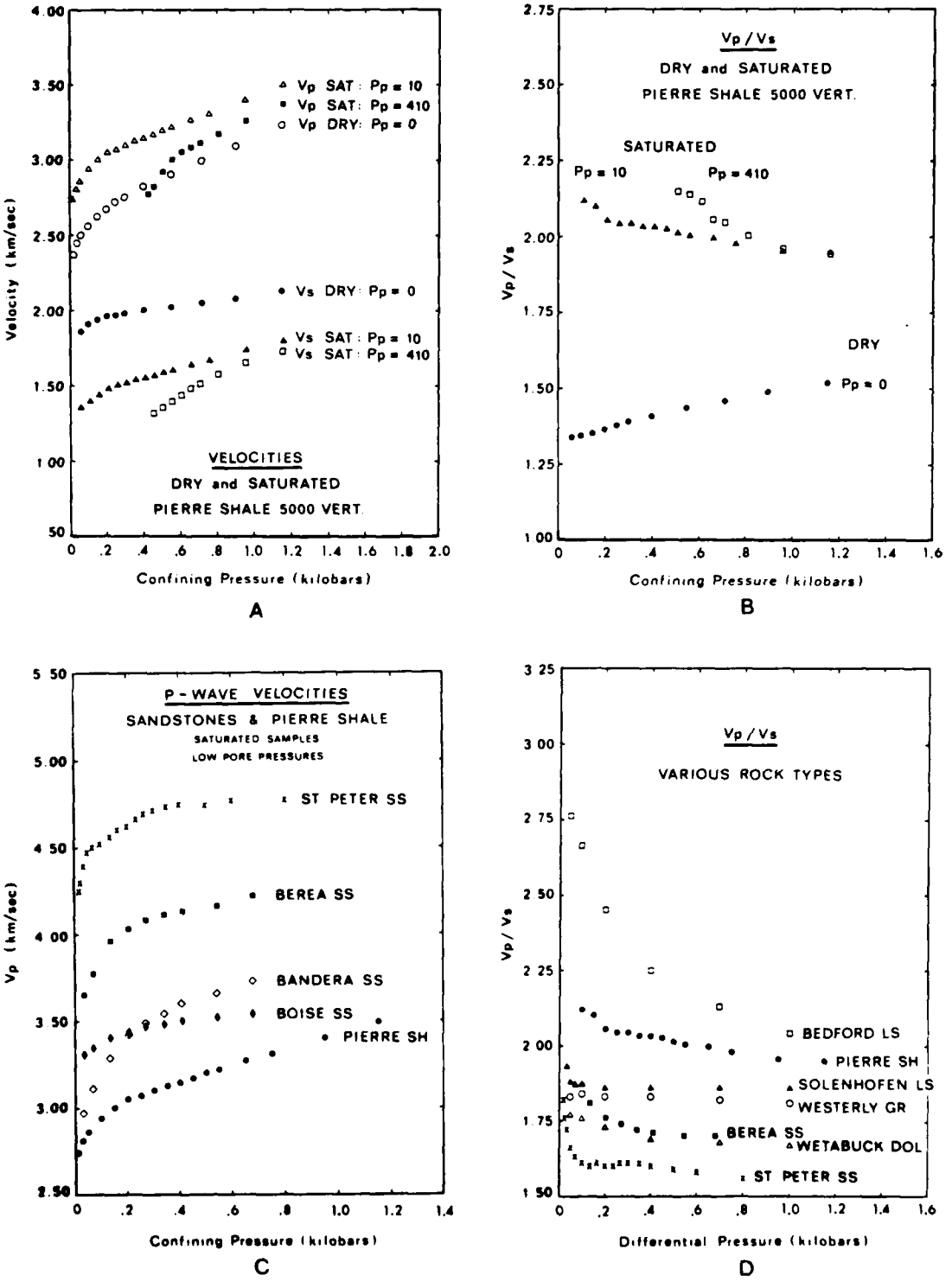

Figure 4-3. Laboratory data on Pierre Shale and other rock (principally from Tosaya (1980)).

Above 250 bars the increase becomes linear. The difference between dry and saturated velocities is about 10% for P waves and over 20% for S waves, however, saturation increases V_P and decreases V_S as expected. The effect of pore pressure, P_P, on saturated samples is also shown but the differences are reduced significantly if velocities are plotted versus differential pressure. This is equivalent to a shift of the $P_P = 410$ bars data points to the left by .4 kilobars.

To compare these velocities with Faust's model the pressure axis can be transformed to depth using the rule of thumb of 1 psi/foot increase in pressure due to overburden. This yields a conversion of 4.42 km/kilobar, hence for a sample depth of 1.5 km the confining pressure is approximately 335 bars and V_P is between 2.8 and 3.1 km/sec depending on the amount of saturation. Faust's model gives a velocity of 3.3 km/sec which is high by 6-15%. The rate of velocity increase versus depth for the speciman can also be compared to the well log data of Haskell (1941). From Tosaya's data the linear rate of increase of V_P is between .1 and .2 km/sec/km while Haskell found a value averaging about .235 km/sec/km in younger Tertiary shales. The difference can be attributed to the age and presence of sandstone in the well logged shale interval, both of which tend to increase the velocity gradient.

With regard to a shear wave velocity model the most useful data is presented in Figure 4-3b. This shows the variation of V_P/V_S with confining pressure (depth). It is strongly dependent on the degree of saturation and to a lesser extent on the confining pressure. For depths from .5 to 2 km (113 bars to 452 bars) the velocity ratio is $1.39 \pm .05$ for the dry sample and $2.08 \pm .05$ for the saturated sample. Depending on the degree of saturation this allows S wave velocities to be found from the P wave velocity model described above. For comparison the seismic wave velocity ratio is shown for various rock types including Pierre Shale in Figure 4-3d.

Cretaceous sediments in the Denver Basin include sandstones as well as shales. This is a common mix and is implicit in Faust's fit. Figure 4-3c shows P wave velocities in various sandstones and Pierre Shale. The faster St. Peter and Berea sandstones are quite clean while the slower Bandera and Boise sandstones have a significant clay content. Therefore, Faust's finding that sandstones are only slightly faster than shales implies that the sandstone sections in his data were not clean. This is consistent with descriptions of the Denver Basin sandstones although the fact that they are also the principal petroleum reservoirs suggests other factors as well.

The last property required to model the Denver Basin deposits is the density function. Direct measurement of formation density is routinely done in well logging operations using the density (gamma-gamma) log, Telford, et al. (1980). Unfortunately densities from available logs in the Wing V area were widely scattered from 2.1 to 2.6 gm/cm^3 and no useful model could be deduced. The conventional, albeit indirect, approach is to relate density to P wave velocity because both are closely related to porosity. Various equations and graphs relating physical properties of sediments and rock are discussed by Nafe and Drake (1963). More to the point are data in Gardner, et al. (1974) relating the P wave velocity and density of a number of sedimentary rocks. For shale the relation takes the simple form $\rho = 0.316V^{1/4}$ where V is P wave velocity in m/sec and ρ is density in gm/cm^3. The coefficient for sandstones is about 7% lower, with the same exponent. For comparison Tosaya has measured densities for the 1.5 km Pierre Shale sample described above and a 3 km Cotton Valley Shale from Texas. At atmospheric conditions these were 2.24 gm/cm^3 dry and 2.35 gm/cm^3 saturated for the Pierre Shales, and 2.60 gm/cm^3 dry and 2.64 gm/cm^3 saturated for the Cotton Valley Shale. Substituting Faust's fit into the density relation gives 2.43 gm/cm^3 and 2.5 gm/cm^3 for

the Pierre and Cotton Valley Shales, respectively, which amounts to a difference of 3% high and 6% low from the saturated samples.

SECTION 5

SEISMIC RESPONSE OF DENVER BASIN SEDIMENTS

The previous sections contain a comprehensive collection of data describing Wing V seismic input as well as structural, geological and geophysical environment. Earthquakes considered are the Pocatello Valley event at a mean distance of about 700 km and the St. Elias event at a distance of 3350 km. The Wing V system is located within the northern Denver Basin, a shallow depression filled with shale and sandstone, situated between the Rocky Mountains to the west and the Great Plains to the east. Detailed cross sections of the Denver Basin sediments are described and a generalized velocity model constructed. In this section the data and models are used to calculate surface response throughout Wing V to simplified body wave inputs. The extension to surface waves and more complex wave phenomena is discussed but no quantitative results are presented here.

For the two earthquake epicenters considered, ground motion in the Denver Basin is due to body and surface waves incident from outside. Body waves are nearly vertically incident from the distant St. Elias event, and at a shallower incidence angle from the local Pocatello Valley event. Surface waves from St. Elias are highly dispersed and therefore separated from other phases due to the propagation distance, while Pocatello Valley Love type surface waves are superposed in a complex fashion on the S wave arrivals and Rayleigh waves are a distinct later arrival.

Both body and surface wave arrivals interact with the near surface structure of the Denver Basin to produce the observed ground response. A generalized basin structure consists of a boundary or edge, an interface and an interior. It can be classified in terms of geometry and characteristic lengths. Geometry might include overall shape and detailed edge configuration, such as

thrust faults, shallow dips, etc. Characteristic lengths include depth of sediments, basin width and length, radius of curvature of the sediment-basement interface, radius of curvature of the boundary, etc. Although a quantitative consideration of all of these factors is beyond the scope of this study, important factors can be isolated by scaling on the basis of periods and wavelengths of interest. Significant periods for this study are between 2 and 6 seconds. Body wavespeeds range from 1 to 3.5 km/sec in the basin sediments, giving a range of wavelengths from 1 to 21 km. Geologic and topographic features with characteristic lengths significantly outside this range of wavelengths can be ignored.

From this point of view the depth to basement in the Denver Basin, from 2 to 3.5 km, is a significant scale while the basin width and length, both greater than 200 km, are not. Radii of curvature of the sediment-basement interface and basin edge are so large that focusing effects can be ignored. The maximum surface relief in the basin is no greater than 200 meters which compares to the thickness of Tertiary sediments. These lengths are apparently too small to produce significant effects in the 2-6 sec period range. Finite element calculations supporting this conclusion are described in the Appendix. These considerations direct attention to the interaction of seismic waves with the sedimentary column in the basin.

5.1 Sedimentary Column Resonance Calculations

When plane body waves are incident from below on a horizontally layered model of basin sediments over bedrock, it is well known that surface response is amplified by the lower wavespeed, near surface sediments. The mechanism is constructive interference of upgoing and downgoing waves. A number of analytical procedures have been developed to calculate response in a layered medium, both

for seismological and engineering applications, see Aki and Richards (1980). They are basically linear transfer function methods in the frequency domain, the best known being the Haskell-Thomson approach applied here to calculate body wave response over Wing V.

The Denver Basin is shallow with a nearly horizontal interface between the sedimentary fill and the Precambrian basement. The interface has significant dip only along the western side flanking the Laramie and Front Ranges of the Rocky Mountains. Structural contours and cross sections were described in Section 2. Table 5-1 shows the mean total depth and formation thicknesses over each of the 20 flights in Wing V. Uniformity of the deposits in the basin is illustrated in the seismic reflection profiles of Figure 5-1. These were found in an advertising brochure for commercially available speculation surveys in the Denver Basin, Geo-Search Corp. (1980). Exact locations, hence depths are not available but the reflection lines passed somewhere between Flights Q and S. The two profiles shown are said to be representative of others across the northern Denver Basins. Telford, et al. (1980) discuss reflection techniques and have some nonuniform profiles for comparison. Only two flights in Wing V deviate from the uniform layer assumption, T and Q on the Laramie Range flank. A cross section through T is shown in Figure 2-4 as section DD' and a cross section through Q as section BB'. Effects of the 5-10^{o} dips will be discussed later.

It is useful to examine briefly the canonical problem of a single soft layer (thickness h, shear wavespeed β_1, density ρ_1) over a harder half-space (shear wavespeed β_2, density ρ_2). All qualitative results of the models to follow are exhibited by this case. For a vertically incident shear wave the maximum surface response occurs at periods, $T_m = 4h/m\beta_1$, m = 1,3,5,...,

Table 5-1. Average Formation Thicknesses Under Wing V Flights

FLIGHT	SEDIMENT DEPTH (meters)	FORMATION THICKNESS (meters)				
		Pennsylvanian	Permian	Jurassic-Triassic	Cretaceous	Tertiary
A	3208	259	274	168	2294	213
B	2903	244	305	122	2019	213
C	2476	213	366	107	1577	213
D	2831	229	305	122	1962	213
E	3005	274	305	122	2152	152
F	2469	244	366	107	1539	213
G	2173	229	305	107	1319	213 ?
H	2018	198	290	91	1226	213 ?
I	2069	244	274	107	1292	152 ?
J	2400	274	274	122	1639	91 ?
K	2626	259	274	107	1803	183
L	2671	274	305	122	1879	91
M	2447	305	305	122	1715	-0-
N	2795	320	335	152	1988	-0-
O	2949	305	335	137	2081	91
P	3432	259	274	213	2473	213
Q	2438	229	274	290	1462	183
R	3398	244	274	229	2529	122
S	2820	259	335	183	2043	-0-
T	1829	183	244	305	762	335

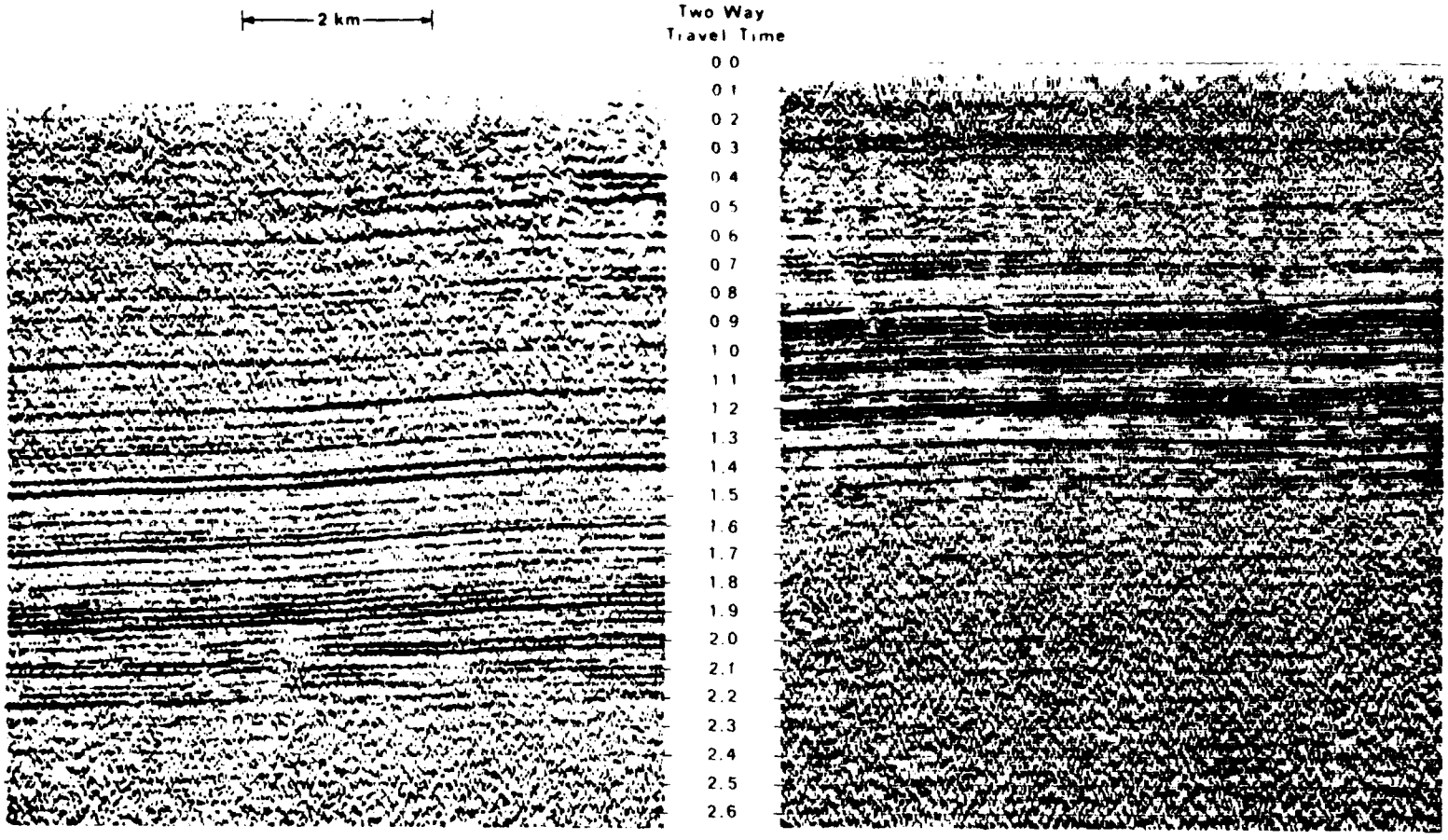

Figure 5-1. Examples of reflection surveys illustrating uniformity of deeper sediments near Flights Q and S in the Denver Basin; vertical travel times in seconds.

i.e. the periods of a free-fixed shear beam. At these maxima the ratio of surface motion with and without the surface layer is just $\rho_2\beta_2/\rho_1\beta_1$, the ratio of characteristic impedences. As an example consider a simple model of Denver Basin sediments consisting of a 3 km thick layer with average shear wavespeed of 1.5 km/sec. Natural periods, T are at 8 sec, 2.67 sec, 1.6 sec, etc. These periods are within the critical period window of the Wing V system. Assuming ρ_1 = 2.4 gm/cm^3, ρ_2 = 2.65 gm/cm^3 and β_2 = 3.3 km/sec gives an amplitude ratio of 2.43. These are representative of the results expected from a more realistic model of Denver Basin sediments overlying Precambrian basement.

This simple model also provides a quantitative estimate of the effects of a soft surface layer, specifically the Tertiary deposits. Assuming for example that the upper 200 meters have a shear wavespeed of 750 m/sec gives natural periods of T = 1.06 sec, .36 sec, etc. A particularly low shear wavespeed of 500 m/sec gives T = 1.6 sec, .53 sec, etc. Therefore the Tertiary overburden must have an anomalously low wavespeed to affect missile response at periods longer than 2 sec. The near surface velocity surveys described in Section 4 give no indication of such low wavespeeds; hence the Tertiary overburden is apparently not a significant contributor to response in the 2 to 6 second period window.

The calculational procedure is to construct velocity and density functions for each of the sedimentary sections given in Table 5-1 and then calculate surface response at each Flight using the Haskell-Thomson approach. The computer program is available in Herrmann (1978) and described by Haskell (1960), Haskell (1962). These latter references also show that the surface response is relatively insensitive to angle of incidence for angles less than 15° from vertical. Therefore only near vertically incident body waves are considered.

Velocity functions are readily constructed from the formation thickness in Table 5-1 using Faust's fit for P wavespeeds, $V_P = AZ^{1/6}$. The constants determined by Faust for each of the formations, excluding Tertiary, are given in Section 4. These are increased here by 2% to fit the available well log data. According to Tosaya's velocity data, Figure 4-3, S wavespeeds are about half of P wavespeeds for saturated Pierre Shale in the depth range considered. This corresponds to a Poisson ratio of 1/3. Although some deep well data in the Wattenberg oil field, north of Denver, Colorado indicate only partial saturation, Matuszczak (1976), it will be assumed here that the Denver Basin sediments are saturated. Therefore V_S is just $.5\ V_P$ in the following models. Finally, the density function of Gardner for shales, also described in Section 4, is used to calculate density directly from V_P as $\rho = .32\ V_P^{1/4}$.

The velocity and density functions at Flights P and S in the Goshen Hole area are shown in Figure 5-2. These are piecewise constant (layered) approximations of the smooth models for use in the Haskell-Thomson formalism. The upper 100 meters representing part of the Tertiary deposits are assigned approximate properties because 2-6 sec response is insensitive to the variations noted in Section 4. The Precambrian basement is assigned properties based on granite wavespeeds at depth given by Press (1966). These are 5750 km/sec, 3324 km/sec and 2.65 gm/cm^3 for P and S wavespeeds and density, respectively.

Amplitude spectra at Flights H, S and P are plotted in Figure 5-3 for S or SH wave input, and in Figure 5-4 for P wave input, both at normal incidence. Three curves are plotted for each flight; the middle curve is for the nominal velocity function while the other two are the $\pm$ 15% bounds, which bracket the original well log data in Figure 4-1a. Flights H, S and P have mean depths of 2018 meters, 2820 meters and 3432 meters respectively. In

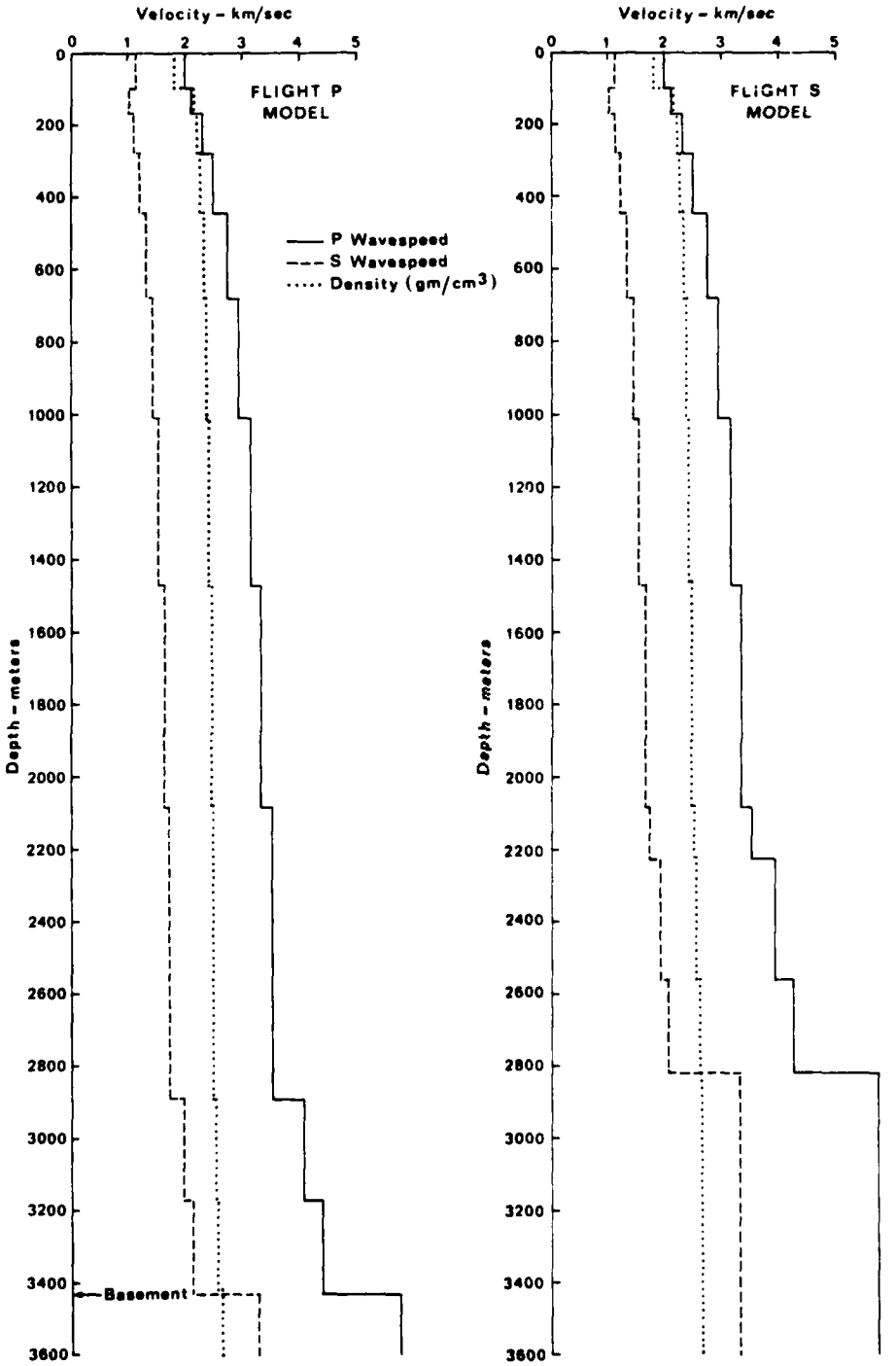

Figure 5-2. Velocity and density functions at Flights P and S.

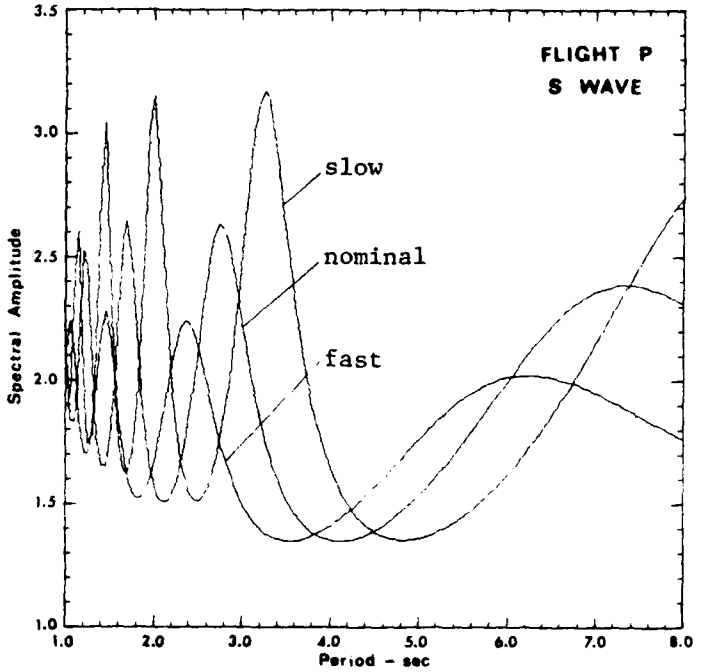

Figure 5-3a. Amplitude spectra for slow, nominal and fast velocity models with S wave input at normal incidence. See also Figs. 5-3b and 5-3c.

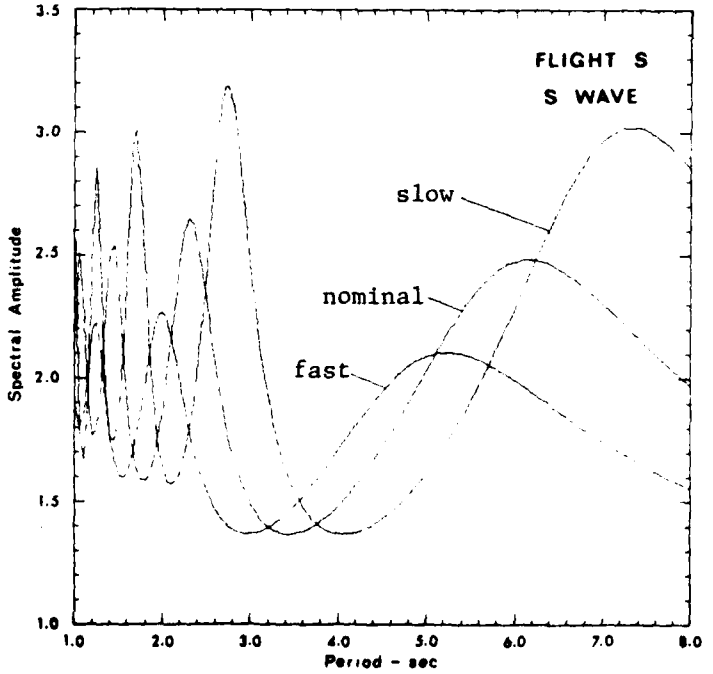

Figure 5-3b. (see Fig. 5-3a)

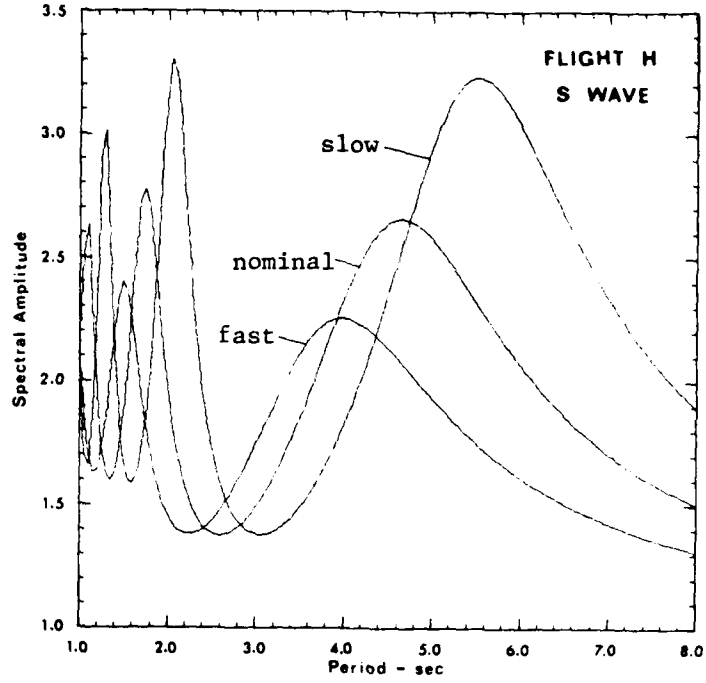

Figure 5-3c. (see Fig. 5-3a)

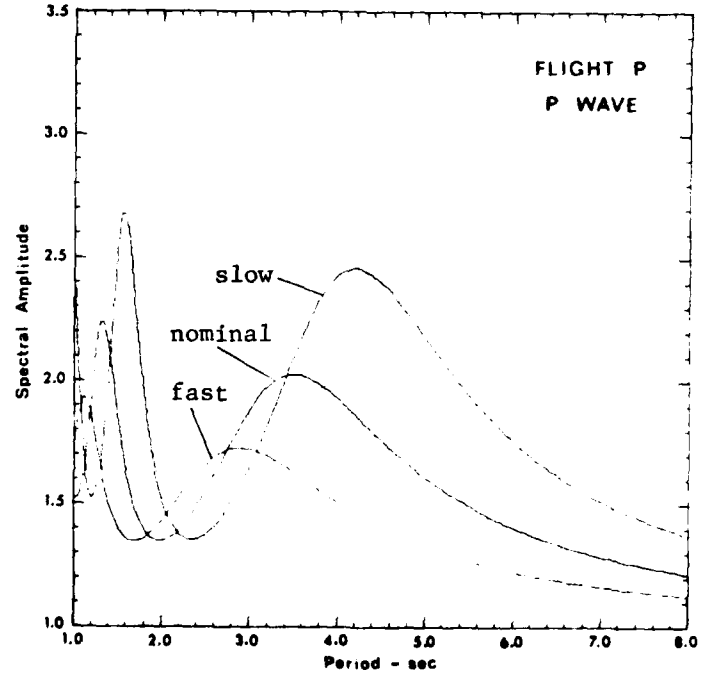

Figure 5-4a. Amplitude spectra for slow, nominal and fast velocity models with P wave input at normal incidence. See also Figs. 5-4b and 5-4c.

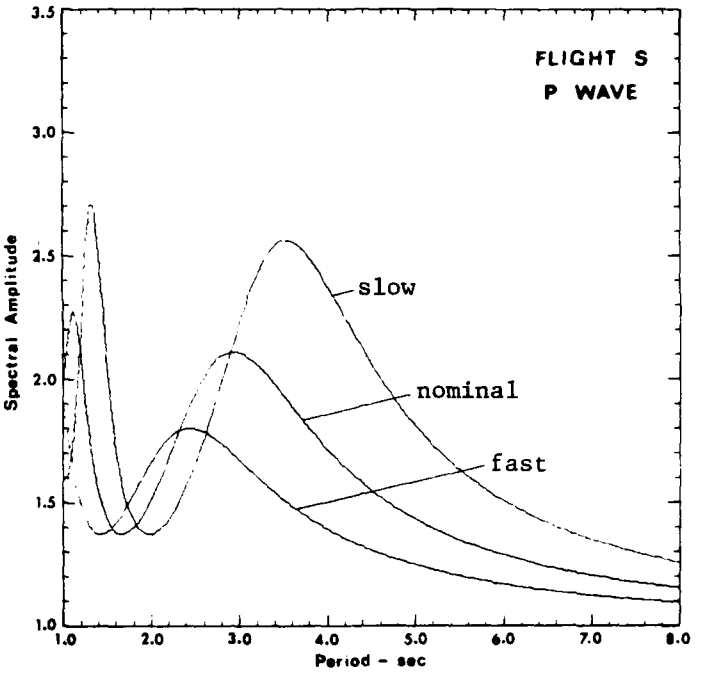

Figure 5-4b. (see Fig. 5-4a)

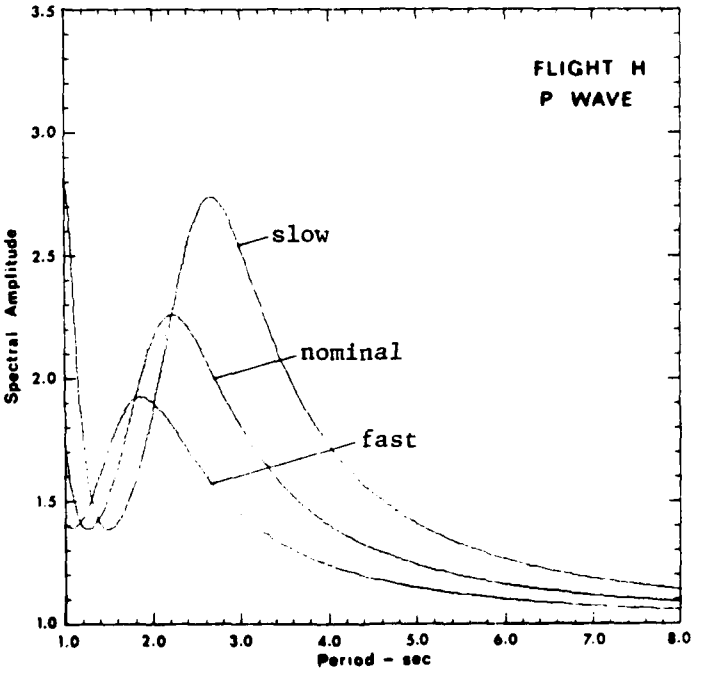

Figure 5-4c. (see Fig. 5-4a)

general, decreasing the overall velocity function shifts the peak response to longer periods and higher amplitude, while increasing the velocity function decreases the peak period and amplitude. The peaks at the longer periods are the fundamental mode of the layered model and consecutive peaks at shorter periods are the overtones.

Consider Figure 5-3 showing response to S waves at normal incidence. The fundamental mode at Flight H ranges from 4 to 5.5 sec and the first overtone ranges from 1.5 to 2.2 sec. At Flight S, where bedrock is 0.8 km deeper, the fundamental is from 5.2 to 7.3 sec and the overtone from 2 to 2.7 sec. At Flight P, 1.4 km deeper than H, the fundamental range is 6.2 to over 8 sec and the overtone range is 2.3 to 3.3 sec. Spectral amplitudes of the fundamental and first overtone generally range from 2 for the + 15% velocity function, to over 3 for the - 15% function. These amplitudes give the increase in surface response due to the presence of sediments, i.e. amplitude on an outcrop of basement rock would be unity.

Figure 5-4 shows the surface response to normally incident P waves. Here the fundamental mode ranges are 1.8 to 2.7 sec. for Flight H, 2.4 to 3.5 sec for S and 2.9 to 4.2 sec for P. The first overtone is less than 1 sec for H, reaches 1.4 sec for S and ranges from 1.1 to 1.6 sec for P. Spectral amplitudes of the fundamental and first overtone range from 1.75 to 2.5 for the + 15%, nominal and - 15% velocity functions.

The most notable result of these calculations is that the best velocity function estimate for Denver Basin sediments exhibits natural periods in the range of Wing V missile suspension system natural periods, 2 to 6 seconds. In particular Flight P, which consistently had a high percentage of seismic alarms from both earthquakes, rests on sediments which amplify in a window

close to the suspected critical period of the Missile Guidance Set (MGS), 3 to 4 seconds. Comparison of response at P and S shows that periods at Flight S, although lower than those at P, are still close to the critical MGS window. However, Flight S in the Goshen Hole had the lowest percentage of seismic alarms. Note also that amplifications at the natural periods are not particularly high because the mean velocity and density contrasts between sediment and basement are not great.

As mentioned above, Flight S in the Goshen Hole lowland was relatively insensitive to the seismic inputs from the Pocatello Valley and St. Elias earthquakes. Recognizing that absolute estimates of ground motion at any one flight are subject to the uncertainties of the geophysical model, a better estimate of response might be spectral ratios with respect to Flight S. Such ratios would tend to cancel certain biases of the model. Two examples are illustrated in Figure 5-5. These show spectra at Flights P and H divided by the spectrum at Flight S for S wave input to the nominal velocity models. There are actually three velocity models at each flight, - 15%, nominal, + 15%, to be considered in computing these spectral ratios. This gives nine combinations per flight ratio, or a total of 180 combinations over the twenty flights for each body wave input (P or S). In what follows all ratios are with respect to the Flight S (lowland) spectra with either a slow (- 15%), medium (nominal) or fast (+ 15%) velocity function. For example, spectral ratios at Flights P and H are shown in Figure 5-6 when Flight S has a fast model and Flights P and H have slow models. Comparing Figures 5-5 and 5-6 shows that the Flight P ratio has a peak near 3 seconds in both cases.

All possible spectral ratios were calculated for normal incidence of P and S waves. Rather than show the 360 curves, a less cumbersome approach is

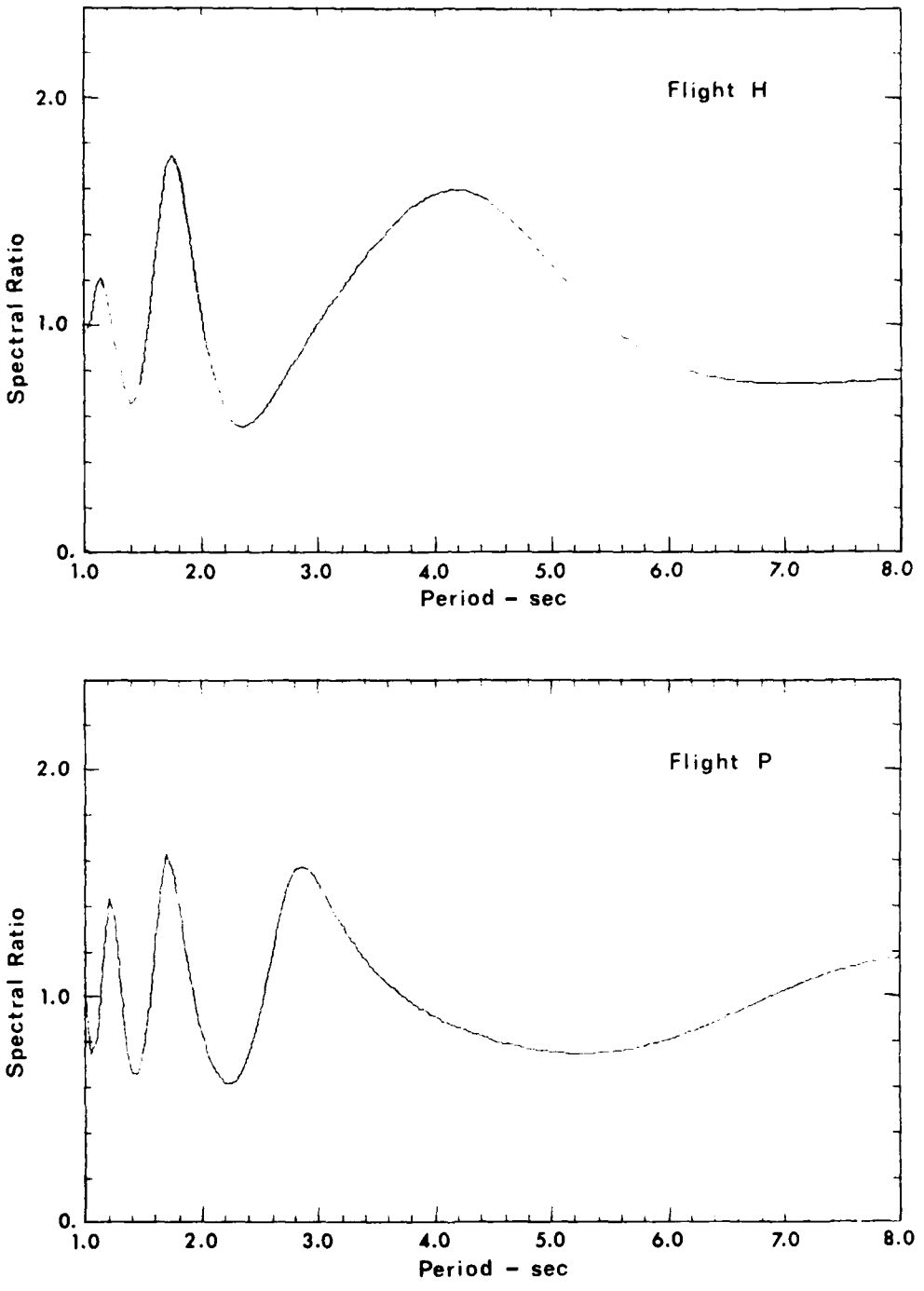

Figure 5-5. Spectral ratios for S wave input with nominal velocity models (Flights P and H spectra divided by Flight S spectrum).

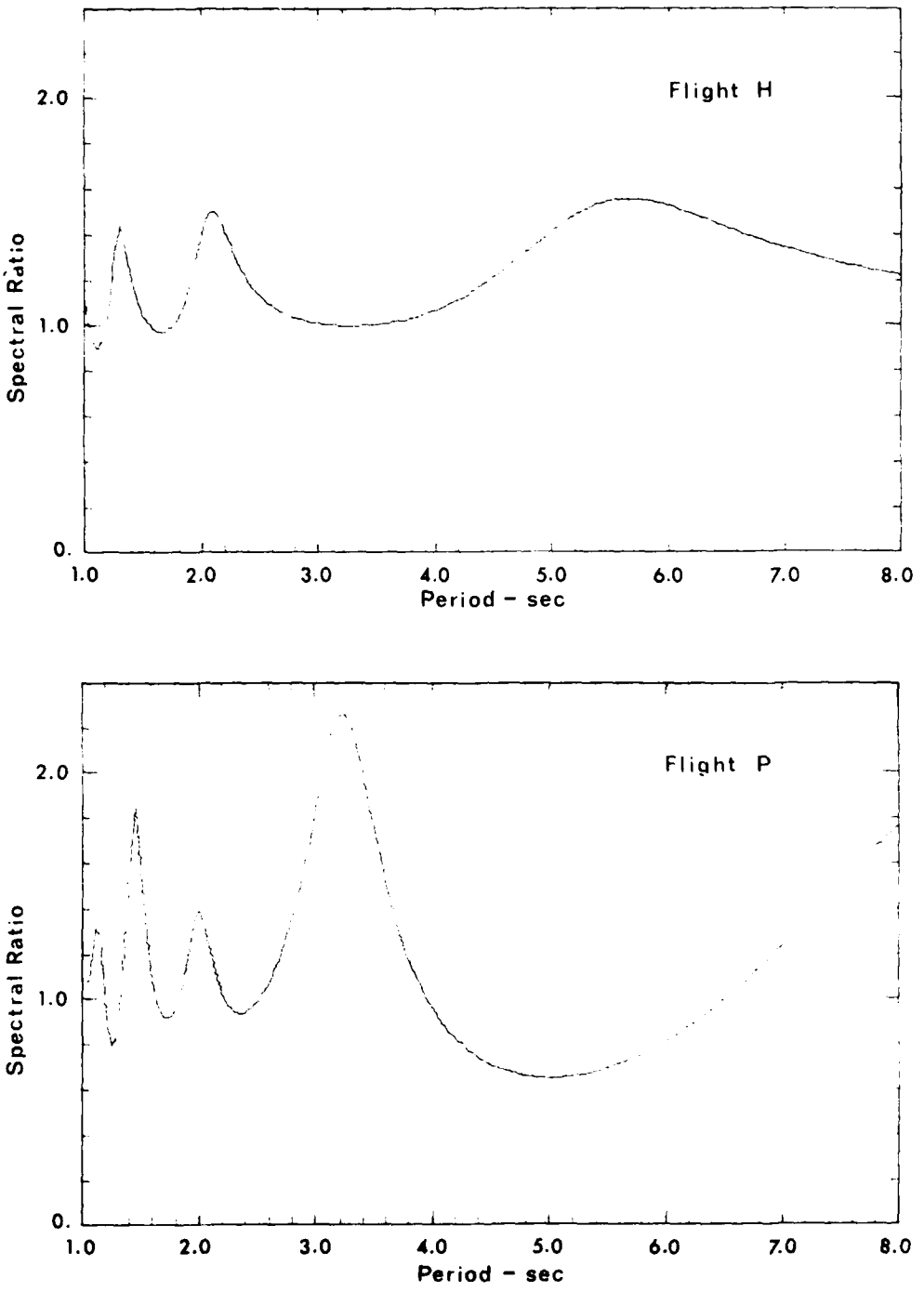

Figure 5-6. Spectral ratios for S wave input with a fast model at Flight S and slow model at Flights P and H (Flights P and H spectra divided by Flight S spectrum).

to indicate the distribution of flights exhibiting spectral ratios greater than some level within a period window of interest. This is effectively a distribution of synthetic seismic alarms. They indicate relative amplification with respect to Flight S, hence susceptibility to higher amplitude motion. They do not correspond to any absolute motion, specifically that required to trigger a seismic alarm. Figure 5-7 shows those flights with spectral ratios above 1.35 or 1.5 in the period window of 2.5 to 3.5 sec. The first (a) is for the nominal velocity model at each flight, the second (b) is for the slow model and the third (c) is for the fast model. Figure 5-8 shows similar results for the extreme case of a slow model at all flights except the reference Flight S which has a fast model; this combination is referred to as slow/fast. This case exhibits the highest spectral ratios within the more restrictive period window from 3 to 3.5 seconds. Observe that some of the flights are included because they amplify P wave input while others amplify S wave input, the amplification being with respect to the corresponding response at Flight S. Other period windows exhibit similar patterns, as in Figure 5-9 for a window from 2 to 2.5 seconds with a nominal/slow combination. To show correlation with depth to basement, sediment depths are indicated in Figure 5-10.

These results indicate that the relative response between Flight S (lowland) and most of the other flights (highland) is probably no greater than a factor of two or so. The spectral ratios are generally higher for S wave inputs than for P wave inputs. When the velocity functions are on the fast side of the nominal function the spectral ratios decrease, typically less than 1.3, and the peak periods tend to decrease. If the velocity functions are higher than those considered here the spectral ratios are fairly flat indicating no significant differences in the 2 to 6 second window. The synthetic

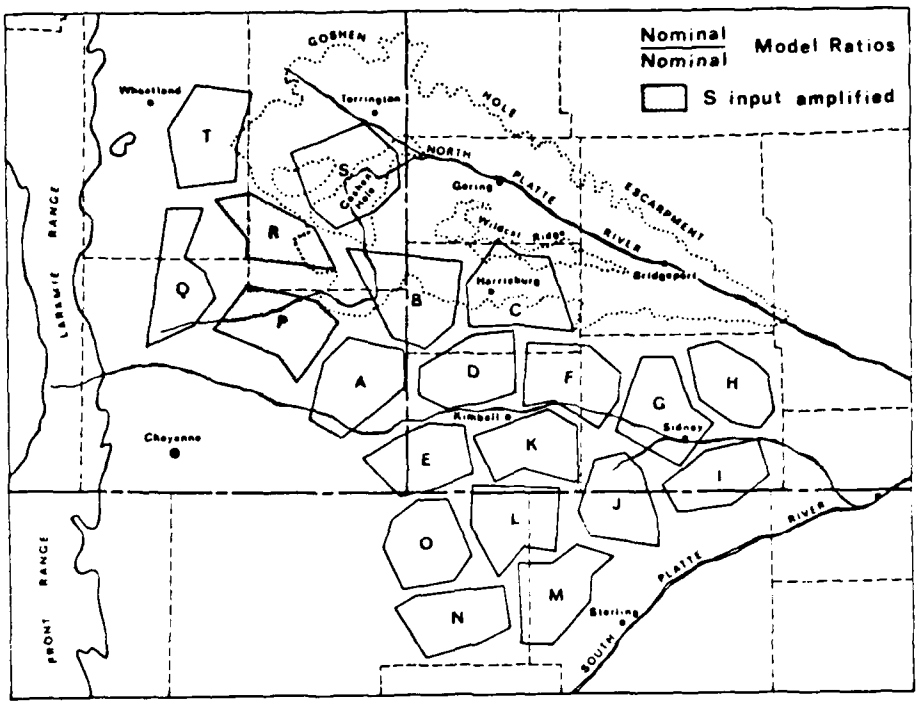

Figure 5-7a. Shaded flights show spectral ratios > 1.5 for 2.5 <period <3.5 seconds.

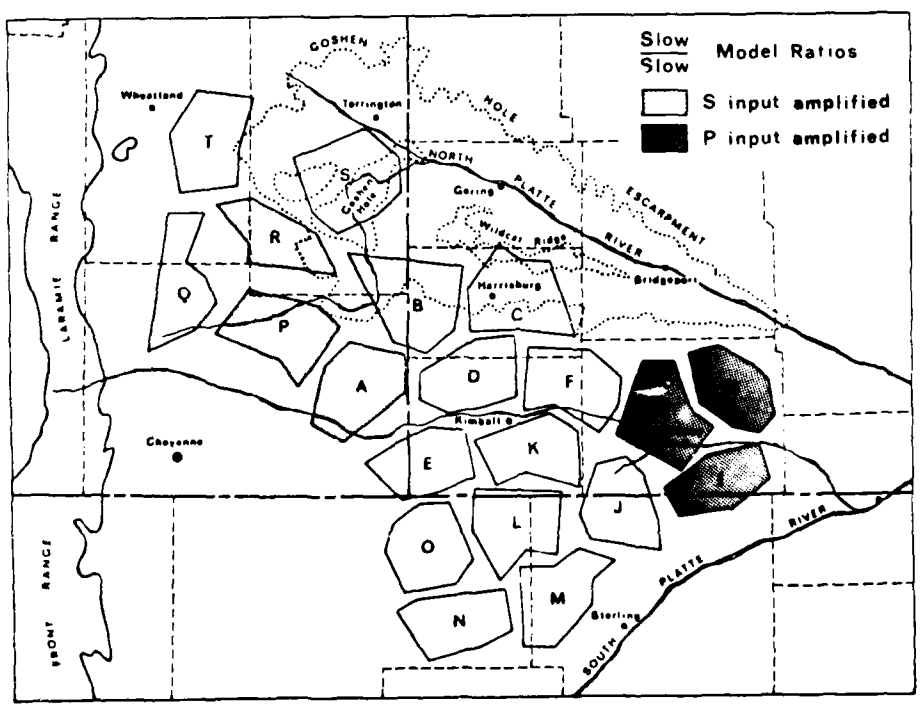

Figure 5-7b. Shaded flights show spectral ratios > 1.5 for 2.5 <period <3.5 seconds.

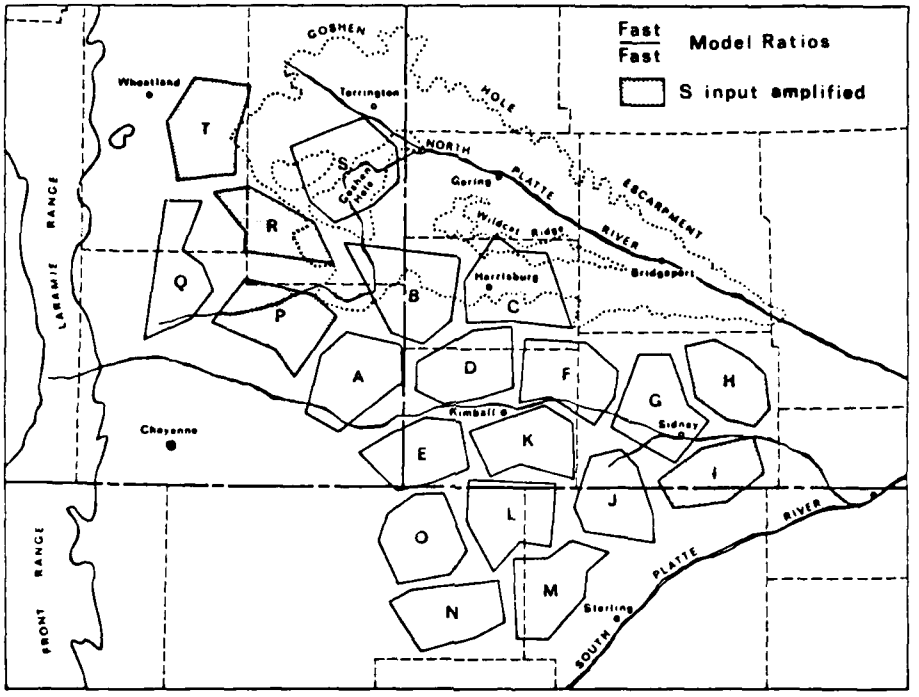

Figure 5-7c. Shaded flights show spectral ratios >1.35 for 2.5 <period <3.5 seconds.

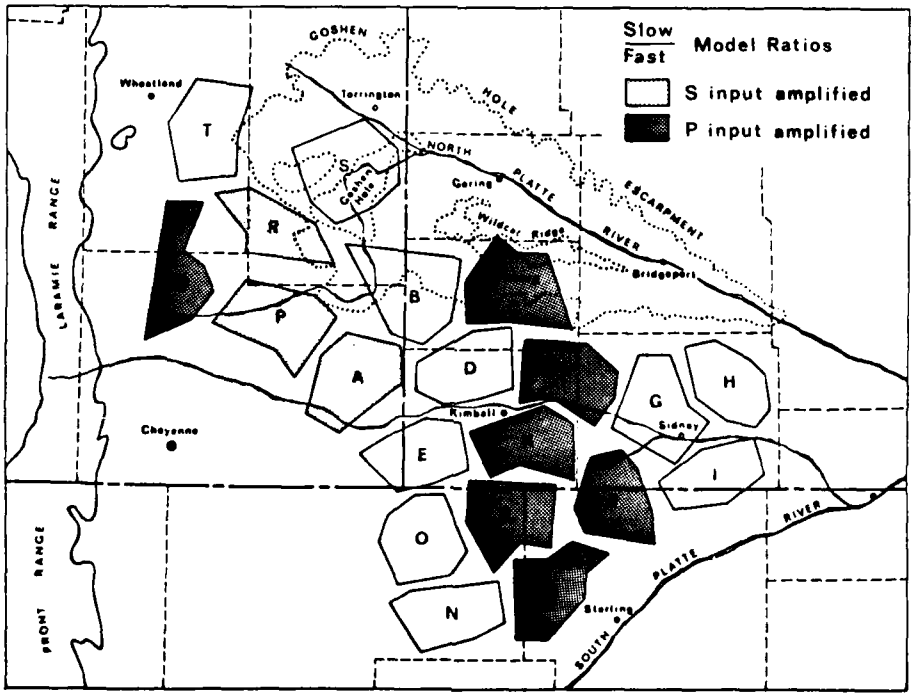

Figure 5-8. Shaded flights show spectral ratios > 1.5 for 3 <period <3.5 seconds.

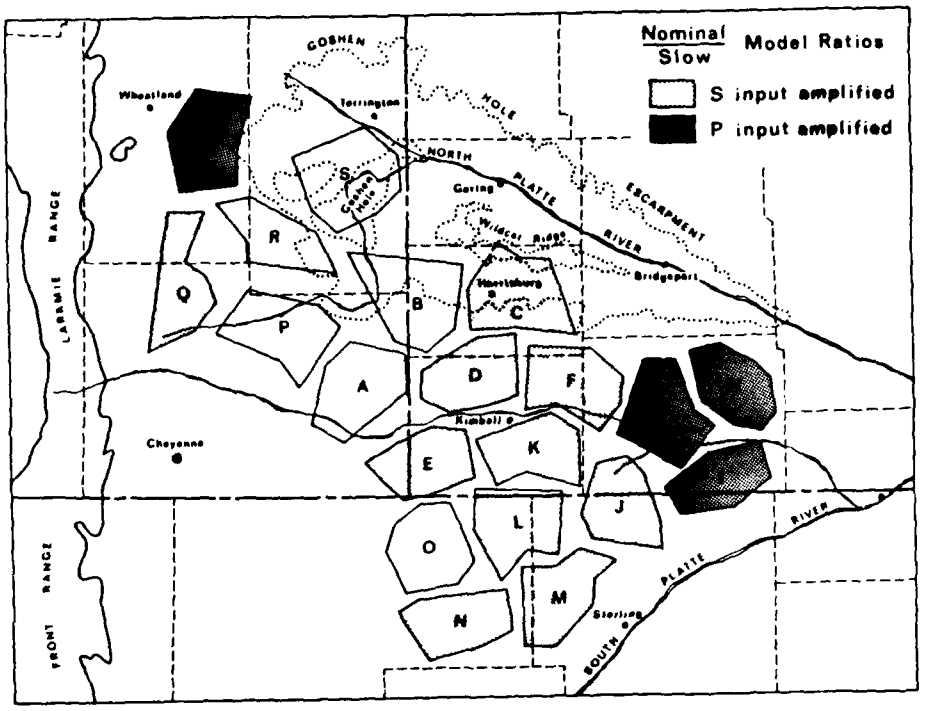

Figure 5-9. Shaded flights show spectral ratios > 1.5 for 2 <periods <2.5 seconds.

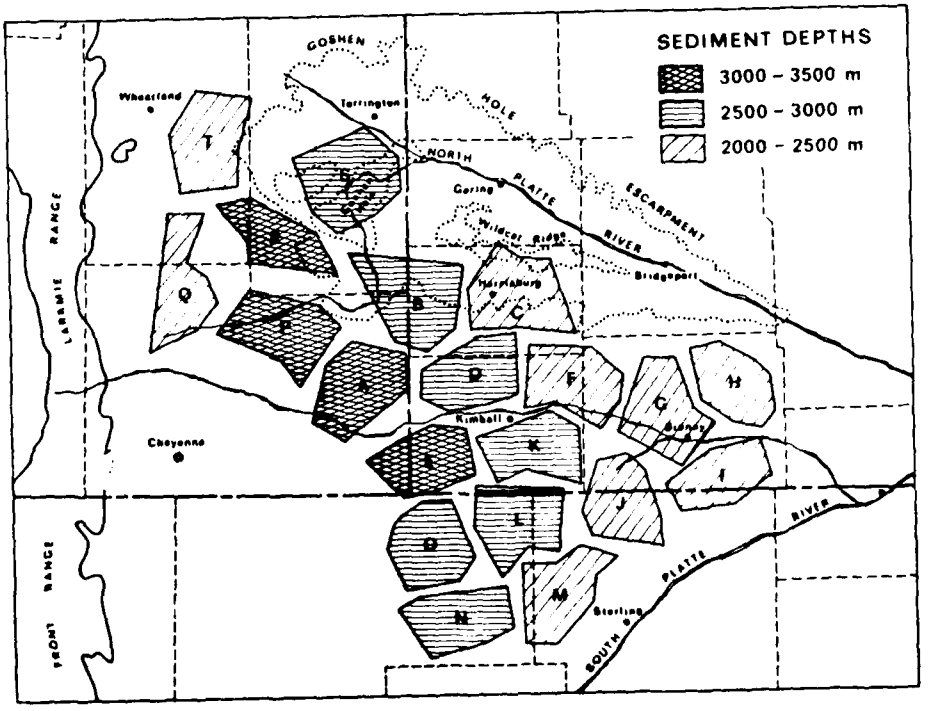

Figure 5-10. Approximate sediment depths over Wing V.

distribution of seismic alarms depends strongly on the location and width of the chosen period window. Referring to Figure 5-10 showing depth of sediments, there is a correlation between depth and the synthetic alarm distributions. Flights P, R and A are the deepest, averaging 3350 meters, and have higher spectral ratios in the window between 2.5 and 3.5 sec. Flights G, H and I are the shallowest, averaging 2090 meters and show much lower ratios in this window.

The spectral ratio peaks and their dependence on velocity functions is due to the relative periods of fundamental and higher mode resonances at each flight. Perturbations in the velocity function may shift the fundamental or overtone into or out of a particular period window. Consequently the flight where spectral ratios are maximized is still sensitive to biases of the chosen velocity model, while the range of relative amplitudes is probably less sensitive. Concerning a viable mechanism for the patterns of seismic alarms observed from the two earthquakes, Figure 1-3, these calculations demonstrate that within the observed bounds of data scatter about a nominal velocity model there is a mechanism for selective amplification at some of the flights. The pattern depends on the type of body wave input, on the critical period window and details of seismic velocity distributions on a flight by flight basis.

5.2 Additional Wave Propagation Mechanisms

These calculations demonstrate a mechanism for observed patterns of seismic alarms over Wing V due to distant earthquakes. To say whether this is the actual mechanism or not requires further data on Minuteman III silo mounted ICBM response to earthquake ground shaking, as well as measurements (rather than estimates) of velocity structure at the 20 flights. However, the coincidence of sedimentary column resonance periods and estimated Missile Guidance

Set natural periods strongly suggest the likelihood of this or a similar mechanism. These calculations were for body wave input and a natural extension is to surface waves which are present in the actual seismic input described in Section 3. For example, relative surface wave response could be found by assuming the same energy flux for a surface wave mode common to all flights and calculating ground motion. Amplitude spectra or spectral ratios could then be determined and presented in much the same manner as was done here for body wave inputs. A similar procedure was applied by Murphy and Hewlett (1975) to explain relative seismic response in a preliminary microzonation of Las Vegas, Nevada.

Other more complex wave propagation phenomena may also contribute to Wing V anomalies in the Denver Basin. One possibility is focusing of shallow body waves from the Pocatello Valley event nonuniformly over the Wing V area due to lateral variations in upper mantle structure under the Rocky Mountains, Julian (1970). The fact that such focusing could not occur for the St. Elias event, due to the different travel path, argues against this. Another possibility is the conversion of incident body waves to surface waves along the Laramie Range flank. Recent numerical calculations by Harmsen and Harding (1980) show the Rayleigh wave to be the dominant scattered phase from a 26.5° flank. The Laramie Range flank is variable and recent COCORP deep reflection surveys, Allemdinger (1980), have shown it to be a shallow overthrust as in Figure 2-3c. However, well logs indicate that flank structure is closer to that shown in Figure 2-3a (see Figure 2-6). Therefore, estimating the amplitude of scattered Rayleigh waves requires numerical calculations for various geometries. Scattered amplitudes on the order of 30% of the incident wave are expected. In any event, the effect of the scattered

waves would be greatest near the flank. Because most seismic alarms occurred farther from the flank and flights on the flank were relatively undisturbed, this mechanism is of doubtful importance. In addition to mode conversion, the shallow dip of the flank can also cause energy trapping of body waves, Wojcik (1979), but to be significant the incidence angle must be quite shallow, which is not the case for either the Pocatello Valley or St. Elias events.

The possibility of anomalous motions due to variations in crustal structure has also been considered. In Section 2 it was noted that core rocks of the Front and Laramie Ranges changed type across the Nash Fork-Mullen Creek shear zone indicated in the tectonic map, Figure 2-1. The COCORP reflection survey mentioned above crosses this zone and results indicate a thickening of the crust by about 25%. Reflections and velocity data north of the shear zone give a thickness of 38 to 40 km while those south of the zone give 48 to 50 km. Further details of crustal structure under the Laramie and Front Ranges are given by Prodehl and Pakiser (1980) from refraction surveys conducted by the U.S. Geological Survey. Predominant body wave periods of their crustal model are entirely too long to be relevant to this study. Furthermore, the crustal thickness change across the shear zone would modify the modal distribution of surface wave energy, Alsop (1966), but would not be expected to amplify or modify Wing V ground response on the scale indicated by alarm distributions.

SECTION 6

SUMMARY AND CONCLUSIONS

Wing V, the 90th strategic missile wing near Cheyenne, Wyoming, consists of 20 flights of Minuteman III ICBMs (10 per flight), distributed over the tri-state area of Wyoming, Nebraska and Colorado. Due to two recent North American earthquakes, the Wing experienced significant operational mode changes (seismic alarms). The earthquakes consisted of a near event, 700 km west in Pocatello Valley, Idaho (1975), and a more distant event, 3350 km northwest near St. Elias, Alaska (1979). The Pocatello Valley, Idaho (M_L = 6.0) and the 1979 St. Elias, Alaska (M_S = 7.1) earthquakes triggered seismic alarms in 42% and 46%, respectively, of the Wing V silos. The alarm pattern differed considerably between the two events. In addition, the tectonic province and source mechanism as well as incident seismic wave types, amplitudes and durations differed considerably. The number of alarms indicated some characteristic common to both events as the causitive factor.

The missile and its suspension system are essentially an inverted pendulum. Motion is registered at the Missile Guidance Set in the form of disruption counts. Seismic alarms over Wing V were due to longer period (2 to 6 seconds), lightly damped ($\lesssim$ 1% critical damping) modes of the suspension system. The amplification factors (i.e. response at resonance) for these modes are high (50-75) but are only achieved after a large number of input wave cycles. For example, over three minutes of shaking at a 3.4 second period are required to achieve 90% of the maximum amplification for the 3.4 second suspension system mode.

Seismograms recorded 200 km south of Wing V on bedrock at Golden, Colorado were overdriven by the Pocatello Valley event. However, the more distant St. Elias event showed distinct body and surface wave arrivals. The shortest periods and longest duration discernable on the record are from body wave

phases. Although the bandpass of the Wood-Anderson Seismometer hinders a direct amplitude comparison, the body waves are generally lower amplitude, shorter period and longer duration than the surface wave phases (LQ, Lg, Rg, etc.). Alarm timing and the relative period and duration of body and surface waves indicated that body waves were the probably cause of the Wing V alarms.

Wing V is situated over the Denver Basin, a broad, shallow (2 to 3 km) sedimentary basin, separating the Central/Southern Rocky Mountains to the west and the Great Plains to the east. Response over the Wing V area is influenced by the interaction of seismic waves with local geologic features, characterized by some length scale. If the seismic wavelength is much larger or smaller than the geologic feature, then little interaction occurs. For the period window of interest, 2 to 6 seconds, the most significant geologic feature is the sedimentary cover, in contrast to topography such as escarpments, low velocity surface layers or crustal depth to Moho.

The predominant sediment in the Denver Basin is cretaceous age Pierre Shale, with significant deposits of sandstone and limestone. Oil well seismic velocity logs of the sedimentary columns are well approximated by Faust's fit. The well log scatter from available data is bounded by ±15% excursions in the velocity. Therefore, three velocity models were used in the calculations. The Nominal Model used Faust's values, the Fast Model used 15% higher velocity and the Slow Model used 15% lower velocity. From well logs and other data, individual formation thicknesses and total depth under each flight were determined. Velocity and density functions were found for each of the twenty Wing V flights using Faust's fit, laboratory data on seismic velocity ratios for Pierre Shale at depth and density models based on porosity. The sedimentary

cover is quite uniform over the Denver Basin. Consequently, a calculational procedure for a uniform layered halfspace was adequate to investigate the sediment's effect on body waves.

Near vertical body waves from the distant St. Elias event are incident on Wing V. The steep incidence angle is due to the high velocity gradient in the upper crust. Therefore, surface response for P and S body waves at vertical incidence was examined using a Haskell-Thomson layered halfspace program. Response at Flight S in the Goshen Hole was used as reference motion because this lowland flight was relatively insensitive to both earthquakes. Spectral ratios were developed for each flight by dividing its response by that at Flight S. Values greater than unity indicate periods where response is amplified with respect to the lowland flight. All possible combinations of spectral ratios (with Flight S as the reference) were calculated for P and S input to the 20 flights with either a slow, nominal or fast velocity model. Results showed that relative response up to a factor of 2 or so could be expected. The amplification was due to the relative period and amplitude of fundamental and higher mode sedimentary column resonances.

The spectral ratios calculated over Wing V with respect to the Flight S lowland spectrum show that amplification occurs in certain period windows, which depend on the resonant column periods. These are functions of the incident wave type (P or S) and the seismic velocity model (fast, nominal or slow) assumed at each flight. Within the range of assumed velocity models and period windows of interest, patterns of amplification are seen which correlate with sediment depth. It was noted that if velocities were all higher than the nominal measured values, the response became uniform over the wing.

In conclusion, within the rather narrow scatter of velocity and depth data used in the calculations, patterns of amplification with respect to a reference lowland flight were found for vertically-incident body waves. The relative response is probably no greater than a factor of 2 or so and the pattern of amplification depends on the period window and body wave type, among other factors.

The observation that relative amplification between nearby flights can occur at or near natural periods of the Missile Guidance Set (MGS) suggests this as the causative factor of Wing V seismic alarm distributions. That is, the sedimentary column under certain flights amplifies ground response near natural periods of the MGS. The body wave ground response from distant events is low amplitude; however, the MGS gain at resonance is sufficiently large to cause significant MGS motion.

It appears that the Wing V alarm patterns are therefore due to coincidence of three factors:

1. High gain of 2 to 6 second period missile suspension system modes.
2. Incident body waves with periods covering the window of the suspension system modes.
3. Sedimentary column resonance periods close to the suspension system periods.

Factors 1 and 2 are sufficient to trigger seismic alarms, while factor 3 would tend to cause anomalous alarm patterns due to relative amplification between flights.

Prior to the 1979 St. Elias event, explanations for Wing V seismic alarm patterns centered on a topographic effect due to the Goshen Hole escarpment

and/or peculiar earthquake phases from the Pocatello Valley event. However, the St. Elias seismic alarms suggested that simple body waves were responsible and the calculations reported here support this hypothesis. On this basis, future North American earthquakes with significant body wave energy in the period range of 2 to 6 seconds would be expected to trigger seismic alarms over Wing V in a pattern depending on the depth and velocity of sedimentary cover and the incident body wave type. A quantitative description of the phenomenon would require: measured (versus inferred) seismic velocities under a number of flights; the inclusion of material damping, which is significant for Pierre Shale, in the calculation; and more complete data on MGS response based on large scale seismic vibration tests.

SECTION 7

REFERENCES

Aki, K. and P. G. Richards (1980). Quantitative Seismology, W. H. Freeman and Co.

Allemdinger, R. (1980). Personal communication, Dept. of Geological Sciences, Cornell University.

Alsop, L. E. (1966). Transmission and Reflection of Love Waves at a Vertical Discontinuity, J. Geophys. Research 71, 3969-3984.

Anderman, G. G. and E. J. Ackman (1963). Structure of the Denver-Julesburg Basin and Surrounding Areas, in Bolyard and Katich (1963).

Arabasz, W. J., W. D. Richens and C. J. Langer (1980). The Pocatello Valley (Idaho-Utah Border) Earthquake Sequence of March-April 1975, Bull. Seism. Soc. Am. 71, 803-826.

Battis, J. C. (1978). Geophysical Studies for Missile Basing: Seismic Risk Studies in the Western United States, Texas Instruments Inc. report to the Air Force Office of Scientific Research, Bolling AFB.

Battis, J. C. and K. J. Hill (1977). Analysis of Seismicity and Tectonics of the Central and Western United States, Texas Instruments Inc. report to the Air Force Office of Scientific Research, Bolling AFB.

Boatwright, J. (1980). Preliminary Body-Wave Analysis of the St. Elias Earthquake of February 28, 1979, Bull. Seism. Soc. Am. 70, 419-436.

Bolt, B. A. (1976). Nuclear Explosions and Earthquakes, W. H. Freeman and Co.

Bolyard, D. W. and P. J. Katich, editors (1963). Guidebook to the Geology of the Northern Denver Basin and Adjacent Uplifts, Fourteenth Field Conference, Rocky Mountain Association of Geologists, Denver, Colorado.

Bouchon, M. (1973). Effect of Topography on Surface Motion, Bull. Seism. Soc. Am. 63, 615-632.

Cram, I. H., editor (1971). Future Petroleum Provinces of the United States—Their Geology and Potential, The American Association of Petroleum Geologists, Tulsa, Oklahoma.

Day, S. M., T. C. Bache, T. G. Barker and J. T. Cherry (1978). A Source Model for the 1975 Pocatello Valley Earthquake, Systems, Science and Software report to the Air Force Geophysics Laboratory, Hanscom AFB, Massachusetts.

Denson, N. M. and M. H. Bergendahl (1961). Middle and Upper Tertiary Rocks of Southeastern Wyoming and Adjoining Areas, U.S. Geological Survey Professional Paper 424-C.

Droullard, E. K. (1963). Tectonics of the Southeast Flank of the Hartville Uplift, Wyoming, in Bolyard and Katich (1963).

REFERENCES (CONTINUED)

Ewing, W. M., W. S. Jardetsky and F. Press (1957). Elastic Waves in Layered Media, McGraw-Hill Book Co.

Faust, L. Y. (1951). Seismic Velocity as a Function of Depth and Geologic Time, Geophysics 16, 192-206.

Gardner, E.H.F., L. W. Gardner and A. R. Gregory (1974). Formation Velocity and Density—The Diagnostic Basics for Stratigraphic Traps, Geophysics 39, 770-780.

Gassmann, F. (1951). Elastic Waves Through a Packing of Spheres, Geophysics 16, 673-685.

Geo-Search Corp. (1980). Speculative Seismic Survey, Denver Basin, Chadron Arch, Kennedy Basin; Advertising Brochure from Geo-Search Corp. and Western Geophysical.

Harmsen, S. and S. Harding (1980). Surface Motion Over a Sedimentary Valley for Incident Plane P and SV Waves, Bull. Seism. Soc. Am. 71, 655-670.

Harris, D. V. (1963). Geomorphology of Larimer County, Colorado, in Bolyard and Katich (1963).

Haskell, N. A. (1941). The Relation Between Depth, Lithology and Seismic Wave Velocity in Tertiary Sandstones and Shales, Geophysics 6, 318-326.

Haskell, N. A. (1960). Crustal Reflections of Plane SH Waves, J. Geophys. Research 65, 4147-4150.

Haskell, N. A. (1962). Crustal Reflections of Plane P and SV Waves, J. Geophys. Research 67, 4751-4767.

Herrmann, R. B., editor (1978). Computer Programs in Earthquake Seismology, 1,2, NSF Sponsored, Dept. of Earth and Planetary Sciences, Saint Louis University.

Hume, R. (1980). Personal communication, Navigation Systems Engineering Dept., TRW, Redondo Beach, California.

Julian, B. R. (1970). Regional Variations in Upper Mantle Structure Beneath North America, Ph.D. Thesis, California Institute of Technology.

Keller, G. R., R. B. Smith, L. W. Braile, R. Heaney and D. H. Shurbet (1976). Upper Crustal Structure of the Eastern Basin and Range, Northern Colorado Plateau, and Middle Rocky Mountains from Rayleigh-Wave Dispersion, Bull. Seism. Soc. Am. 66, 869-876.

King, P. B. (1969). Tectonic Map of North America, U.S. Geological Survey.

King, P. B. (1977). The Evolution of North America, Princeton University Press, Princeton, New Jersey.

REFERENCES (CONTINUED)

King, P. B. and H. M. Beikman (1974). Geologic Map of the United States, U.S. Geological Survey.

Lahr, J. C. (1980). Personal communication, U.S. Geological Survey, Menlo Park, California.

Matuszczak, R. A. (1976). Wattenberg Field, Denver Basin, Colorado, in North American Oil and Gas Fields, edited by J. Braunstein, The American Association of Petroleum Geologists, Tulsa, Oklahoma.

Moore, F. E. (1963). Tertiary Stratigraphy of the High Plains, in Bolyard and Katich (1963).

Murphy, J. R. and R. A. Hewlett (1975). Analysis of Seismic Response in the City of Las Vegas, Nevada: A Preliminary Microzonation, Bull. Seism. Soc. Am. 65, 1575-1597.

Nafe, J. E. and C. L. Drake (1963). Physical Properties of Marine Sediments, The Sea, 3, Interscience Publishers, 794-815.

Ossing, H. A. and F. A. Crowley (1978). Wing V Ground Motion Study, Air Force Surveys in Geophysics, No. 401, Air Force Geophysics Laboratory, Hanscom AFB, Massachusetts.

Porter and O'Brien, Consulting Engineers (1960). Subsurface Site Investigations, F. E. Warren Air Force Base, Wyoming Development Area, 1-20.

Press, F. (1966). Seismic Velocities, Handbook of Physical Constants, Geol. Soc. Am., Memoir 97.

Prodehl, C. and L. C. Pakiser (1980). Crustal Structure of the Southern Rocky Mountains from Seismic Measurements, Bull. Geol. Soc. Am. 91, 147-155.

Rapp, J. R., F. N. Visher and R. T. Littleton (1957). Geology and Groundwater Hydrology of Goshen County, Wyoming, Water Supply Paper #1377, U.S. Geological Survey.

Richter, C. F. (1958). Elementary Seismology, W. H. Freeman and Co.

Riecker, R. E. (1975). Literature Reconnaissance: Geology of Northeastern Colorado, Southeastern Wyoming, and the Nebraska Panhandle, Terrestrial Sciences Laboratory, Air Force Cambridge Research Laboratories.

Rodi, W. L., T. C. Bache, J. J. Swanger, T. G. Barker and J. T. Cherry (1979). Synthesis of Regional Ground Motion from Western U.S. Earthquakes, Systems, Science and Software report to the Air Force Geophysics Laboratory, Hanscom AFB, Massachusetts.

Smith, F. A. and V. L. Souders (1975). Groundwater Geology of Banner County, Nebraska, Nebraska Water Supply Paper 39.

AD-A107 667 WEIDLINGER ASSOCIATES MENLO PARK CA F/G 8/11
SITE-DEPENDENT GROUND MOTIONS FROM DISTANT EARTHQUAKES. REVISED--ETC(U)
DEC 80 G L WOJCIK, J ISENBERG, W S DUNBAR F49620-80-C-0009
UNCLASSIFIED R-8065 AFOSR-TR-81-0723 NL

2 OF 2
AD A
107 667

END
DATE FILMED
1 -82
DTIC

REFERENCES (CONCLUDED)

Smith, R. B., W. J. Arabasz and K. Kilty (1980). Preliminary Geological and Geophysical Data from the Wing V Area, Consultants' Report to Weidlinger Associates.

Smith, R. B. and M. L. Sbar (1974). Contemporary Tectonics and Seismicity of the Western United States with Emphasis on the Intermountain Seismic Belt, Bull. Geol. Soc. Am., 85, 1205-1218.

Summers, T. S. (1980). Personal communication, Eyring Research Institute, Inc., Provo, Utah.

Telford, W. M., L. P. Geldart, R. E. Sheriff and D. A. Keys (1980). Applied Geophysics, Cambridge University Press.

Tosaya, C. (1981). Ultrasonic Velocities and Attenuation in Shales: Identification of Shale Lithologies and Delineation of Abnormal Pore Pressures, Stanford Rock Physics Project, 10, Amos Nur, Principal Investigator, 61-101.

Volk, R. W. (1971). Petroleum Potential of Eastern Colorado, Western Nebraska, Southeastern Wyoming and Northeastern New Mexico, in Cram (1971).

Wojcik, G. L. (1979). Resonance Zones on the Surface of a Dipping Layer due to Plane SH Seismic Input, NSF Grant Report, Weidlinger Associates, Menlo Park, California.

APPENDIX A

NUMERICAL ANALYSIS OF TOPOGRAPHIC SCATTERING EFFECTS

A.1 Introducton

Scattering of waves by the Goshen Hole escarpment was investigated as a possible contributor to the observed distribution of seismic alarms. As is discussed above, sources of shaking in the period range 2 to 6 seconds are of interest in explaining the distribution. Scaling laws suggest that the dimension of the Goshen Hole escarpment (<200 meters) is too small to interact with these longer period waves. To support this conclusion, an analysis of shorter wave periods for which interaction is expected to be maximum was performed.

The present study considers normally incident P and S waves. A two-dimensional finite element model of a 250 meter escarpment was generated for a 2 to 8 Hz frequency range (.125-.5 second period). The finite element model was used to develop a Green's function for each type of body wave input. By means of superposition, a range of input time histories were considered and seismograms and spectra were generated without further time domain finite element analysis.

In Ref. A-1, Boore et al. used a finite difference model to examine scattering from a vertical and 45° escarpment for a particular time history input. Earlier, Bouchon, Ref. A-2, considered scattering from ridges and valleys using a semi-analytical frequency domain analysis. Boore et al. showed the shape of the escarpment was significant at the relatively high frequencies where scattering occurred. Bouchon's results indicated that the highland response exceeded that of the adjacent lowland.

A.2 Numerical Method

The basic numerical tool used in this study was TRANAL, a three-dimensional, explicit, nonlinear finite element code with constant strain elements in which

single point integration is used to compute stresses, Ref. A-3. The code was specialized to treat two-dimensional, linear problems for this study.

The model of the Goshen Hole escarpment is shown in Fig. A-1. Since the model is assumed to be linear, superposition of elementary solutions (Green's functions) can be used to obtain the response to complex inputs. The Green's function best suited to TRANAL is a ramp in velocity. The function is developed by applying to the bottom boundary of the grid in Fig. A-1 a horizontal (S wave) or vertical (P wave) velocity-time history which increases linearly with time. The procedure is illustrated in Fig. A-2. The responses of nodes on the free surface are stored for future use in response calculations. At surface nodes far from the escarpment, the response is due to the direct wave only and is equal to the input multiplied by a factor of 2. At surface nodes close to the escarpment, the response includes both the direct wave and scattered waves.

By superposition, the responses to a ramp input can be combined to obtain a wide range of smooth time domain input functions. The function used here is the Ricker wavelet, Ref. A-4, which is illustrated in Fig. A-3 along with its spectrum. In the time domain, the wavelet is dispersed as a result of frequency limitations of the finite element grid. However, the distortion appears negligible when examined in the frequency domain.

A.3 Application to Goshen Hole Escarpment

Seismograms resulting from P wave input are shown in Figs. A-4 and A-5. These seismograms are observed at highland and lowland stations which are equally spaced from the edges of the escarpment. The first signal is the input wavelet, which arrives simultaneously at all lowland points, and soon thereafter

at all highland points. The next signal is the scattered P wave which is a weak diffracted wave from the corner of the escarpment. The next significant signal is the scattered Rayleigh wave. Superposed on this signal is the scattered S wave which is difficult to distinguish from the Rayleigh wave because of low amplitude and comparable seismic wavespeed. The scattered surface wave is significantly stronger in the highlands than in the lowlands. To investigate the relative amplitudes of scattered waves, the incident wave was subtracted from the total responses of the highlands and lowlands. A typical result for the highlands is shown in Fig. A-6 where the vertical component of scattered surface waves is about ten times greater than the scattered body waves. These results were also studied in the frequency domain by imposing wavelets covering the frequency range of interest. Typical results are presented in Figs. A-7 and A-8 in the form of power spectral density ratios for one station in the lowland and highland. The ratio at each frequency is formed by dividing the spectral density of the scattered signal by the spectral density of the incident signal. At the lowlands point shown in Fig. A-7, the scattered signal reaches a peak of about 3% of the incident signal density at a frequency of about 5.3 Hz. At the highlands point shown in Fig. A-8, the scattered signal reaches its maximum of about 22% of the incident signal density at about 5.7 Hz with a lesser peak of 20% near 2.5 Hz. Peak amplitudes and frequencies at which they occur vary depending on location and type of input.

A.4 Conclusions and Suggestions for Extending the Method

The principal scattered signal is a free surface Rayleigh wave whose amplitude in the highlands is 20-25% of the free surface body wave amplitude; scattered surface Rayleigh waves in the lowlands are about one-fourth as strong

as in the highlands. Resonances occur at frequencies in the range 4-6 Hz, which is related to the characteristic dimension of the topography (250 m) and the wavespeed (c_s = 1240 m/sec). The diffracted body waves are much weaker than the surface waves in the frequency range considered. Since this numerical model does not consider response in the period range 2-6 sec, where resonance occurs in the fundamental mode of the MGS, we cannot conclude that seismic alarms are independent of topography. However, nothing in the results of these studies suggests that significant interaction would occur between wavelengths of the order of 2 km (for 1 sec waves) and the escarpment even if the numerical model were expanded to include such longer period waves.

Recent extensions of TRANAL have made it possible to consider a wider range of frequencies for significantly less computer time (on the order of 250 times faster). These extensions include specialization of the code for problems of this type and adaptation to vector machines such as the CRAY-1.

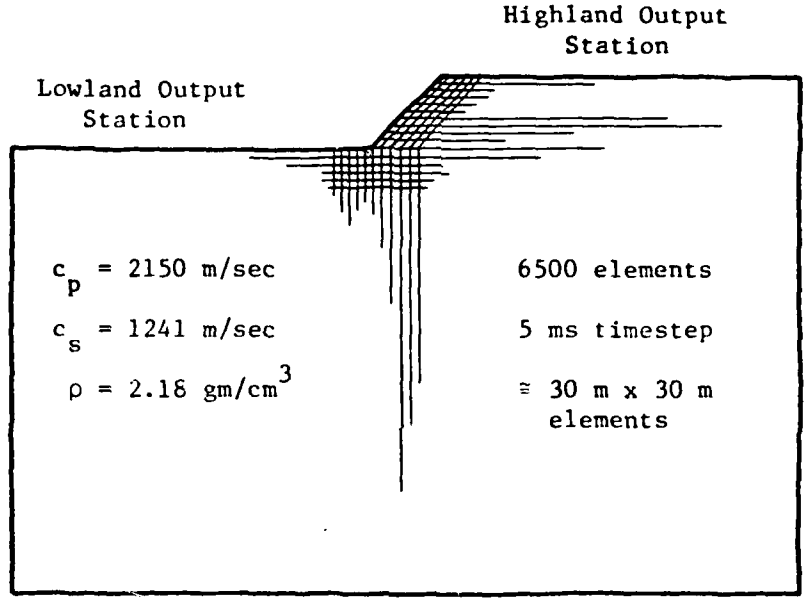

Figure A-1. Finite element model of escarpment (Wing V highlands-lowlands seismic alarm anomaly).

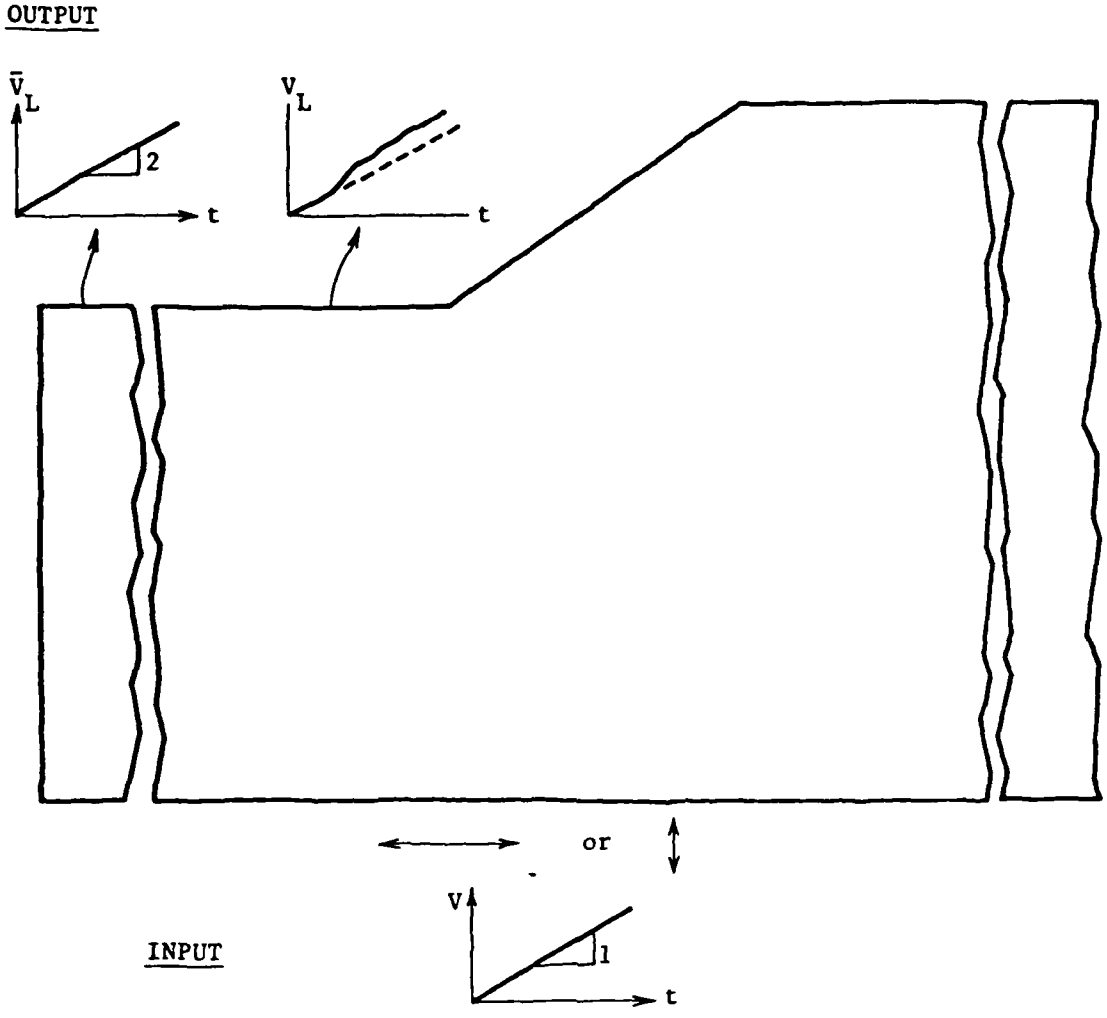

Definitions

V: input velocity-time history (velocity ramp)

$V_{L,H}$: lowland or highland velocity response on surface including incident and scattered waves

$\bar{V}_{L,H}$: one-dimensional soil column response (without scattered waves)

$V^*_{L,H}$: scattered velocity response (i.e. $V^*_L = V_L - \bar{V}_L$)

Figure A-2. Application of Green's function approach to example of Wing V seismic alarm anomaly.

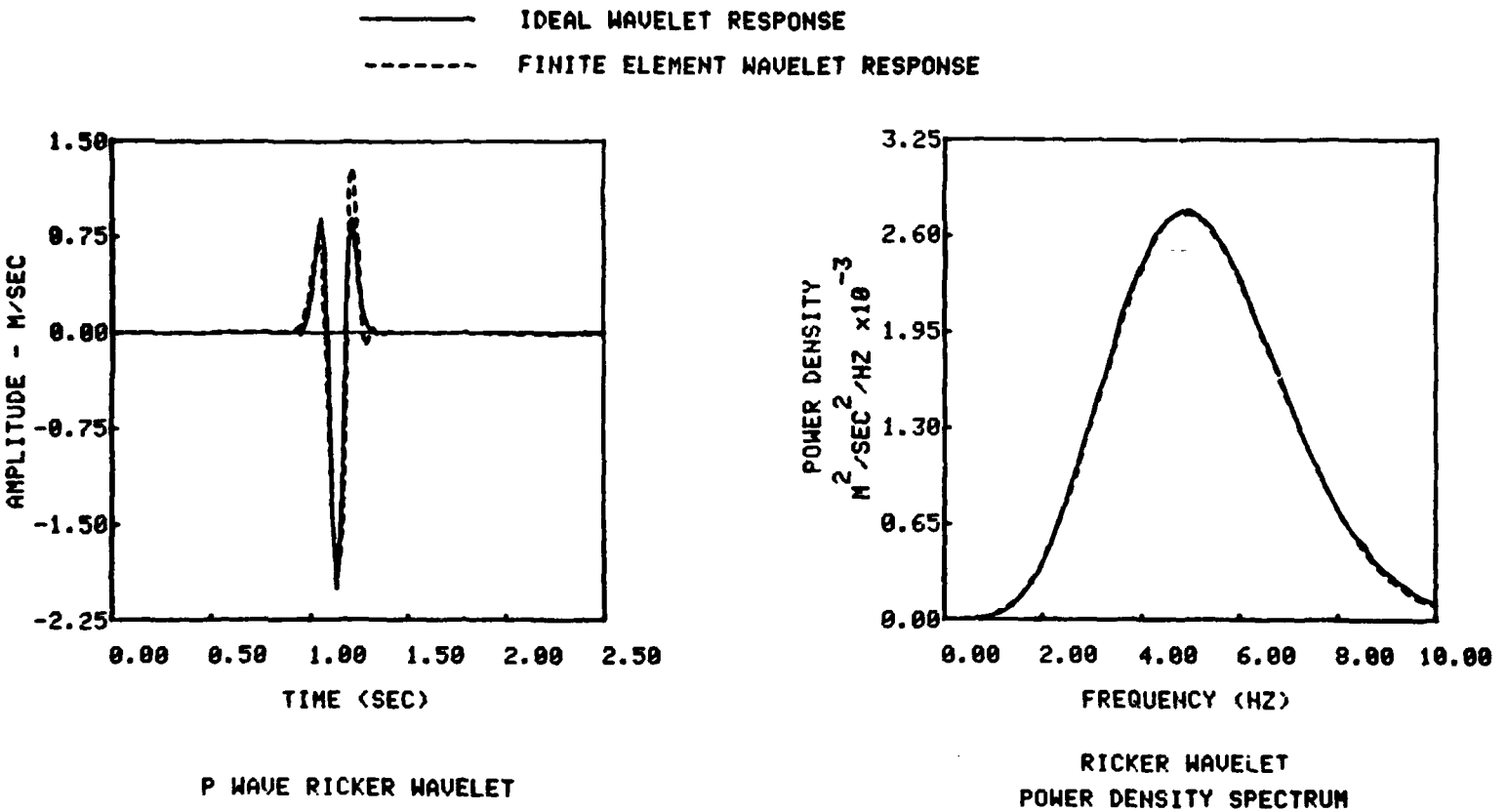

Figure A-3. Ricker wavelet obtained by a superposition of finite element ramp responses for the highland soil column.

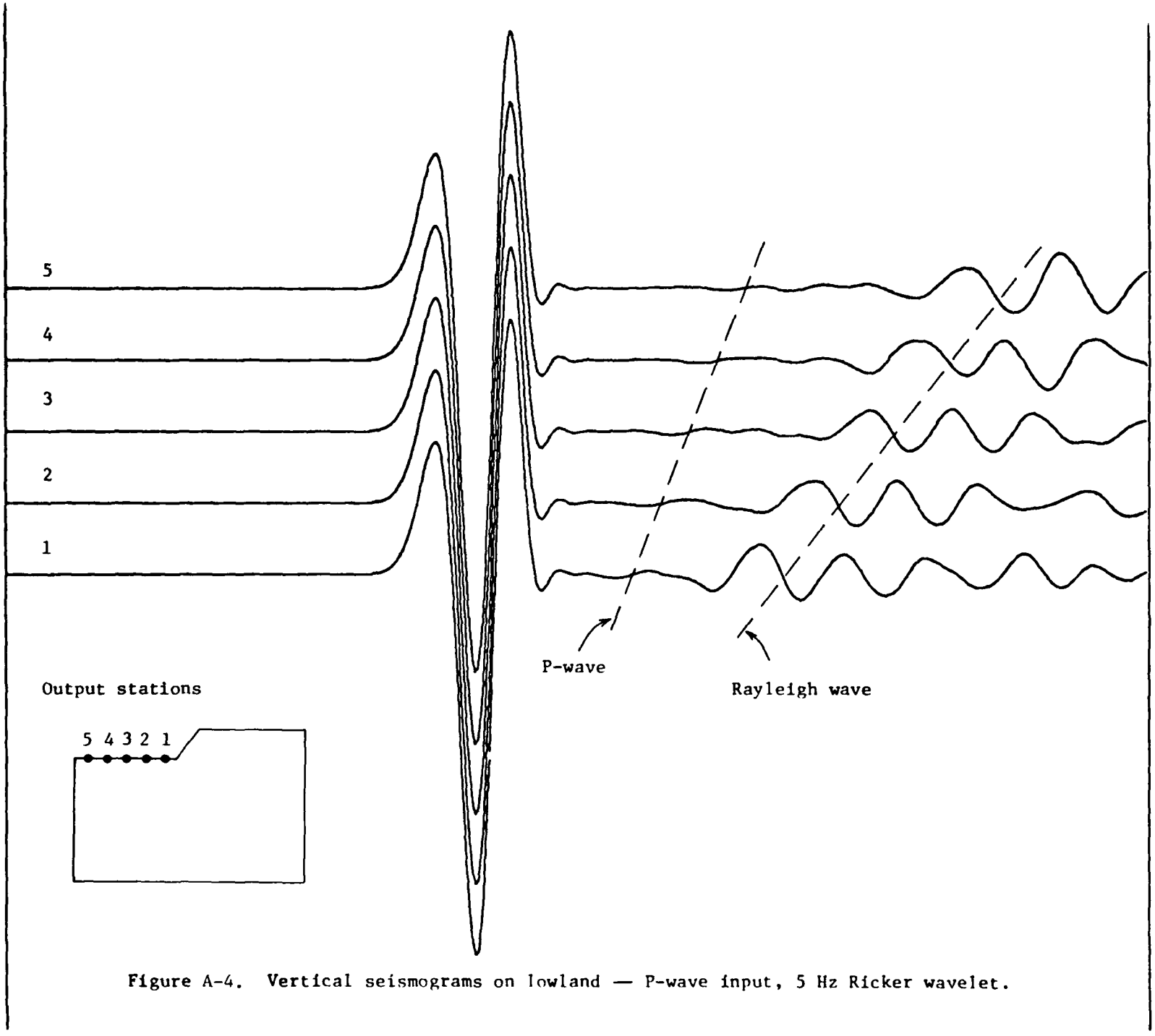

Figure A-4. Vertical seismograms on lowland — P-wave input, 5 Hz Ricker wavelet.

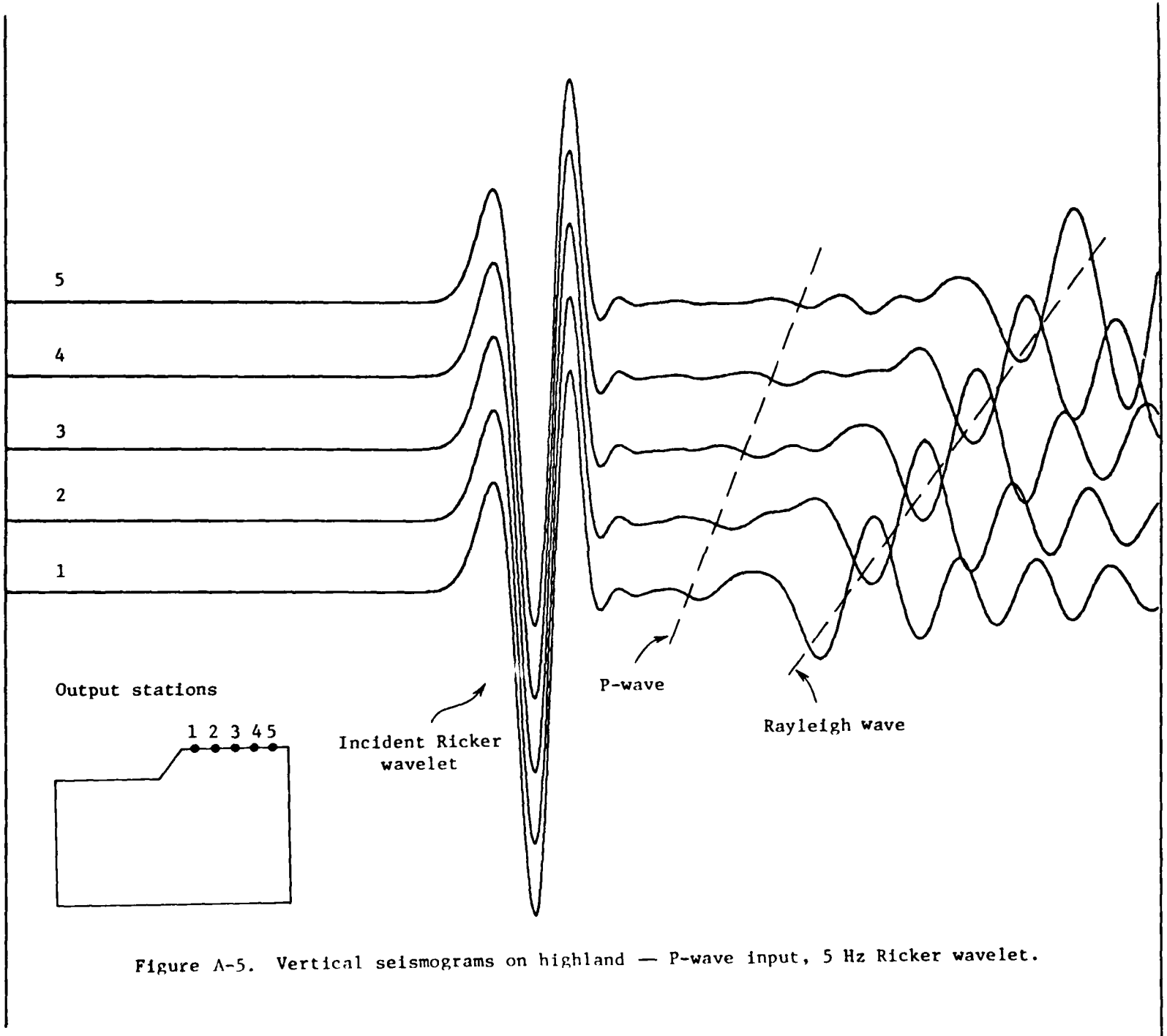

Figure A-5. Vertical seismograms on highland — P-wave input, 5 Hz Ricker wavelet.

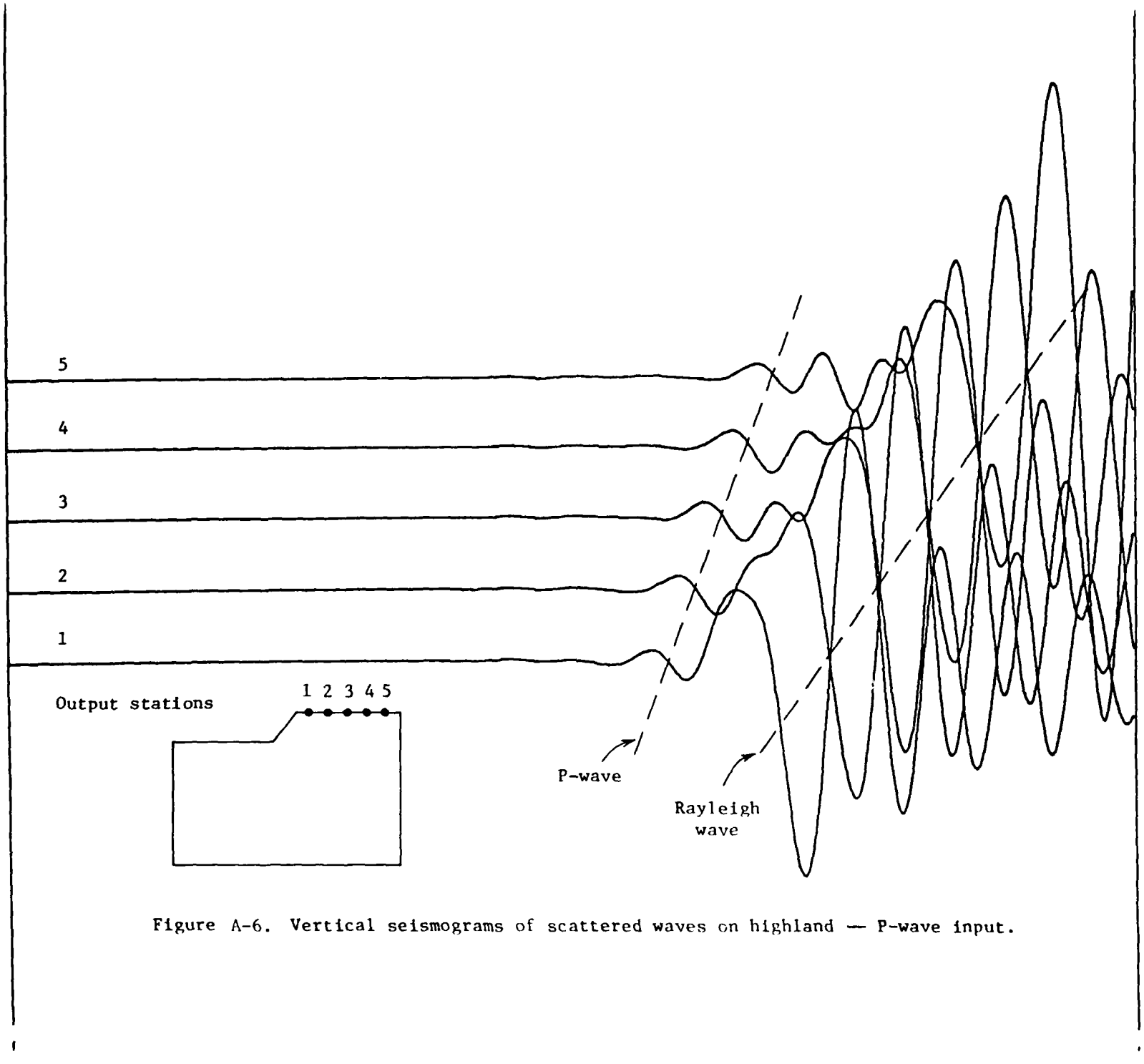

Figure A-6. Vertical seismograms of scattered waves on highland — P-wave input.

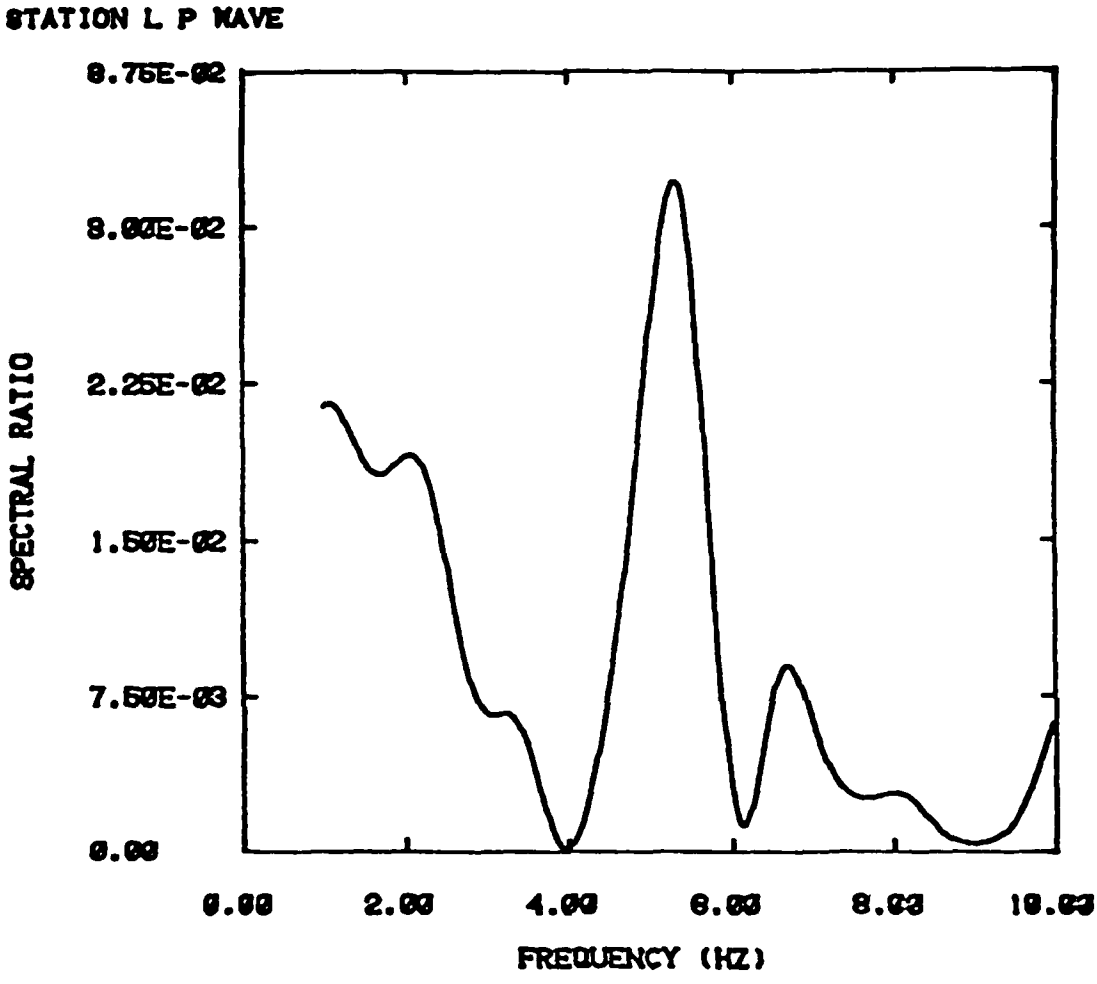

Figure A-7. Power spectral density ratio (vertical)

$$\frac{\text{scattered spectrum}}{\text{incident spectrum}}$$

for a lowlands point with P-wave input.

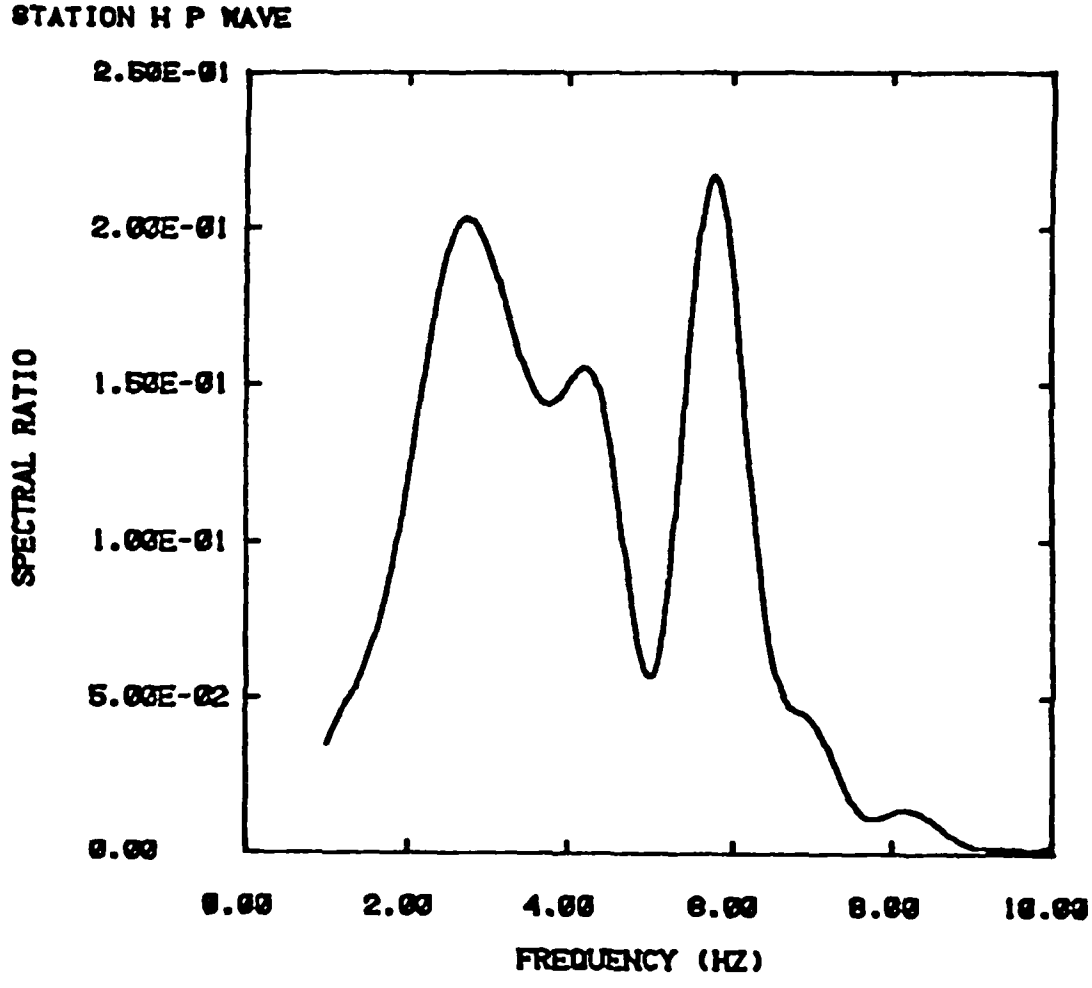

Figure A-8. Power spectral density ratio (vertical)

$$\frac{\text{scattered spectrum}}{\text{incident spectrum}}$$

for a highlands point with P-wave input.

APPENDIX A

REFERENCES

A-1. Boore, D. M., S. C. Harmsen and S. T. Harding (1981). Wave Scattering from a Step Change in Surface Topography, Bull. Seism. Soc. Am. 63, 117-125.

A-2. Bouchon, M. (1973). Effects of Topography on Surface Motion, Bull. Seism. Soc. Am. 63, 615-632.

A-3. Baylor, J. L., J. P. Wright and C. F. Chung (1979). Tranal User's Guide, Part I (small strain, small displacement), Weidlinger Associates, prepared for Director, Defense Nuclear Agency.

A-4. Ricker, N. (1953). The Forms and Laws of Propagation of Seismic Wavelets, Geophysics 18, 10-40.